The Pennsylvania State University

The Graduate School

College of Engineering

PSEUDO PIN-BY-PIN CALCULATION METHODOLOGY FOR PIN POWER RECOVERY

A Dissertation in

Nuclear Engineering

by

Baocheng Zhang

Submitted in Partial Fulfillment

of the Requirements

for the Degree of

Doctor of Philosophy

December 2010

The dissertation of Baocheng Zhang was reviewed and approved[1] by the following:

Kostadin N. Ivanov
Distinguished Professor of Nuclear Engineering
Dissertation Adviser
Chair of Committee

Maria N. Avramova
Assistant Professor of Nuclear Engineering

Seungjin Kim
Assistant Professor of Nuclear Engineering

Ludmil Zikatanov
Associate Professor of Mathematics

Jeffery Brown
Consultant Engineer
Westinghouse Electric Company
Special Member

Arthur Motta
Professor of Nuclear Engineering and Material Science
Chair of Nuclear Engineering Program

[1] Signatures are on file in the Graduate School

ABSTRACT

With the increasing demand of nuclear energy, nuclear energy suppliers are interested in safe and effective margin management in their operations. Moreover, seeking extra financial benefit, the nuclear energy suppliers up-rate their plants, which takes away a lot of original design margin and pushes the fuel and core design very close to the design limits. In such environment, it is more and more important to reduce the uncertainty of the calculations and improve the accuracy of the design codes in both global solution and detailed local distribution such as fuel rod (pin) power predictions so that the reactor capabilities and operation behavior can be precisely predicted and simulated.

At the same time, in the new generation PWR core designs such as AP1000™, the role of the control rods has been completely changed since the control rods are heavily involved in the core operation. The use of control rods for normal operation has brought significant challenges to the current PWR methodologies. One of the most affected methodologies is the conventional pin power calculation. The insertion of the control rods dramatically changes the heterogeneity of the fuel assemblies, which in turn leads to completely different pin power distribution. The accumulation effect of this re-distribution is a history modeling problem of the conventional pin power recovery methodology since the actual strategy of control rod insertion and withdrawal is not available in advance. Therefore it is difficult to generate pin-wise data at the core design phase to simulate the actual operation condition.

The main objective of this PhD research is to develop a novel Pseudo Pin-by-Pin

Calculation (P3C) methodology for pin power recovery, which can be directly applied in the Westinghouse core design code ANC. The P3C methodology should be robust enough to simulate all control rod insertion scenarios for all different fuel types and provide accurate pin power predictions. In addition, compared to direct pin-by-pin embedded calculation, this method is more efficient so that the methodology is fast enough to be used in the current code system for routine design calculation and core monitoring. This study focuses on PWR application. However, feasibility study for BWR application is also included.

TABLE OF CONTENTS

LIST OF ABBREVIATIONS

1-,2- or 3D	One-, Two- or Three Dimensional
ANC	Westinghouse Advance Nodal Code
ANM	Analytic Nodal Method
AO	Axial Offset
ARO	All control Rod Out
BA	Burnable Absorber
BCs	Boundary Conditions
BWR	Boiling Water Reactor
CD	Cell Data
CHF	Critical Heat Flux
CR	Control Rod
DF	Discontinuity Factor
DNB	Departure from Nucleate Boiling
FA	Fuel Assembly
HFP	Hot Full Power
HZP	Hot Zero Power
IFBA	Integral Fuel and Burnable (Boron) Absorber
LRF	Lattice code Result File
LWR	Light Water Reactor
MOX	Mixed-Oxide
MTU	Metrics Ton Uranium
NEM	Nodal Expansion Method
NEXUS	Westinghouse New Cross-Section Generation System
NGM	Next Generation Methodology
NPP	Nuclear Power Plant
NRC	Nuclear Regulatory Commission
P3C	Pseudo Pin-by-Pin Calculation

PSU	The Pennsylvania State University
PWR	Pressurized Water Reactor
RMSE	Root Mean Square Error
SANM	Semi-Analytic Nodal Method
T-H	Thermal-Hydraulic
UOX	Uranium-Oxide
UA	Unit Assembly
WABA	Wet Annular Burnable Absorber

LIST OF FIGURES

ACKNOWLEDGMENTS

I would like to thank my advisor, Dr. Kostadin Ivanov, for his support, encouragement and assistance during the course of this work.

I wish to acknowledge Dr. Erwin Muller, Dr. Yung-An Chao, and Mr. Larry Mayhue for the guidance and suggestions they have given me during my thesis research.

I would like to express my great appreciation to Dr. Petri Forslund Guimaraes, Dr. Fausto Franceschini, and Westinghouse NEXUS system development team for their hard work on the implementation of the required changes in the NEXUS system and the generation of basic assembly data for the qualification. Because of their support, this research work could be carried out successfully.

Further, I would like to thank the committee members Dr. M. Avramova, Mr. Jeff Brown, Dr. Seungjin Kim, and Dr. Ludmil Zikatanov for reading and making additional suggestions to improve this thesis.

I also wish to thank Core Engineering Department of Westinghouse Electric Company for providing funding during the course of my graduate studies and supporting my research work.

Finally, I want to thank my family, my son Eddie and my wife Bo for their lasting love, encouragement, and creating a comfortable environment at home so that I could complete all assigned courses and concentrate on my research work.

CHAPTER 1

INTRODUCTION AND BACKGROUND

1.1 Introduction

A focused effort to merge and modernize the methods employed in the PWR and BWR steady-state reactor physics codes of Westinghouse was launched a few years ago. A new core design package, NEXUS/ANC9[1], is being developed to replace the current ALPHA/PHOENIX/ANC (APA) system. This new system is illustrated in Figure 1.1.

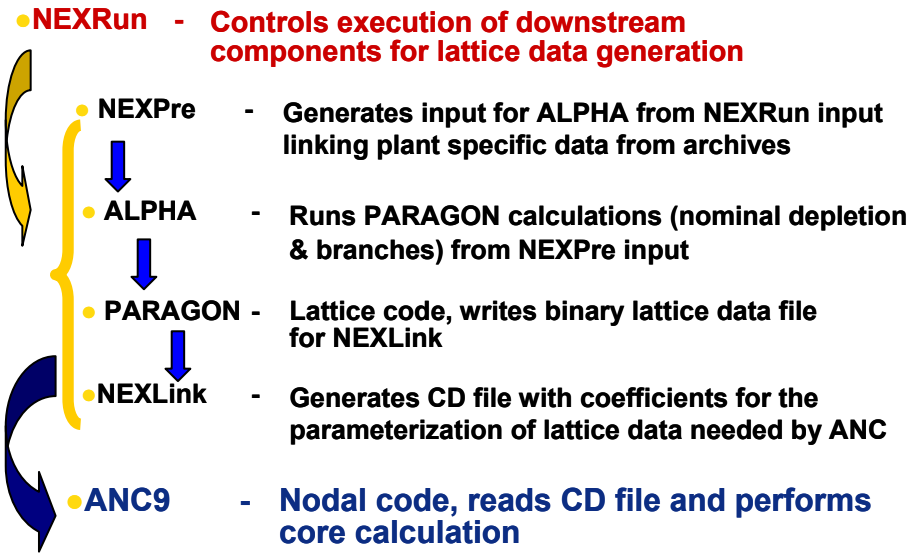

Figure 1.1 Illustration of NEXUS/ANC9 system

In the first phase of the development project, a new once-through nodal cross-section generation and representation methodology was developed [2] and incorporated in NEXUS. After completion of the cross-section representation model, a new pin power recovery (reconstruction) methodology has been under development for the Westinghouse suite of core analysis codes. One of its main features is to enable capturing the impact of control rod history on pin power distributions in an explicit on-the-fly procedure, thus overcoming an important limitation of the existing BWR implicit methodology that requires complicated data generation procedures. Since the next generation of PWRs such as the AP1000 will be operated with control rods inserted into the core, the effect of control rod history has become relevant also in the PWR analysis.

This research focuses on development of a new pin power recovery methodology. Its trademark name is the Pseudo Pin-by-Pin Calculation ("P3C"). There are several requirements for this new methodology. First, this new method should improve the pin power recovery calculations in PWR applications. Second, the method should be able to account for control rod history and spectrum interaction effects. Besides accuracy, another important requirement for this new methodology is the computational efficiency, which would allow the application not only in routine core design calculations but also in the Westinghouse on-line core monitoring systems.

In addition, the control rod history problem, that has been a challenge to the BWR core design codes for many years, will need to be resolved so that this new developed method could be applied in both PWR and BWR cores.

1.2 Background information

In most core analysis codes, the neutron diffusion equations are solved using nodal methods, which solve the diffusion equation over large mesh sizes, i.e. nodes. Typically, the size of each node in the radial plane is either the size of an assembly or the size of an quarter fuel assembly.

In order to solve the problem, the nodal code uses the homogenized cross-sections and discontinuity factors generated through lattice code single assembly calculations. The Analytic Nodal Method (ANM), Semi-Analytic Nodal Method (SANM), or Nodal Expansion Method (NEM) are commonly used to solve the diffusion equations [3][4][5] [6][7] and obtain the nodal fluxes and power distributions.

In addition to the nodal methods, the pin power recovery [8] has been adopted by the core design codes in order to calculate the power of each fuel rod. The accurate prediction of these pin powers is very important as this guarantees that all fuel rod power densities meet the safety limit, e.g. DNB limits, during the plant operation. Among the pin power recovery methods, the modulation method has been widely adopted by the nodal codes in the nuclear industry due to its efficiency. The modulation method computes the pin powers through multiplying pre-generated pin power form factors to the homogeneous, smooth pin power distribution. This means that those pin power form factors, generated from the lattice code single assembly calculation during the homogeneous cross-section generation, carry all heterogeneity information of the fuel.

Past experience shows that the conventional modulation method has adequate accuracy in the pin power predictions for the conventional PWR cores. However, in certain conditions the modulation method shows significant discrepancies in the pin power predictions. Some of those are:

- Significant heterogeneity change during the fuel assembly exposure, typically fuel burning with inserted control rod. The conventional method has difficulty to accurately capture the control rod history effect.

- Strong interaction effect between unlike fuel assemblies such as Mixed-oxide (MOX) fuel assembly and UO_2 assembly.

In recent years, instead of improving the conventional pin power recovery methods, more and more studies, especially in the national labs and universities, focused on developing advanced methods that directly adopt fine mesh transport calculation within each fuel node (Embedded Method) [9][10] or full direct core transport simulation [11][12]. Definitely, those advanced methods, normally called "Next Generation Methods (NGM)", are the future of the reactor core calculations. But the current limitations on computer power capability seem to set their implementation and practical application well ahead in the future.

1.3 Research objectives

The main objective of this thesis is the development, implementation, and qualification of

the Pseudo Pin-by-Pin Calculation (P3C) methodology for pin power recovery. The new methodology is directly adopted by the Westinghouse core design code ANC. The P3C methodology is robust and able to simulate all control rod insertion scenarios for all different fuel types and provide accurate pin power predictions. In addition, compared to direct pin-by-pin embedded calculation, this method is much simpler so that the methodology is fast enough to be used in the current code system for routine design calculation and core monitoring. The qualification in this thesis is focused on PWR application. A feasibility study for BWR application is also included.

It should be pointed out that the "pin" referred throughout this document stands for the smeared pin-cell. Typically, a fuel "pin" is the smeared area of the pellet, cladding, and moderator of a pin-cell.

1.4 Thesis outline

CHAPTER 2 presents the current conventional pin power recovery methodology used in core design calculations. In addition, the improvements of the conventional methodology made around the world will be discussed.

CHAPTER 3 describes the philosophy of the Pseudo Pin-by-Pin Calculation (P3C) methodology and focuses on the development of the pin cross-section representation model.

CHAPTER 4 continues the discussion of the P3C methodology, while focusing on the pin

flux calculation.

CHAPTER 5 describes the implementation and qualification of the P3C methodology based on the comparison between ANC and lattice calculations for PWR fuel assemblies.

CHAPTER 6 covers the preliminary study of the P3C concept for BWR pin power prediction.

CHAPTER 7 summarizes the development work, envisions the potential application of the P3C methodology and corresponding development.

CHAPTER 2

CONVENTIONAL METHODOLOGY

2.1 Description of the Conventional Modulation Methodology for Pin Power Recovery

This chapter presents the conventional modulation methodology widely used in the simulator codes for performing pin power calculations for nuclear core designs. In addition, some improvements of the conventional methodology are also described.

In most core design codes based on nodal methods (e.g. ANC [13] and POLCA7 [14]) a modulation method is used to recover the heterogeneous pin power distribution from the nodal results. Heterogeneous pin power form factors are used in this process which are either energy group dependent (as in ANC) or group independent (as in POLCA7). The power in pin "*k*" can generally be expressed as:

$$P^k = \sum_g P_g^{k,Hom} \cdot p_g^k \tag{2.1a}$$

or

$$P^k = P^{k,Hom} \cdot p^k \tag{2.1b}$$

Here P^k and $P^{k,Hom}$ are the heterogeneous (actual) and the homogeneous pin powers respectively.

Originally, the homogeneous pin power distribution was directly computed using the nodal average and surface powers through two-dimensional polynomial expansions. With the continuous development of the pin power recovery methodologies, it become standard to calculate the homogeneous pin power through constructing the homogeneous pin cross-sections and fluxes [8] [15] [16] [17]. Therefore:

$$P^k = \sum_g (\kappa\Sigma_{f,g}^{k,Hom} \cdot \phi_g^{k,Hom}) \cdot p_g^k \tag{2.1}$$

Here $\kappa\Sigma_{f,g}^{Hom}$ is the homogeneous intra-node kappa-fission cross-section in energy group g, and ϕ_g^{Hom} the pin homogeneous flux.

Generally speaking, the conventional modulation method assumes that the heterogeneity can be fully captured by the heterogeneous power form factors p_g^k. The power form factors are usually generated from unit assembly lattice calculations at selected fuel exposures. Figure 2.1 illustrates the ratio of the homogeneous to heterogeneous relative power (the form factor) for selected row that crosses the central pin.

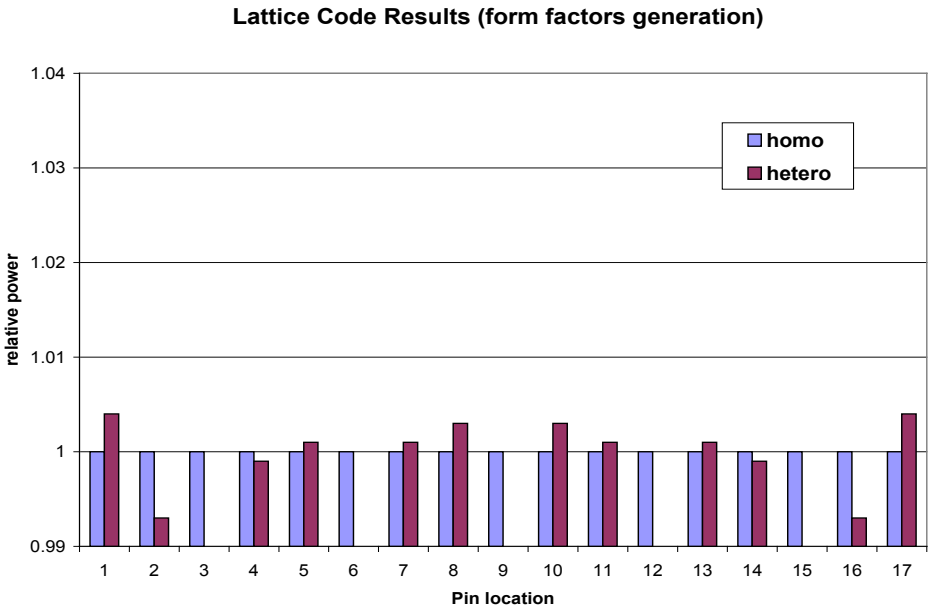

Figure 2.1 Illustration of pin power form factors generation

The form factors are defined as:

$$p_g^k = \frac{P_g^{k,Het,Lat}}{P_g^{k,Hom,Lat}} = \frac{\kappa\Sigma_{f,g}^{k,Het} \cdot \phi_g^{k,Het}}{\kappa\Sigma_{f,g}^{k,Hom} \cdot \phi_g^{k,Hom}} \tag{2.2}$$

Here $P_g^{k,Het,Lat} = \kappa\Sigma_{f,g}^{k,Het} \cdot \phi_g^{k,Het}$ is the heterogeneous pin power of the energy group "g" from the lattice code calculations, and $P_g^{k,Hom,Lat} = \kappa\Sigma_{f,g}^{k,Hom} \cdot \phi_g^{k,Hom}$ is the homogeneous one. Since the reflective boundary condition is used in the unit lattice calculations, the homogeneous power distribution is flat and the uniform power can be simply computed as:

$$P_g^{k,Hom,Lat} = \kappa\Sigma_{f,g}^{Avg,Lat} \cdot \phi_g^{Avg,Lat} = P_g^{Avg,Lat} \tag{2.3}$$

The notation "*Avg*" in Eq.(2.3) stands for the assembly average values.

To match the actual environmental and assembly conditions, the pin power form factors are normally represented as a function of fuel average burnup and of selected instantaneous state parameters.

Besides the pin power form factors, two homogeneous pin data sets capturing the environmental assembly conditions, homogeneous pin kappa-fissions and fluxes, are needed to compute the pin powers. Constructions of these two parameters are discussed in the subsections 2.1.1 and subsection 2.1.2, respectively.

2.1.1 Homogeneous Pin-cell Cross-section Calculation

As described above, the pin power form factors are generated through single assembly lattice code calculation with reflective boundary condition, which assumes a uniform distribution of homogeneous pin-cell cross-sections.

In the real core conditions, most assemblies are normally surrounded by different assembly types with different enrichment, exposure history, or fuel type. That creates non-zero currents at the assembly surfaces and leads to a power and fuel exposure gradients within the fuel node (or assembly). During the nodal calculation, the so-called intra-nodal model [18] accounts for the above gradient through introducing nodal surface cross-sections in conjunction with nodal average ones.

In most of the conventional pin power recovery methods, the pin-cell homogeneous cross-sections are obtained through polynomial expansion [15] preserving the nodal

average and surface values.

2.1.2 Homogeneous Pin-cell Flux Calculations

The homogeneous fluxes can be generated through polynomial fitting or solving the diffusion equation of each homogeneous node. The latter one is commonly taken by most industrial core design codes including ANC [16] and SIMULATE [17] as well as in some developments in academia for transient applications [31]. The discussion below will focus on the method of directly solving the diffusion equations.

For a given homogeneous fuel node, the diffusion equation of energy group "g" is expressed as:

$$-D_g \nabla^2 \phi_g + \left(\Sigma_{a,g} + \sum_{g' \neq g} \Sigma_{g',g} \right) \phi_g = \frac{\chi_g}{k_{eff}} \sum_{g'} \nu \Sigma_{f,g'} \phi_g + \sum_{g' \neq g} \Sigma_{g,g'} \phi_{g'}$$

or

$$\nabla^2 \phi_g + \frac{1}{D_g} \left(-\left(\Sigma_{a,g} + \sum_{g' \neq g} \Sigma_{g',g} \right) \phi_g + \frac{\chi_g}{k_{eff}} \sum_{g'} \nu \Sigma_{f,g'} \phi_{g'} + \sum_{g' \neq g} \Sigma_{g,g'} \phi_{g'} \right) = 0$$

In general, the multi-group diffusion equation can be expressed as:

$$\nabla^2 \cdot \vec{\phi} + \hat{\mathrm{B}} \cdot \vec{\phi} = 0 \tag{2.4}$$

Here

$$\vec{\phi} = \{\phi_g\}$$

$$(\mathrm{B})_{i,j}=\begin{cases}\dfrac{1}{D_i}\left(-\left(\Sigma_{a,i}+\sum_{g'\neq i}\Sigma_{g',i}\right)+\dfrac{\chi_i}{k_{eff}}\nu\Sigma_{f,i}\right) & i=j\\ \dfrac{1}{D_i}\left(\dfrac{\chi_i}{k_{eff}}\nu\Sigma_{f,j}+\Sigma_{i,j}\right) & i\neq j\end{cases}$$

Assume $\left\{B_g^2, g=1,G\right\}$ are the eigenvalues of the matrix $\hat{\mathrm{B}}$, $\hat{R}$ and $\hat{R}^{-1}$ are the corresponding eigenmode and inverse eigenmode respectively, i.e. $\hat{R}=\left(\vec{\varphi}_1,\vec{\varphi}_2,\cdots,\vec{\varphi}_G\right)$ and $\vec{\varphi}_g$ is an eigenvector of matrix $\hat{\mathrm{B}}$ belonging to the eigenvalue B_g^2. So $\hat{\mathrm{B}}=\hat{R}^{-1}\cdot\hat{\Lambda}\cdot\hat{R}$ and $\hat{\Lambda}=diag\left(B_g^2\right)$.

2.1.3 Expression of Pin-cell Fluxes

Introducing a vector $\vec{\psi}=\left\{\psi_g, g=1,G\right\}$ and let:

$$\vec{\psi}=\hat{R}^{-1}\cdot\vec{\phi} \text{ or } \vec{\phi}=\hat{R}\cdot\vec{\psi} \tag{2.5}$$

Bringing Eq. (2.5) into (2.4) and multiplying it by $\hat{R}^{-1}$ results in:

$$\nabla^2\vec{\psi}+\Lambda\cdot\vec{\psi}=0 \text{ or } \nabla^2\psi_g+B_g^2\cdot\psi_g=0 \tag{2.6}$$

So far, the multi-group diffusion equation has been transferred into a group of buckling equations. The solution (called buckling fluxes or flux modes throughout the paper) corresponding to the eigenvalue B_g of the above equation is:

$$\psi_g=\int_0^{2\pi}A_g(\alpha)e^{iB_g\vec{n}_\alpha\cdot\vec{r}}d\alpha$$

Here B_g can be either a real ($B_g^2 \geq 0$) or an imaginary ($B_g^2 < 0$).

If "*M*" certain directions are chosen, this solution can be expressed using Fourier expansion as:

$$\psi_g = \sum_m \left\{ A_{g,m}^+ \cos\left(B_g r \cos\left(\theta - \alpha_m\right)\right) + A_{g,m}^- \sin\left(B_g r \cos\left(\theta - \alpha_m\right)\right) \right\} \tag{2.7a}$$

or

$$\psi_g = \sum_m \left\{ A_{g,m}^+ \cos\left(B_g \left(x\cos\left(\alpha_m\right) + y\sin\left(\alpha_m\right)\right)\right) + A_{g,m}^- \sin\left(B_g \left(x\cos\left(\alpha_m\right) + y\sin\left(\alpha_m\right)\right)\right) \right\} \tag{2.7b}$$

Up to this point, the calculation of the pin homogeneous fluxes is turned into the buckling flux calculation, or the computation of the above expansion coefficients. These coefficients can be expressed differently using different nodal boundary conditions. Based on results [19][20], nodal surface and corner fluxes are chosen as the boundary conditions in this work. Other choices for surface boundary conditions can be surface net currents and surface partial currents, with the later shown to be the most accurate choice [31]. From the nodal average cross-sections and 3D nodal solution, the detailed process and equations to derive the expansion coefficients ($A_{g,m}^{\pm}$) and the computation of the pin wise homogeneous fluxes are described in Appendix A.

2.2 Challenge to Handle Control Rod History Effect

2.2.1 Introduction

In the conventional method, only the homogeneous pin-cell cross-sections and fluxes are computed, and these data doesn't contain any information regarding the change of assembly heterogeneity. Therefore the conventional method completely relies on the pin power form factors to capture the heterogeneities in the assembly.

As mentioned above, in order to get the pin power form factors at different conditions, they are normally formulated as a function of the local state parameters through tabulation [21] or parameterization [22]. By including control rod insertion status in the local state parameters, an instantaneous effect of control rod insertion on the pin power distribution can be well recovered through the pin power form factors.

Figure 2.2 shows the change of the pin power distribution after control rod insertion in a standard Westinghouse 17x17 4.95wt% UO_2 assembly. Due to the strong absorption of the control rod material, the insertion of the control rod causes depression of the local fluxes, i.e. control rod shadow that makes the pin-cell powers around the control rod fingers (or blade in BWR) significantly below the others. Comparing with the unrodded fuel assembly, the heterogeneity of the rodded assembly in pin-cell flux and power distribution is significantly different.

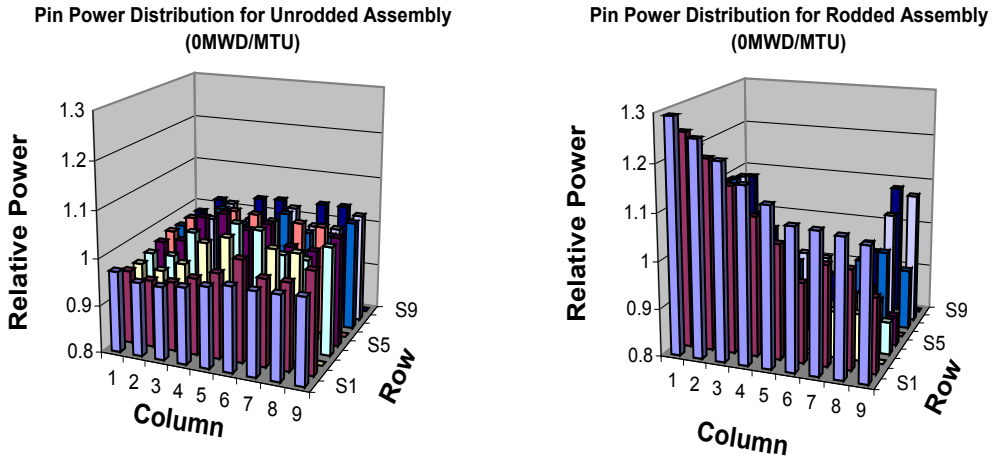

Figure 2.2 Illustration of control rod impact on the pin power distribution

As mentioned above, the conventional pin power recovery method can easily capture the instantaneous effect of control rod insertion on the pin power distribution by using the pin power form factors for the rodded situation. Those pin power form factors can be simply produced through lattice code single assembly calculation with control rod insertion.

However, once the fuel assembly is exposed in the core with control rod inserted during operation, the above control rod impact on the pin power will accumulate with the fuel depletion. This accumulation may lead to significant difference of the pin power distribution from the one where the control rods are inserted instantaneously. To demonstrate the control rod history effect, a 17x17 fuel assembly was modeled and 4 cases were setup and calculated with Westinghouse lattice code PARAGON [23]. They are:

- Case 1: Regular depletion calculation without control rod insertion.

- Case 2: Read the history data file generated from Case 1 at each burnup step, and perform branch calculation with control rod insertion. Therefore, no control rod history effect is taken into account in the results.
- Case 3: Regular single assembly depletion calculation with control rod insertion.
- Case 4: Read the history data file generated from Case 3 at each burnup step, and perform branch calculation with control rod removed.

As an example, the pin power distributions at 22GWD/MTU are displayed in the Figure 2.3 and Figure 2.4. In the figures, "CR/GT" is the control rod or guide thimble location, and "IT" is the location for the instrumentation. The "CR history" is defined as the pin power difference in % between cases with and without consideration of the control rod history. Comparing case 2 and case 3 results, Figure 2.3 shows that, if the control rod history effect is ignored, there is a maximum over 7% error in the pin power prediction for rodded case. Similarly, if the control rod is inserted in the fuel assembly from the beginning and removed at 22GWD/MTU, without consideration of the control rod history effect, the conventional pin power method may give as much as about 7% error in the pin power result as shown in Figure 2.4.

		1	2	3	4	5	6	7	8	9
Case 1	1	0.977	0.964	0.964	0.971	0.978	0.986	0.985	0.985	0.988
Case 2		1.296	1.259	1.22	1.177	1.142	1.105	1.103	1.098	1.085
Case 3		1.201	1.173	1.147	1.119	1.097	1.072	1.07	1.065	1.057
CR history		-7.33	-6.83	-5.98	-4.93	-3.94	-2.99	-2.99	-3.01	-2.58
	2	0.964	0.95	0.955	0.968	0.982	1.014	0.986	0.986	1.013
		1.259	1.209	1.158	1.096	1.041	0.964	1.012	1.01	0.954
		1.173	1.134	1.101	1.062	1.028	0.983	1.007	1.004	0.974
		-6.83	-6.20	-4.92	-3.10	-1.25	1.97	-0.49	-0.59	2.10
	3	0.964	0.955	0.973	1.017	1.03	CR/GT	1.024	1.022	CR/GT
		1.22	1.158	1.067	0.945	0.89		0.894	0.895	
		1.147	1.101	1.045	0.972	0.934		0.932	0.932	
		-5.98	-4.92	-2.06	2.86	4.94		4.25	4.13	
	4	0.971	0.968	1.017	CR/GT	1.041	1.037	0.999	0.996	1.025
		1.177	1.096	0.945		0.836	0.84	0.92	0.927	0.866
		1.119	1.062	0.972		0.893	0.893	0.941	0.945	0.909
		-4.93	-3.10	2.86		6.82	6.31	2.28	1.94	4.97
	5	0.978	0.982	1.03	1.041	1.017	1.036	1.001	0.999	1.028
		1.142	1.041	0.89	0.836	0.872	0.84	0.914	0.92	0.861
		1.097	1.028	0.934	0.893	0.911	0.892	0.936	0.94	0.905
		-3.94	-1.25	4.94	6.82	4.47	6.19	2.41	2.17	5.11
	6	0.986	1.014	CR/GT	1.037	1.036	CR/GT	1.031	1.029	CR/GT
		1.105	0.964		0.84	0.84		0.862	0.87	
		1.072	0.983		0.893	0.892		0.907	0.913	
		-2.99	1.97		6.31	6.19		5.22	4.94	
	7	0.985	0.986	1.024	0.999	1.001	1.031	1	0.999	1.029
		1.103	1.012	0.894	0.92	0.914	0.862	0.941	0.965	0.926
		1.07	1.007	0.932	0.941	0.936	0.907	0.957	0.975	0.957
		-2.99	-0.49	4.25	2.28	2.41	5.22	1.70	1.04	3.35
	8	0.985	0.986	1.022	0.996	0.999	1.029	0.999	1	1.03
		1.098	1.01	0.895	0.927	0.92	0.87	0.965	1.035	1.079
		1.065	1.004	0.932	0.945	0.94	0.913	0.975	1.025	1.068
		-3.01	-0.59	4.13	1.94	2.17	4.94	1.04	-0.97	-1.02
	9	0.988	1.013	CR/GT	1.025	1.028	CR/GT	1.029	1.03	IT
		1.085	0.954		0.866	0.861		0.926	1.079	
		1.057	0.974		0.909	0.905		0.957	1.068	
		-2.58	2.10		4.97	5.11		3.35	-1.02	

Figure 2.3 Comparison of pin power for rodded assembly with and without consideration of control rod history at 22GWD/MTU

		1	2	3	4	5	6	7	8	9
Case 1	1	0.977	0.964	0.964	0.971	0.978	0.986	0.985	0.985	0.988
Case 4		0.912	0.904	0.91	0.924	0.939	0.955	0.953	0.954	0.96
CR history		-6.65	-6.22	-5.60	-4.84	-3.99	-3.14	-3.25	-3.15	-2.83
	2	0.964	0.95	0.955	0.968	0.982	1.014	0.986	0.986	1.013
		0.904	0.896	0.91	0.937	0.967	1.03	0.976	0.976	1.03
		-6.22	-5.68	-4.71	-3.20	-1.53	1.58	-1.01	-1.01	1.68
	3	0.964	0.955	0.973	1.017	1.03		1.024	1.022	
		0.91	0.91	0.95	1.041	1.074	CR/GT	1.059	1.056	CR/GT
		-5.60	-4.71	-2.36	2.36	4.27		3.42	3.33	
	4	0.971	0.968	1.017		1.041	1.037	0.999	0.996	1.025
		0.924	0.937	1.041	CR/GT	1.101	1.088	1.01	1.005	1.065
		-4.84	-3.20	2.36		5.76	4.92	1.10	0.90	3.90
	5	0.978	0.982	1.03	1.041	1.017	1.036	1.001	0.999	1.028
		0.939	0.967	1.074	1.101	1.049	1.085	1.012	1.008	1.069
		-3.99	-1.53	4.27	5.76	3.15	4.73	1.10	0.90	3.99
	6	0.986	1.014		1.037	1.036		1.031	1.029	
		0.955	1.03	CR/GT	1.088	1.085	CR/GT	1.071	1.067	CR/GT
		-3.14	1.58		4.92	4.73		3.88	3.69	
	7	0.985	0.986	1.024	0.999	1.001	1.031	1	0.999	1.029
		0.953	0.976	1.059	1.01	1.012	1.071	1.005	0.998	1.054
		-3.25	-1.01	3.42	1.10	1.10	3.88	0.50	-0.10	2.43
	8	0.985	0.986	1.022	0.996	0.999	1.029	0.999	1	1.03
		0.954	0.976	1.056	1.005	1.008	1.067	0.998	0.981	1.01
		-3.15	-1.01	3.33	0.90	0.90	3.69	-0.10	-1.90	-1.94
	9	0.988	1.013		1.025	1.028		1.029	1.03	
		0.96	1.03	CR/GT	1.065	1.069	CR/GT	1.054	1.01	IT
		-2.83	1.68		3.90	3.99		2.43	-1.94	

Figure 2.4 Comparison of pin power for unrodded assembly with and without consideration of control rod history at 22GWD/MTU

Clearly, the control rod history effect has to be considered properly in order to correctly predict the pin powers. Unfortunately, it is not an easy task for the conventional pin power method to consider the control rod history effect since the control rod insertion and withdrawal is not pre-defined. Consequently, it is difficult for the method to pre-generate the pin power form factors to match the real control rod insertion history.

2.2.2 Implicit Pin Power Form Factor Generation Method

The conventional pin power recovery method has been used for core design and safety calculations since 1980's [16][17][18][31]. For a traditional PWR, since it is essentially operated with all control rods out (ARO), the actual fuel depletion in the core doesn't make a considerable difference in the heterogeneity of the assembly as compared to the reference condition adopted in the pin power form factors generation. Past experience [24] has confirmed that the conventional method is highly accurate for the traditional PWR core designs. Because of that, until the recent Westinghouse AP1000 design, there has been no effort made to improve the pin power form factor generation for the conventional pin power method in PWR application.

In contrast, BWR is using the control blades in operation to control both reactivity and axial power shape. As discussed earlier, the insertion of the control blade creates significant change of the assembly heterogeneity. The control blade history effect has been a challenge to the conventional pin power recovery method. As a prevailing approach in the conventional method, to account for the control blade history effect, the form factors are implicitly generated as a function of the control rod history parameters [36]. For convenience, the term "control rod" is used in this paper for both standard PWR finger type control rod and BWR control blades.

Typically, these history cases involve a straight-forward lattice depletion calculation with the control rod continually inserted from selected fuel burnup steps. This implicit pin

power form factor generation method can give an accurate pin power distribution if the real history of the modeled fuel is close to the pre-calculated scenarios. However, in the real plant operation, a fuel assembly may experience control rod history with multiple periods of control rod insertion and withdrawal, with the same control rod or different control rod type (in the different cycles). Therefore, it is difficult to simulate actual control rod history scenarios where repeated insertion and withdrawal of control rods in different computational nodes in the nodal core model can be expected. Therefore, in the Westinghouse BWR methodology, fixed (pre-determined) sequences of rod insertion and withdrawal are simulated in the control rod history lattice calculations. The problem with this approach is that the actual sequence of control insertions and withdrawals cannot be determined a priori for a given cycle, but is, at best, known only to some partial extent. Besides, application of these control rod history data sets requires very complicated procedures in the simulator to track and combine various periods of rod insertion and withdrawal in each node that has been subjected to such sequences. Experience has shown that this method can induce unphysical spikes (or dips) in the axial profile of pin powers within partially rodded nodes.

2.2.3 Next Generation Methodology (NGM)

In the conventional modulation method, the nodal average history, e.g. control rod history (CRH) and boron history (BH), is usually used as parameter to represent the heterogeneity factors (e.g. pin power form factors). It is well-recognized that the challenge to the conventional modulation method comes from the missing detailed

information, i.e. pin-by-pin data, since the pin heterogeneous history is not followed and applied in the conventional pin power methodology.

In contrast to the modulation method, more and more studies are focused to the next generation methodology (NGM), i.e. fine mesh (pin-by-pin) calculation. Through the fine mesh transport or diffusion calculation, the pin power can be obtained as the total product of pin kappa-fission and flux. These fine mesh calculations can be done for each node (so called embedded method) or on full-core base. Regardless embedded or directly full-core fine mesh calculation method, it is necessary to perform the pin-by-pin isotopic tracking so that the real history is precisely represented in the pin cross-sections.

As a future method, the fine mesh calculation along with pin-by-pin isotopic tracking involves a large amount of calculations and requires tremendous computer memory and data storage. However, current available computing power precludes implementation of such a scheme in standard core design applications.

2.2.4 Sub-Zoning Method

In view of computer power barriers, a compromised approach, “sub-zoning method” was proposed and developed by Studsvik [34] and implemented in the Simulate code [33]. Instead of the direct pin-by-pin calculation in NGM, the sub-zoning method divides each radial mesh into several sub-meshes, e.g. 5x5, so that, within each sub-mesh, the flux and power distribution is relatively flat, the heterogeneity change during the depletion can be ignored and the conventional pin power recovery method is applicable. Compared with

the conventional pin power recovery method, the sub-zoning method shifts the focus from pin power calculation to the generation of sub-mesh results.

With the sub-zoning method, the accuracy of fuel rod power depends on how the sub-meshes are defined and whether sub-zoning results are good enough. In order to overcome the computer power barrier and avoid tracking a large number of isotopes on sub-mesh level while keeping the high quality of the global solution, the proposed method performs two levels depletion calculation. One is following the average history in detail through explicitly tracking a large amount of isotopes on regular radial mesh (node) basis. The second is tracking the minimum selected isotopes for each sub-mesh and using the sub-mesh data to derive the intra-assembly distribution.

According to the papers [34][35], the preliminary results demonstrate that sub-zoning method improves the fuel rod power prediction considerably when 5x5 sub-zoning is adopted for BWR assembly.

However, there are several issues to solve before the sub-zoning method can be actually used in the routine core design calculations. Compared to NGM, the sub-zoning method takes significantly less cpu time. Even though, due to an extra calculation step, the sub-mesh cross-section and flux/power computations take more than affordable time and cannot meet the practical speed requirements for regular design application.

In addition, to get highly accurate fuel rod powers, the assembly (or regular radial node) should be divided in such way that the heterogeneity within each sub-mesh will not be

impacted by the actual depletion history. For BWR assembly, it is easy to satisfy the requirement by specifying the outmost layer of pins as a sub-mesh because the control rod (control blade) is inserted in the outside of the assembly. For PWR assembly, since the control rod fingers spread throughout the assembly, the sub-mesh has to be small enough to cover the influence of each individual control rod finger. The more sub-meshes the calculation adopts, the less efficient it will be. Also the structure of sub-mesh has to be pre-defined during the assembly cross-section data generation, which cannot change afterwards. Considering the method limitations along with the implementation difficulties, it is too early to conclude whether the sub-zoning method is practical or not.

2.3 Concluding remarks

This chapter presented the conventional pin power methodology and the Next Generation Methods. The efforts made to capture the history effects of the control rod insertion on the pin power distribution were also discussed. However, due to the fundamental weakness without explicitly following the real history of each pin and impractical computing power requirements, neither the extension to the conventional method nor NGM are considered as an available option to meet the needs of the design calculation for both BWR and the new type of PWR (e.g. AP1000). A complete review of the pin power recovery methodology was carried out and a new Pseudo Pin-by-Pin Calculation (P3C) methodology has been developed.

CHAPTER 3

DEVELOPMENT OF PSUEDO PIN-BY-PIN CALCULATION (P3C) METHODOLOGY – PIN CROSS-SECTION REPRESENTATION

3.1 Introduction

In a nodal code, widely used in the core design calculation, the average homogeneous history of each node can be easily followed by extensive depletion calculations. In general, the node-wise homogeneous results represent the true history of the node. To obtain the detail fuel rod power distribution from the node-wise results through the pin power recovery, the pin power form factors are used to give the heterogeneity information of the fuel assembly. Since the power form factors are the only heterogeneity data and the real pin history is not involved in those factors computation, the performance of the conventional method strongly relies on the pin power form factors generation. As discussed in the Chapter 2, the challenge to the conventional pin power method is how to obtain precise pin power form factors that match the real pin history. When the control rod is inserted in the core during the operation, the pre-generation of actual pin power form factors becomes very difficult because the information of when, where, and how long the control rods are inserted in the core is not available in advance of the reactor operation.

Clearly, following each pin and making use of the real pin history is the way to fundamentally resolve the issue, and there is no doubt that NGM (direct pin-by-pin calculation) is the ideal method to compute the pin power distribution. However, the ideal method involves fine mesh transport calculations, either embedded or direct 3D full-core. In addition, the NGM method requires pin-wise isotopic tracking so as to get the precise pin-by-pin cross-sections. As mentioned earlier, both calculations are time consuming and require tremendous memory and disk space. The computing power currently available still precludes the implementation of these schemes in standard core design applications.

Even though the NGM is away from the standard core design use, the fundamental idea of using pin cross-sections and fluxes for heterogeneous assemblies in combination with the tracking of individual fuel rod depletion histories is exploited in the pseudo pin-by-pin calculation (P3C) methodology. Only the manner in which the pin average parameters are obtained is different from the direct (transport) approach.

The following two Chapters will derive the pin power expression of the P3C methodology, and the detailed discussion on the calculation method for the pin cross-sections and pin fluxes will be presented respectively.

3.2 Derivation of P3C Pin Power Equation

For any pin k, the pin power could be computed directly in terms of pin average cross-sections $\kappa\Sigma_{f,g}^{k,Het}$ and fluxes $\phi_g^{k,Het}$ for the heterogeneous assembly over all energy groups

(g):

$$P^k = \sum_g \kappa\Sigma_{f,g}^{k,Het} \cdot \phi_g^{k,Het} \tag{3.1}$$

In the conventional pin power method, the pin power is expressed as:

$$P^k = \sum_g \left(\kappa\Sigma_{f,g}^{k,Hom} \cdot \phi_g^{k,Hom}\right) \cdot p_g^k \tag{3.2}$$

Comparing above equations one can find that the pin power form factor actually represents two heterogeneity factors, i.e. pin cross-section form factor (ζ_g^k) and pin flux form factor (f_g^k), and $p_g^k = \zeta_g^k \cdot f_g^k$.

Here $\zeta_g^k = \dfrac{\kappa\Sigma_{f,g}^{k,Het}}{\kappa\Sigma_{f,g}^{k,Hom}}$ and $f_g^k = \dfrac{\phi_{f,g}^{k,Het}}{\phi_{f,g}^{k,Hom}}$. Bringing the definitions into Eq.(3.2) yields:

$$P^k = \sum_g \left(\kappa\Sigma_{f,g}^{k,Hom} \cdot \phi_g^{k,Hom}\right) \cdot \left(\zeta_g^k \cdot f_g^k\right) = \sum_g \kappa\Sigma_{f,g}^{k,Het} \cdot \left(\phi_g^{k,Hom} \cdot f_g^k\right) \tag{3.3}$$

Eq.(3.2) looks similar to Eq.(3.3), except that the homogeneous pin cross-section is replaced by heterogeneous one and the pin power form factor is substituted for by the flux form factor. However, these substitutions completely change the calculation scheme. The conventional method is based on the nodal average information only, while the P3C method follows the history of each individual pin in order to construct the pin cross-sections.

Further investigation on the pin power errors shown in the Figure 2.3 and Figure 2.4 found that the control rod history leads to the pin-wise thermal kappa-fission deviation up to over 10% while the pin thermal flux distribution deviation is about 4% in opposite direction at 22GWD/MTU.

Recalling the homogeneous flux calculation in the conventional method, to reconstruct pin power, it is important for P3C method to have accurate pin cross-sections and flux form factors.

The details of the pin cross-section calculation are presented in the following sections. For convenience, the notation "*ref*" is used in the following discussion to represent data at reference condition and "*refh*" stands for the data with the reference depletion history.

3.3 Pin Cross-Section Calculation

For pin "k", the macroscopic cross-section is the total contribution of all isotopes. So the macroscopic cross-section of the reaction "x" is expressed as:

$$\Sigma_{x,g}^{k} = \sum_{i} N_i^k \sigma_{x,g}^{i,k} = \sum_{i} N_i^{k,ref} \sigma_{x,g}^{i,k} + \sum_{i} \left(N_i^k - N_i^{k,ref} \right) \sigma_{x,g}^{i,k} \tag{3.4}$$

Where $N_i^{k,ref}$ is the number density of isotope "*i*" inside the pin with the reference depletion history, while N_i^k is the actual value of the isotope in the pin. $\sigma_{x,g}^{i,k}$ is the effective microscopic cross-section of energy group "*g*" for isotope "*i*" in the pin, and

$$\sigma_{x,g}^{i,k} = \frac{\int_g \sigma_x^{i,k}(E)\phi^k(E)dE}{\int_g \phi^k(E)dE} = \frac{\int_g \sigma_x^{i,k}(E)\phi^k(E)dE}{\bar{\phi}_g^k} \tag{3.5}$$

$\bar{\phi}_g^k$ is the average pin flux of group "g". Definitely, the difference in the neutron spectrum $\phi(E)$ will give a different group microscopic cross-section for each isotope. Therefore the first term of the right hand side of Eq.(3.4) includes the instantaneous spectrum impact on the pin macroscopic cross-section.

The second term of the right hand side of Eq.(3.4) is the correction accounting for the effect of number density deviation for both instantaneous and the historic reason. For a pin, the change of composition may be caused by

- The status change of the movable component (or inserts), for instance, control rod insertion, removal of discrete burnable absorbers, etc.

- Change of actinides and fission products burnout or buildup due to off-reference depletion history, i.e. history effect.

Therefore, the second term in the right hand side of Eq.(3.4) can be re-written as:

$$\begin{aligned}\sum_i \left(N_i^k - N_i^{k,ref}\right)\sigma_{x,g}^{i,k} &= \sum_{i\in Comp}\left(N_i^k - N_i^{k,ref}\right)\sigma_{x,g}^{i,k} + \sum_{i\in depl}\left(N_i^k - N_i^{k,ref}\right)\sigma_{x,g}^{i,k} \\ &= W^{Comp}\cdot\Delta\Sigma_{x,g}^{Comp} + \Delta\Sigma_{x,g}^{hist}\end{aligned} \tag{3.6}$$

W^{Comp} is the component insertion status; 1 is for inserted or differentiated from the origin, 0 for non-insertion or staying at original status. And the Eq.(3.4) becomes:

$$\Sigma_{x,g}^{k} = \Sigma_{x,g}^{k,free} + W^{Comp} \cdot \Delta\Sigma_{x,g}^{Comp} + \Delta\Sigma_{x,g}^{hist} \tag{3.7}$$

Here $\Sigma_{x,g}^{k,free}$ is the "free" pin-cell macroscopic cross-section, in which the contribution from control rod insertion or discrete BP extraction is removed.

3.3.1 Instantaneous Spectrum Correction to Pin-cell Cross-section

The "free" cross-section defined by Eq.(3.7) is not really free of everything, and it actually varies with the isotopic microscopic cross-sections. Indeed, Eq.(3.4) shows that two factors will determine the value of $\Sigma_{x,g}^{k,free}$, i.e. the behavior of the microscopic cross-section and the local neutron spectrum.

Approximately, the combination of fission spectrum, $1/E$ spectrum, and Maxwell spectrum is used to generate the basic fine group library for a light water reactor (LWR) [25]. Fission spectrum represents the neutron spectrum at high energy range (820eV~) where fission neutron source dominates. In this energy range, if the material composition is defined, the fission spectrum can be considered as unchangeable, $1/E$ slowing-down spectrum represents the neutron energy distribution in the resonance energy range (0.125eV~820eV) with extremely low resonance absorber concentrations (infinite dilute). Maxwell thermal spectrum describes the neutron energy distribution in the thermal energy range (~0.125eV) and the spectrum changes with the media temperature (*T*) as:

$$\phi(E) = \frac{E}{kT}\exp\left(-E/kT\right)$$

However, the actual neutron spectrum in each pin region differs from the above approximation, and varies with the local condition, such as material composition, temperature, geometry. The effect of the material composition and the pin geometry has been taken into account during lattice code calculation through resonance integration, while the impact of local actual fuel and moderator temperatures and density effect couldn't be considered at the lattice code level since they are not available yet. This information is obtained by the thermal hydraulic calculation of the simulator code during feedback iteration based on the power distribution through 3D core calculation. Unfortunately, the simulator code uses few-group diffusion calculation and cannot give the detailed neutron spectrum. Parameterization is widely used to represent the neutron spectrum as well as the microscopic cross-sections at different conditions and the group effective cross-sections are tabulated or fitted as a function of these spectrum parameters [21][22][26].

Theoretically, the isotopic microscopic cross-section $\sigma_x(E,T)$ is a function of neutron energy and media temperature (or Doppler temperature for the isotopes within the pellet). It has been widely accepted that resonance integral can be expressed as a function of square root of fuel Doppler temperature, and quadratic interpolation is normally applied in the lattice code to obtain the isotopic resonance integral based on the actual Doppler temperature of the fuel pellet [27].

In addition to the Doppler temperature, the neutron spectrum is also affected by the moderator condition due to the moderation. In another words, the neutron spectrum in the

low energy range strongly depends on the state of the moderator (e.g. moderator temperature).

During the past several years, according to the general behavior of the isotopic cross-sections discussed above, Westinghouse has successfully developed a new cross-section representation model [2] and implemented it in the new ANC code for constructing the nodal average feedback-free cross-sections. In the new representation model, Westinghouse uses spectrum index (S) and moderator and fuel temperatures (T_m, T_f) as spectrum parameters. Thus, the nodal average feedback-free cross-section for the reaction "x" is expressed as a function of local state parameters, i.e.

$$\Sigma_{x,g}^{free} = \Sigma_{x,g}^{free}(E,\{p\}) = \Sigma_{x,g}^{free,ref}(E)\cdot F_{x,g}(E,\{p\})$$

Here $(\{p\}) = (S, T_m, T_f)$ are the local state parameters, and $F_{x,g}$ is the spectrum correction factor to cross-section type "*x*" of group "*g*". In the spectrum parameters, spectrum index represents the general hardness of the neutron spectrum while the Doppler and the moderator temperatures are expected to characterize the detail local state impact on the effective cross-sections.

By extending the Westinghouse cross-section representation model for nodal cross-sections to pins (with spatial smearing over pin regions), for the reaction type (*x*), one can compute the spectrum corrected macroscopic feedback-free cross-section of a pin (k) as:

$$\Sigma_{x,g}^{k,free} = \Sigma_{x,g}^{k,free}(E^k,\{p\}) = \Sigma_{x,g}^{k,free,ref}(E^k)\cdot F_{x,g}^{k}(E^k,\{p\}) \qquad (3.8)$$

where E^k is the local burnup of the pin (k), $\{p\}$ is the set of instantaneous nodal average state parameters as discussed above.

3.3.2 Movable Component Correction

The movable component effect on the pin macroscopic cross-sections can be computed through tracking the composition of the component, and explicitly calculating the total isotopic contribution of each component pin as:

$$\Delta\Sigma_{x,g}^{k,Comp} = \sum_{i\in Comp}\left(N_i^k - N_i^{k,ref}\right)\sigma_{x,g}^{i,k}$$

This model requires isotopic tracking for each individual component rod, which is not affordable in the current computer condition. Besides, the above model hardly captures the indirect impact of the component on the neighbor pins due to the local leakage change.

Instead, lump effective component corrections to the pin macroscopic cross-sections ($\Delta\Sigma_{x,g}^{k,Comp}$) are directly obtained from component branch calculation by lattice code to represent the component effect.

3.3.3 Pin History Correction

Summarizing the above instantaneous corrections, the pin-cell macroscopic cross-section with the reference fuel depletion history is

$$\Sigma_{x,g}^{k,refh} = \Sigma_{x,g}^{k,free} + W^{Comp} \cdot \Delta\Sigma_{x,g}^{k,Comp} \tag{3.9}$$

Eq.(3.4) can be expressed as:

$$\Sigma_{x,g}^{k} = \Sigma_{x,g}^{k,refh} + \Delta\Sigma_{x,g}^{k,hist} \tag{3.10}$$

where the history correction is derived from the number density deviation of all depletable isotopes inside the pin, i.e.:

$$\Delta\Sigma_{x,g}^{k,hist} = \sum_{i \in depl} \left(N_i^k - N_i^{k,ref} \right) \sigma_{x,g}^{i,k} \tag{3.11}$$

(i) Pin-wise Micro-Depletion Correction Method

Due to the simplification of the depletion chain, the depletion calculation is no longer able to give accurate number densities for the tracked isotopes and the error will accumulate with the fuel exposure time. Therefore, Eq.(3.11) won't provide a correct adjustment to the macroscopic cross-sections even for the tracked isotopes. To overcome this problem, the reference number densities for the tracked isotopes must be recalculated at the reference condition using exactly the same simplified chain so that the error in both reference number densities and the actual number densities due to the simplification would cancel out. Even though, the simplified depletion still needs to calculate the isotopic cross-sections and solve the transmutation for each pin, which significantly increases *cpu* time and memory and is hardly used in the routine core design calculations.

(ii) Spectrum History Correction Model

The following figure displays the typical nuclear transmutation of isotope "C".

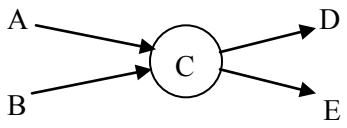

Figure 3.1 Illustration of nuclear transmutation

Here "A" and "B" are the parents of isotope "C" through capture and decay respectively, while the absorption and decay of "C" will respectively produce the daughters "D" and "E". Therefore the transmutation equation of isotope "C" can be written as:

$$\frac{dN^C}{dt} = -\left(\sigma_a^C \phi + \lambda^C\right) \cdot N^C + \lambda^B \cdot N^B + \sigma_\gamma^A \phi \cdot N^A \tag{3.12}$$

If the parents' number densities are known, since the decay constants never change, the following factors will impact the behavior of the isotope "C" transmutation.

1) The effective capture rate ($\sigma_\gamma^A \phi$) of the parent "A", which impacts the build-up of "C"

2) The effective absorption rate ($\sigma_a^C \phi$) of "C", which impacts its burn-out and the daughter generation ratio of "D" to "E".

Generally speaking, the variation of isotope transmutation is caused by both effective isotopic cross-sections and local flux level.

In view of the importance of each individual isotope in respect of the contribution to the total macroscopic cross-section, it is noticed that the majority of the depletion history correction to the macroscopic cross-sections is from the actinides, especially the transmutation of ^{238}U to plutonium chain.

Without the parent isotopes and decay constants, the transmutation equation of ^{238}U is simplified from Eq.(3.12) as:

$$\frac{dN^8}{dt} = -\sigma_a^8 \phi \cdot N^8 = -R_a^8 \cdot N^8$$

The above equation clearly shows that the transmutation rate of ^{238}U to plutonium through ^{239}Np depends on the effective absorption rate of ^{238}U. For a typical 2-group model in thermal reactor physics, the ^{238}U effective absorption cross-section ratio of fast to thermal group is significantly larger than that of ^{235}U. And, as the main thermal fission source, ^{235}U has large thermal absorption and fission cross-sections. Thus, to get the same total fission rate (fuel, i.e. ^{235}U, burn-out rate) from a thermal reactor, the harder spectrum gives a higher transmutation rate of ^{238}U. In other words, the changes of actinides number densities from the pin depletion are determined by the history of the spectrum (so called "spectrum history") that the pin has experienced.

Moreover, for a certain total flux, the hard spectrum means a high flux level in the high energy range. As a result the pin spectrum history can be represented by the time integration of flux high energy range, i.e.

$$SH = \Phi = \int_0^t \phi^{high} dt$$

Based on the above discussion, an alternative method has been developed in P3C to avoid tracking isotopic number densities on pin level, which assumes that the pin nuclide number densities can be functionalized in terms of the pin spectrum history, Φ^k, that is:

$$\begin{aligned} N_i^k &= N_i^k\left(E^k, \Phi^k\right) \\ N_i^{k,ref} &= N_i^k\left(E^k, \Phi^{k,ref}\right) \end{aligned}$$

Therefore, Eq.(3.9) can be re-written as:

$$\begin{aligned} \Sigma_{x,g}^k &= \Sigma_{x,g}^{k,refh}\left(E^k, \{p\}, \Phi^{k,ref}\right) \cdot \left(1 + \frac{\sum_i \left(N_i^k\left(E^k, \Phi^k\right) - N_i^k\left(E^k, \Phi^{k,ref}\right)\right)\sigma_{x,g}^{k,i}}{\Sigma_{x,g}^{k,refh}\left(E^k, \{p\}, \Phi^{k,ref}\right)}\right) \\ &= \Sigma_{x,g}^{k,refh}\left(E^k, \{p\}, \Phi^{k,ref}\right) \cdot \left(1 + \frac{\Delta\Sigma_{x,g}^{k,hist}\left(E^k, \Phi^k\right)}{\Sigma_{x,g}^{k,refh}\left(E^k, \{p\}, \Phi^{k,ref}\right)}\right) \\ &= \Sigma_{x,g}^{k,refh}\left(E^k, \{p\}, \Phi^{k,ref}\right) \cdot \left(1 + H_{x,g}^k\left(E^k\right) \cdot \Delta\Phi^k\right) \end{aligned} \tag{3.14}$$

where $\Sigma_{x,g}^{k,refh}\left(E^k, \{p\}, \Phi^{k,ref}\right)$ is the pin macroscopic cross-section (x) at the burnup E^k and the local spectrum condition $\{p\}$ with the reference depletion history. The spectrum history correction coefficient $H_{x,g}^k\left(E^k\right)$ is defined as

$$H_{x,g}^k\left(E^k\right) = \frac{\Sigma_{x,g}^k\left(E^k, \Phi^k\right) - \Sigma_{x,g}^{k,refh}\left(E^k, \Phi^{k,ref}\right)}{\Sigma_{x,g}^{k,refh}\left(E^k, \Phi^{k,ref}\right)} \Big/ \Delta\Phi^k \tag{3.15}$$

and

$$\Delta\Phi^k = \frac{\Phi^k - \Phi^{k,ref}}{\Phi^{k,ref}}$$

The spectrum history correction coefficient for each pin is pre-generated based on lattice calculation results.

3.4 Improvement of Pin Cross-Section Representation

The above pin cross-section representation consists of three models, i.e. spectrum correction model, component (insertion) correction model, and the spectrum history correction model. As discussed earlier, for a given assembly, the pin cross-section is determined by the pin composition and the local neutron spectrum, and the pin composition may change due to:

- Instantaneous component insertion
- Depletion history
- Instantaneous moderator composition change

Eq.(3.9) and Eq.(3.10) clearly show that the effects of the instantaneous component insertion and depletion history are explicitly modeled in the above representation while the impact of the moderator composition is implicitly captured by the local spectrum correction. Therefore, the spectrum correction model covers both direct (moderator composition) and indirect (neutron spectrum) impact to the pin cross-sections. The test results given later do reveal the weakness of the above cross-section method, especially

for non-fuel pin and in cases with large moderator density change. In view of the results, the pin cross-section representation method has been improved by explicitly applying the moderator correction.

3.4.1 Updated Feedback Free Pin Cross-Section

With the improvement, the spectrum correction model in the pin cross-section representation should express the local spectrum impact only. In other words, the moderator composition effect should be separated from the feedback free pin cross-sections. Focusing on the spectrum correction, for each case with reference fuel depletion history, the feedback free pin cross-section is updated as:

$$\begin{aligned}\Sigma_{x,g}^{k,free} &= \sum_i N_i^{k,ref}\sigma_{x,g}^{k,i} \\ &= \Sigma_{x,g}^{k,refh} - W^{Comp}\cdot\Delta\Sigma_{x,g}^{k,Comp} - \Delta\Sigma_{x,g}^{k,W} - \Delta\Sigma_{x,g}^{k,B}\end{aligned} \tag{3.16}$$

Here $\Delta\Sigma_{x,g}^{k,W}$ and $\Delta\Sigma_{x,g}^{k,B}$ are moderator correction terms for water density and soluble boron, respectively.

The final pin cross-section can be expressed by bringing this definition to the pin cross-section representation model (3.14) and (3.9).

The feedback free pin cross-sections are corresponding to the reference fuel and moderator compositions. With fixed composition in the each pin, the spectrum correction term $F_{x,g}^k\left(E^k,\{p\}\right)$ truly represents the local neutron spectrum impact on the pin cross-

section.

3.4.2 Moderator Correction to Pin Cross-Section

As shown in Eq.(3.16), the moderator correction consists of water correction and soluble boron correction to the pin cross-sections. The water correction accounts for the change of the total amount of water, caused by either deviation of water density or water displacement. The soluble boron correction takes into account the total amount of soluble B10 contribution to the pin absorptions. Thus the correction terms can be written as:

$$\begin{aligned} \Delta\Sigma_{x,g}^{k,W} &= C^{W}\left(\rho\cdot w^{k}-\rho^{ref}\cdot w^{k,ref}\right)\cdot\sigma_{x,g}^{k,W} \\ \Delta\Sigma_{a,g}^{k,B} &= C^{B}\cdot\rho\cdot w^{w}\cdot ppm\cdot\sigma_{a,g}^{k,B} \end{aligned} \tag{3.17}$$

Where ρ is the moderator density, $\sigma_{x,g}^{k,W}$ and $\sigma_{a,g}^{k,B}$ are respectively the water and soluble boron microscopic cross-sections. C^{W} and C^{B} are the factors to convert the water density and boron concentration (in ppm) to the number densities.

w^{k} is the pin wet fraction defined as the volume ratio of moderator region to the total pin, i.e. $w^{k}=\frac{A_{\mathrm{mod}}^{k}}{A^{k}}$. With the consideration of component insertion, the wet fraction is computed as

$$w^{k}=w^{k,ref}+W^{CRtyp}\cdot\Delta w^{k,CRtyp}+W^{BP}\cdot\Delta w^{k,BP} \tag{3.18}$$

and

$$w^{k,ref} = \frac{A_{wet}^{k,ref}}{A_{cell}^{k}}$$

$$\Delta w^{k,CRtyp} = -\frac{A_{CRtyp}^{k}}{A_{cell}^{k}}$$

$$\Delta w^{k,BP} = +\frac{A_{BP}^{k}}{A_{cell}^{k}}$$

The pin wet fraction may change due to the water displacement caused by any removable component insertion or withdrawal.

3.5 Qualification of Pin Cross-Section Calculation

The pin cross-section model is qualified by the cross-section comparison between the model prediction and direct lattice code calculation at the same condition. A unit test code, PINCHECK, was developed for this purpose.

In each lattice calculation at a given condition, the lattice code (PARAGON) writes both assembly conditions (spectrum index, moderator and fuel temperatures, etc.) and calculation results to the Lattice Result File (LRF). As illustrated in Figure 3.2, PINCHECK reads the state parameters from the LRF, and uses the pin cross-section representation model to compute pin-by-pin cross-sections based on the local condition and pin history.

The pin cross-section comparisons have been made for a wide range of fuel assemblies, including different lattice types, ^{235}U enrichments, and burnable absorber (BA) types at

different conditions. The pin thermal absorption and kappa-fission with respectively initial and updated pin cross-section models for a 17x17 non-BA fuel assembly are compared. The enrichment of the fuel assembly is 4.1wt% ^{235}U, and the configuration of the assembly is shown in Figure 3.3.

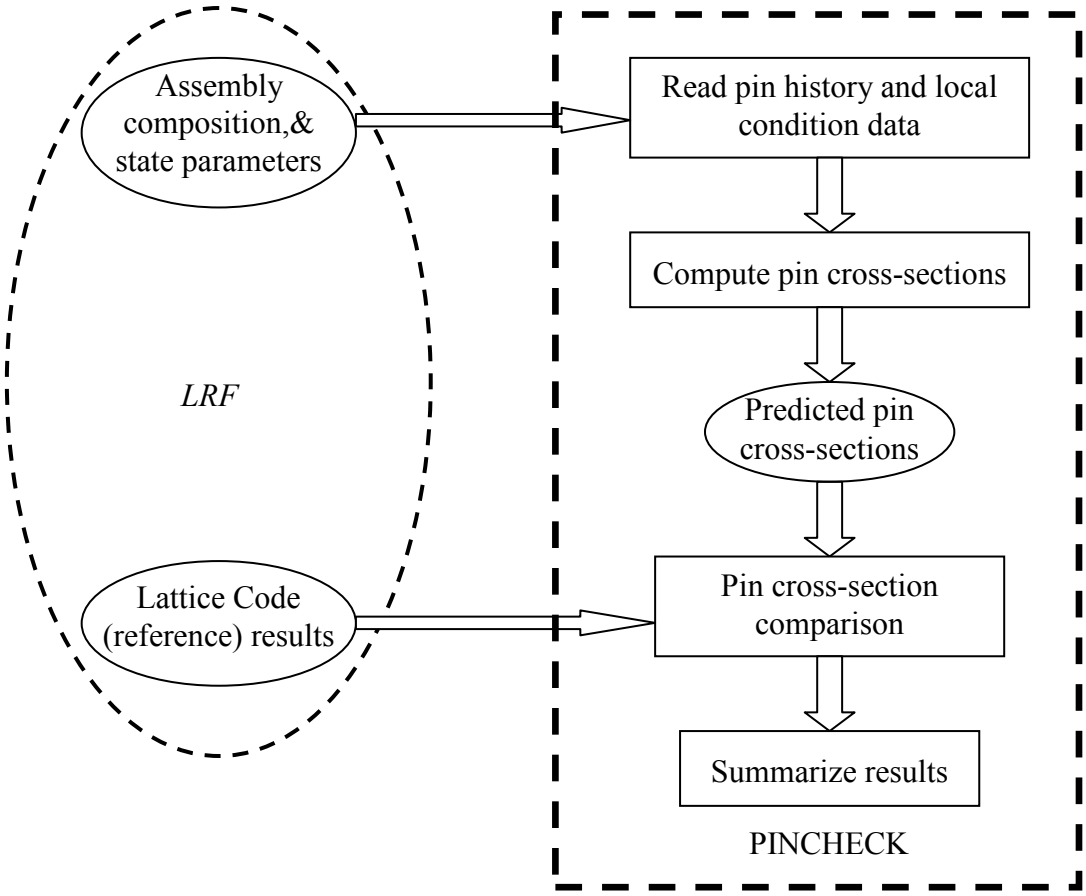

Figure 3.2 Illustration of pin cross-section qualification with PINCHECK

The comparisons of pin cross-sections for an unrodded case at 0.15GWD/MTU with the moderator and fuel temperatures, 598.6K and 847.48K respectively, are provided in Figure 3.4 to Figure 3.7. The relative errors are the prediction against the reference, which are obtained from the lattice code transport calculations.

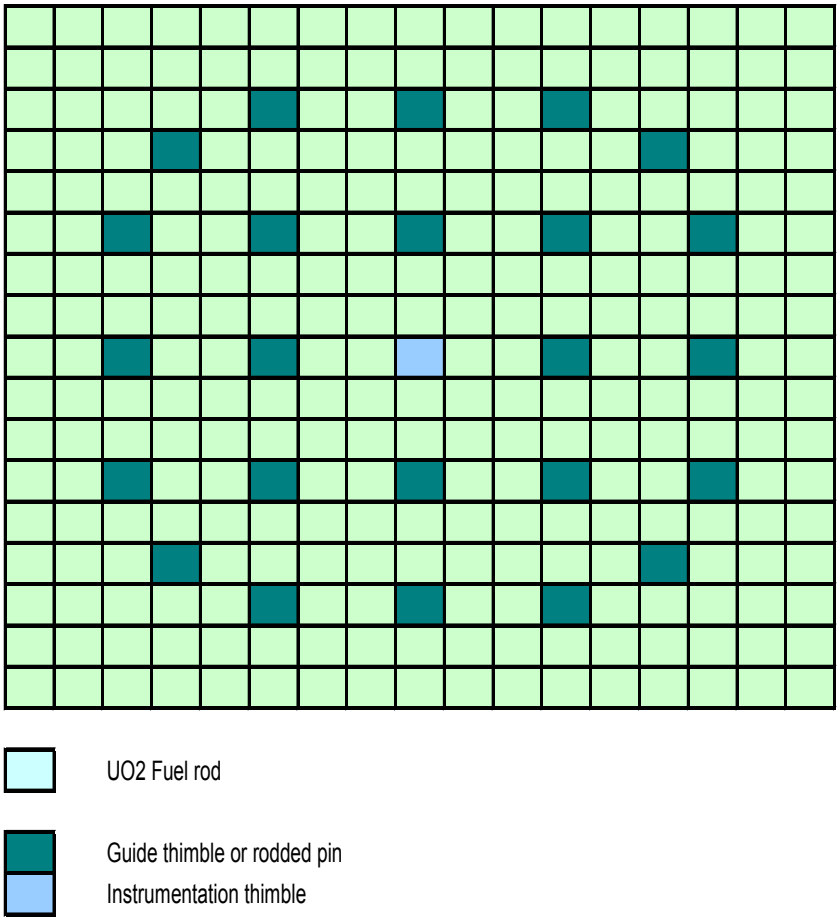

Figure 3.3 Configuration of modeled fuel assembly

0.1112 0.1114 -0.21								
0.1107 0.1110 -0.25	0.1103 0.1106 -0.24		Prediction Reference Error (%)					
0.1107 0.1110 -0.25	0.1105 0.1107 -0.19	0.1108 0.1111 -0.23						
0.1108 0.1111 -0.24	0.1108 0.1111 -0.23	0.1122 0.1124 -0.17	0.0138 0.0143 -3.33					
0.1110 0.1112 -0.19	0.1110 0.1113 -0.23	0.1124 0.1126 -0.17	0.1125 0.1127 -0.16	0.1116 0.1118 -0.21				
0.1111 0.1114 -0.23	0.1121 0.1123 -0.17	0.0138 0.0143 -3.34	0.1126 0.1128 -0.16	0.1125 0.1127 -0.16	0.0138 0.0143 -3.33			
0.1110 0.1113 -0.23	0.1111 0.1113 -0.22	0.1123 0.1125 -0.17	0.1113 0.1115 -0.21	0.1113 0.1115 -0.21	0.1124 0.1126 -0.16	0.1113 0.1115 -0.21		
0.1111 0.1113 -0.18	0.1111 0.1113 -0.22	0.1123 0.1125 -0.17	0.1112 0.1114 -0.22	0.1113 0.1115 -0.21	0.1124 0.1126 -0.16	0.1113 0.1115 -0.21	0.1113 0.1115 -0.21	
0.1111 0.1114 -0.23	0.1121 0.1123 -0.17	0.0138 0.0143 -3.34	0.1123 0.1125 -0.17	0.1124 0.1126 -0.16	0.0138 0.0143 -3.33	0.1124 0.1126 -0.16	0.1124 0.1126 -0.16	0.0137 0.0142 -3.35

Figure 3.4 Comparison of pin thermal absorptions ($\Sigma_{a,2}$) with initial representation model

15.21 15.21 -0.02							
15.16 15.16 -0.01	15.11 15.11 0.00		Prediction Reference Error (%)				
15.15 15.15 0.00	15.12 15.12 0.01	15.16 15.16 0.02					
15.17 15.17 0.00	15.17 15.17 0.01	15.35 15.35 0.02					
15.19 15.19 0.01	15.19 15.19 0.02	15.37 15.37 0.03	15.39 15.39 0.03	15.26 15.26 0.03			
15.22 15.22 0.01	15.33 15.33 0.02		15.40 15.40 0.03	15.39 15.39 0.03			
15.20 15.20 0.01	15.19 15.19 0.02	15.37 15.37 0.03	15.22 15.22 0.03	15.22 15.22 0.03	15.38 15.38 0.03	15.22 15.22 0.03	
15.20 15.20 0.01	15.19 15.19 0.02	15.36 15.36 0.03	15.21 15.21 0.03	15.21 15.21 0.03	15.37 15.37 0.03	15.21 15.21 0.03	15.21 15.21 0.03
15.22 15.22 0.01	15.33 15.33 0.02		15.37 15.37 0.03	15.37 15.37 0.03		15.37 15.37 0.03	15.37 15.37 0.03

Figure 3.5 Comparison of pin thermal kappa-fissions ($\kappa\Sigma_{f,2}$) with initial representation model

0.1114 0.1114 0.02								
0.1110 0.1110 0.02	0.1107 0.1106 0.02		Prediction Reference Error (%)					
0.1110 0.1110 0.02	0.1108 0.1107 0.03	0.1111 0.1111 0.03						
0.1111 0.1111 0.02	0.1111 0.1111 0.03	0.1125 0.1124 0.03	0.0143 0.0143 0.14					
0.1113 0.1112 0.02	0.1113 0.1113 0.03	0.1126 0.1126 0.03	0.1128 0.1127 0.03	0.1119 0.1118 0.03				
0.1115 0.1114 0.02	0.1123 0.1123 0.03	0.0143 0.0143 0.14	0.1128 0.1128 0.03	0.1128 0.1127 0.03	0.0143 0.0143 0.15			
0.1113 0.1113 0.02	0.1113 0.1113 0.03	0.1126 0.1125 0.03	0.1115 0.1115 0.03	0.1115 0.1115 0.03	0.1126 0.1126 0.03	0.1115 0.1115 0.03		
0.1113 0.1113 0.02	0.1113 0.1113 0.03	0.1125 0.1125 0.03	0.1115 0.1114 0.03	0.1115 0.1115 0.03	0.1126 0.1126 0.03	0.1115 0.1115 0.03	0.1115 0.1115 0.03	
0.1115 0.1114 0.02	0.1123 0.1123 0.03	0.0143 0.0143 0.15	0.1126 0.1125 0.03	0.1126 0.1126 0.03	0.0143 0.0143 0.15	0.1126 0.1126 0.03	0.1126 0.1126 0.03	0.0142 0.0142 0.15

Figure 3.6 Comparison of pin thermal absorptions ($\Sigma_{a,2}$) with updated representation model

15.21 15.21 0.00								
15.16 15.16 0.00	15.11 15.11 0.01		Prediction Reference Error (%)					
15.15 15.15 0.00	15.12 15.12 0.01	15.17 15.16 0.01						
15.17 15.17 0.00	15.17 15.17 0.01	15.36 15.35 0.01						
15.19 15.19 0.00	15.19 15.19 0.01	15.37 15.37 0.01	15.39 15.39 0.01	15.26 15.26 0.01				
15.22 15.22 0.00	15.34 15.33 0.01		15.40 15.40 0.01	15.39 15.39 0.01				
15.20 15.20 0.00	15.19 15.19 0.01	15.37 15.37 0.01	15.22 15.22 0.01	15.22 15.22 0.01	15.38 15.38 0.01	15.22 15.22 0.01		
15.20 15.20 0.00	15.19 15.19 0.01	15.36 15.36 0.01	15.21 15.21 0.01	15.22 15.21 0.01	15.37 15.37 0.01	15.22 15.21 0.01	15.21 15.21 0.01	
15.22 15.22 0.00	15.34 15.33 0.01		15.37 15.37 0.01	15.37 15.37 0.01		15.37 15.37 0.01	15.37 15.37 0.01	

Figure 3.7 Comparison of pin thermal kappa-fissions ($\kappa\Sigma_{f,2}$) with updated representation model

The results show that the updated pin cross-section model provides consistently good agreement for both fuel and non-fuel pins. As compared to the initial model, the updated one makes a remarkable improvement in the pin thermal absorption, especially for the non-fuel pins, while the change of the representation model shows no impact on the pin kappa-fission.

To confirm the accuracy of the spectrum history correction model, the cross-section

comparisons for the off-nominal depletion cases were investigated. Among those cases, attention was particularly focused on the cases with the control rod insertion, including different insertion (or withdrawal) scenarios. Figure 3.8 to Figure 3.10 list the comparisons of pin cross-sections, thermal absorption, thermal kappa-fission, and down-scattering, between the updated representation model and reference at 20GWD/MTU for an octant assembly. In this case, the fuel is depleted with the insertion of Ag-In-Cd control rods while the spectrum history correction coefficients are generated with B_4C rods. The results clearly show that the spectrum history correction model is robust and the spectrum history correction coefficients truly capture the impact of the pin depletion history.

3.6 Concluding remarks

This chapter provided the general description of the P3C methodology for pin power calculation. The key step of the P3C methodology, the pin cross-section representation model, was derived and discussed in detail. The pin cross-section representation model takes into account both instantaneous spectrum effect as well as the spectrum history effect. The results for the cross-section model verification confirmed that the model constructs the pin cross-sections in good agreement with the reference that was directly obtained from pin-wise transport calculation at the same condition.

0.1362 0.1361 0.05								
0.1370 0.1369 0.05	0.1373 0.1372 0.05		Prediction Reference Error (%)					
0.1382 0.1381 0.05	0.1385 0.1384 0.05	0.1403 0.1402 0.05						
0.1393 0.1392 0.05	0.1395 0.1394 0.05	0.1415 0.1415 -0.03	0.8713 0.8712 0.01					
0.1404 0.1403 0.04	0.1413 0.1413 -0.03	0.1430 0.1431 -0.11	0.1438 0.1440 -0.17	0.1444 0.1448 -0.25				
0.1405 0.1405 -0.02	0.1417 0.1418 -0.08	0.8687 0.8686 0.01	0.1423 0.1425 -0.18	0.1428 0.1431 -0.23	0.8661 0.8660 0.02			
0.1413 0.1414 -0.07	0.1419 0.1421 -0.14	0.1423 0.1425 -0.17	0.1435 0.1438 -0.25	0.1436 0.1441 -0.29	0.1424 0.1428 -0.27	0.1428 0.1433 -0.34		
0.1414 0.1416 -0.1	0.1419 0.1422 -0.16	0.1422 0.1425 -0.18	0.1434 0.1438 -0.27	0.1435 0.144 -0.31	0.1423 0.1427 -0.27	0.1425 0.1429 -0.34	0.1407 0.1412 -0.35	
0.1409 0.1411 -0.1	0.1418 0.1420 -0.14	0.8670 0.8669 0.01	0.1424 0.1428 -0.23	0.1425 0.1429 -0.26	0.8680 0.8678 0.02	0.1420 0.1424 -0.3	0.1409 0.1414 -0.35	0.0154 0.0153 0.73

Figure 3.8 Comparison of pin thermal absorptions ($\Sigma_{a,2}$) at 20GWD/MTU with Ag-In-Cd rod insertion

15.09 15.09 0.00								
15.27 15.27 0.00	15.40 15.40 0.00		Prediction Reference Error (%)					
15.52 15.52 0.00	15.67 15.67 0.00	16.08 16.08 0.00						
15.76 15.76 0.00	15.94 15.94 -0.01	16.50 16.51 -0.08						
15.99 15.99 -0.01	16.28 16.29 -0.08	16.82 16.85 -0.16	17.08 17.11 -0.23	17.09 17.14 -0.30				
16.1 16.11 -0.08	16.51 16.54 -0.13		16.92 16.96 -0.24	17.00 17.05 -0.29				
16.22 16.24 -0.13	16.46 16.49 -0.19	16.79 16.83 -0.23	16.89 16.95 -0.31	16.94 17 -0.35	16.92 16.97 -0.32	16.80 16.86 -0.40		
16.25 16.28 -0.16	16.48 16.51 -0.22	16.78 16.83 -0.24	16.88 16.93 -0.33	16.92 16.98 -0.37	16.89 16.94 -0.33	16.70 16.77 -0.41	16.37 16.44 -0.42	
16.23 16.25 -0.16	16.58 16.61 -0.20		16.91 16.95 -0.29	16.93 16.99 -0.32		16.73 16.79 -0.36	16.32 16.39 -0.43	

Figure 3.9 Comparison of pin thermal kappa-fission ($\kappa\Sigma_{f,2}$) at 20GWD/MTU with Ag-In-Cd rod insertion

0.0127 0.0127 0.00								
0.0125 0.0125 0.00	0.0122 0.0122 0.00		Prediction Reference Error (%)					
0.0122 0.0122 0.00	0.0119 0.0119 0.00	0.0113 0.0113 0.00						
0.0119 0.0119 0.00	0.0115 0.0115 0.00	0.0104 0.0104 0.01	0.0071 0.0071 0.08					
0.0117 0.0117 0.00	0.0111 0.0111 0.01	0.0099 0.0099 0.02	0.0093 0.0093 0.02	0.0096 0.0096 0.03				
0.0114 0.0114 0.01	0.0105 0.0105 0.02	0.0072 0.0071 0.11	0.0093 0.0093 0.03	0.0093 0.0093 0.03	0.0068 0.0068 0.19			
0.0114 0.0114 0.02	0.0108 0.0108 0.02	0.0098 0.0098 0.03	0.0100 0.0100 0.03	0.0099 0.0099 0.04	0.0096 0.0096 0.04	0.0102 0.0102 0.05		
0.0113 0.0113 0.02	0.0108 0.0108 0.03	0.0099 0.0099 0.03	0.0100 0.0100 0.04	0.0100 0.0100 0.04	0.0096 0.0096 0.04	0.0104 0.0104 0.05	0.0108 0.0108 0.05	
0.0113 0.0113 0.02	0.0104 0.0104 0.03	0.0072 0.0072 0.14	0.0095 0.0095 0.03	0.0095 0.0095 0.04	0.0070 0.0070 0.21	0.0101 0.0101 0.05	0.0112 0.0112 0.05	0.0169 0.0168 0.39

Figure 3.10 Comparison of pin down-scattering ($\Sigma_{1\to 2}$) at 20GWD/MTU with Ag-In-Cd rod insertion

CHAPTER 4

PIN FLUX RECONSTRUCTION IN P3C METHODOLOGY

4.1 Introduction

The Pseudo Pin-by-pin Calculation (P3C) method directly calculates the pin powers through the computation of the pin heterogeneous cross-sections and fluxes. The pin cross-section representation model has been discussed in Chapter 3. Regardless of the pin exposure experiences, once all the pin cross-sections are available, the solution of pin-by-pin fluxes becomes decisive to meet the given nodal boundary conditions (surface/corner fluxes or/and currents, core reactivity).

Ideally, like in the embedded methods, the pin flux distribution within each node can be generated by performing pin-by-pin transport or diffusion calculations. However, a more efficient alternative option, the modulation method, is used in P3C methodology instead of direction pin-by-pin calculation due to the computer power limitation.

In this chapter, the modulation method is presented. And the key of the P3C methodology, the on-fly flux form factors are derived and discussed.

4.2 Pin Flux Calculation

In the modulation method, the pin (k) heterogeneous flux is expressed as:

$$\phi_g^{k,het} = \phi_g^{k,\hom} \cdot f_g^k$$

Here the homogeneous pin flux distribution is obtained using the method described in section 2.1.2. Therefore, the pin flux form factor (f_g^k) becomes the key to derive the heterogeneous flux. This pin flux form factor should represent the real local condition and the depletion history of the pin.

4.2.1 Pin Flux Form Factor with Reference History

For a given fuel assembly with reference depletion history, the pin flux form factors vary with the local spectrum condition. For instance, a high boron concentration leads to less variation of the thermal flux form factor among the pin cells. Similar to the pin cell cross-sections, the spectrum correction $F_{\phi,g}^k\left(E,\{p\}\right)$ is applied to the pin flux form factor to take into account the spectrum effect on the pin flux form factors as:

$$f_g^{k,refh,NoComp} = f_g^{k,ref} \cdot F_{\phi,g}^k\left(E,\{p\}\right) \tag{4.1}$$

In addition to the spectrum effect, the insertion of components like control rod or withdrawal of discrete burnable absorbers induces much larger heterogeneity change, which develops significant pin flux form factor variations. This impact is captured by the utilization of component correction. For a fuel node with status change due to component

insertion, the following expression provides the pin flux form factor with all instantaneous correction:

$$f_g^{k,refh} = f_g^{k,refh,NoComp} + W^{Comp} \cdot \Delta f_g^{k,Comp} \tag{4.2}$$

Here $\Delta f_g^{k,Comp}$ is the component correction factor to the pin factor. Obviously, Eq.(4.2) and Eq. (3.9) respectively generate the pin cell cross-sections and flux form factors at the same conditions and with the reference depletion history.

4.2.2 Pin Flux Form Factor with Actual Depletion History

Eq.(4.2) provides the pin flux form factors with all instantaneous corrections, and these form factors match the pin cross-sections given by Eq.(3.9). Obviously, due to the difference of the pin cross-sections (from the reference history to the real history), the pin fluxes will be re-distributed. In other words, the change of the pin macroscopic cross-sections will change the pin flux form factors.

With the pin cross-sections, the pin flux distribution can be obtained through solving diffusion or transport equations for each node. As discussed in the Section 2.2.3, the iterative process to solve diffusion or transport equations takes significant amount of *CPU* time, which is not affordable in the regular core design and safety analysis calculations. Alternatively, to obtain the flux form factor for the actual depletion history while avoiding solving diffusion or transport equations, it is necessary to utilize a rational approximation.

In 2-group calculations, the diffusion equations for each pin can be written as:

$$\begin{aligned} -D_1^k \nabla^2 \phi_1^k + \left(\Sigma_{a,1}^k + \Sigma_{1\to 2}^k\right)\phi_1^k &= \frac{1}{k_{eff}}\left(\nu\Sigma_{f,1}^k \phi_1^k + \nu\Sigma_{f,2}^k \phi_2^k\right) \\ -D_2^k \nabla^2 \phi_2^k + \Sigma_{a,2}^k \phi_2^k &= \Sigma_{1\to 2}^k \phi_1^k \end{aligned} \tag{4.3}$$

It is noticed that the diffusion length in the first group is long enough compared to the pin pitch so that the impact of the pin cross-section change on the first group flux distribution is negligible. Besides, in the thermal reactor, only about 5% of total energy is released from the first group fission. Investigation did show that the pin history variation has very minor impact on the pin first energy group flux distribution. Based on this observation, it is acceptable to simplify the calculation by ignoring the first group flux form factor difference due to the change of pin cross-sections caused by the different depletion history, i.e. $f_1^k = f_1^{k,refh}$ or $\phi_1^k = \phi_1^{k,refh}$.

So the last piece of the puzzle of getting the actual flux distribution is to derive the thermal group flux form factor for each pin.

Model 1: Ignore the Change of Pin-wise Thermal Neutron Leakage

Re-writing the Eq.(4.3) for thermal group by using the buckling, there is

$$D_2^k \left(B^k\right)^2 \phi_2^k + \Sigma_{a,2}^k \phi_2^k = \Sigma_{1\to 2}^k \phi_1^k$$

If the total thermal neutron leakage ($D_2^k \left(B^k\right)^2 \phi_2^k$) of each fuel pin is not affected by the

pin depletion history (or the change of the pin cross-sections), the correlation of the pin thermal fluxes at reference and actual depletion history can be built as:

$$\Sigma_{1\to 2}^{k}\phi_1^k - \Sigma_{a,2}^{k}\phi_2^k = \Sigma_{1\to 2}^{k,refh}\phi_1^{k,refh} - \Sigma_{a,2}^{k,refh}\phi_2^{k,refh} \tag{4.4}$$

Dividing Eq.(4.4) by ϕ_1^k and noticing $\phi_1^k = \phi_1^{k,refh}$ yields:

$$\frac{\phi_2^k}{\phi_1^k} = \frac{\Sigma_{1\to 2}^{k} - \Sigma_{1\to 2}^{k,refh}}{\Sigma_{a,2}^{k}} + \frac{\Sigma_{a,2}^{k,refh}}{\Sigma_{a,2}^{k}} \cdot \frac{\phi_2^{k,refh}}{\phi_1^{k,refh}} \tag{4.5a}$$

If the pin leakage rate ($D_2^k\left(B^k\right)^2$) of thermal neutron remains unchanged, then

$$\Sigma_{1\to 2}^{k}\frac{\phi_1^k}{\phi_2^k} - \Sigma_{a,2}^{k} = \Sigma_{1\to 2}^{k,refh}\frac{\phi_1^{k,refh}}{\phi_2^{k,refh}} - \Sigma_{a,2}^{k,refh}$$

Hence

$$\frac{\phi_1^k}{\phi_2^k} = \frac{\Sigma_{1\to 2}^{k,refh}}{\Sigma_{1\to 2}^{k}}\frac{\phi_1^{k,refh}}{\phi_2^{k,refh}} + \frac{\Sigma_{a,2}^{k} - \Sigma_{a,2}^{k,refh}}{\Sigma_{1\to 2}^{k}} \tag{4.5b}$$

Both expressions of Eq.(4.5a) and (4.5b) were evaluated by verifying the data of Case 1 against Case 4, and Case 2 against Case 3 described in Chapter 2. A discrepancy over 4% in thermal group pin flux was given by both models as compared to lattice code results. This means that the change of the leakage caused by the difference in the depletion history cannot be ignored.

Model II: Spectrum Index Approach

To keep the neutron balance, the change of the pin cross-section will lead to change of the local neutron spectrum and the neutron leakage. From the thermal group diffusion equation, the pin spectrum index *S* (the flux ratio of the epithermal to thermal group) can be derived as:

$$S^k = \frac{\phi_1^k}{\phi_2^k} = \frac{D_2^k \left(B^k\right)^2 + \Sigma_{a,2}^k}{\Sigma_{1\to 2}^k} \tag{4.6}$$

As mentioned above, the pin neutron leakage rate ($D_2^k \left(B^k\right)^2$) depends on the pin cross-sections, or $D_2^k \left(B^k\right)^2 = L^k \left(\Sigma_x^k\right)$. Here "$\Sigma_x^k$" is the representative of pin cross-sections. Therefore, Eq.(4.6) can be re-written as:

$$S^k = \frac{L^k \left(\Sigma_x^k\right) + \Sigma_{a,2}^k}{\Sigma_{1\to 2}^k} = \delta^k \left(\Sigma_x^k\right) \tag{4.7}$$

For the sample fuel assembly mentioned in Chapter 3, Figure 4.1 to Figure 4.4 show that the spectrum index (SI) changing with the representative (Σ_x^k) of the pin cross-sections for both corner pin and the pin next to the guide thimble (GT) at burnups of 18GWD/MTU and 42GWD/MTU, respectively.

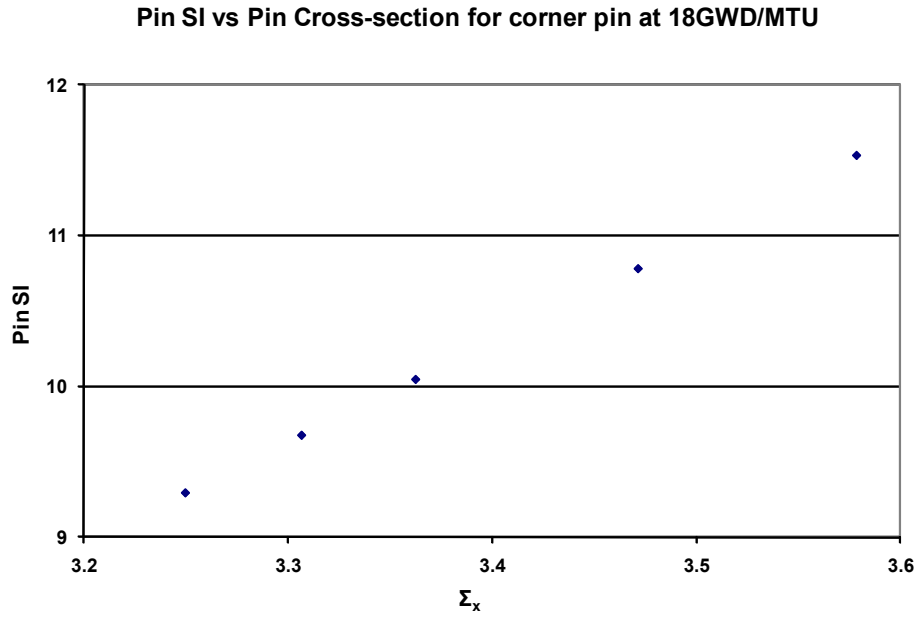

Figure 4.1 Spectrum index changes with pin cross-sections for corner pin at 18GWD/MTU

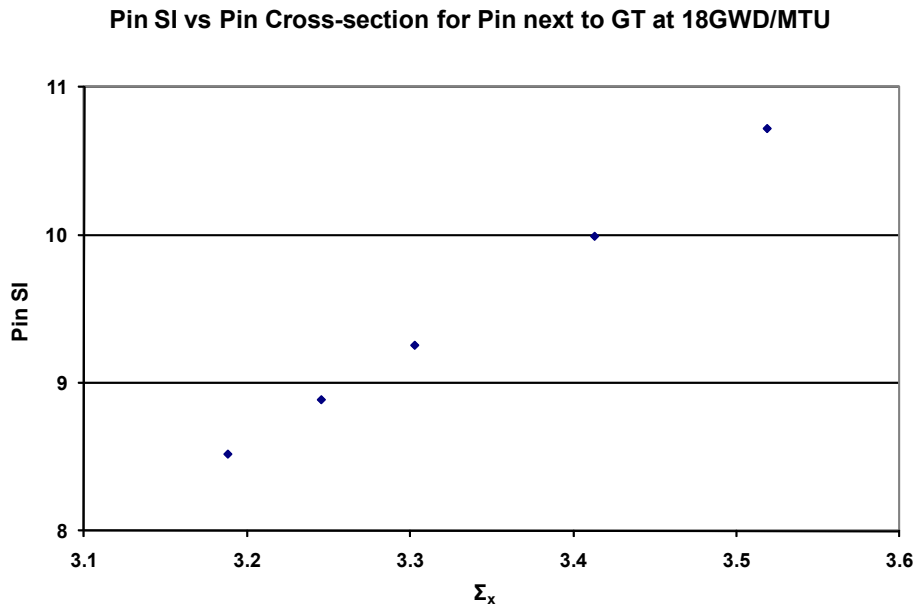

Figure 4.2 Spectrum index changes with pin cross-sections for pin next to guide thimble at 18GWD/MTU

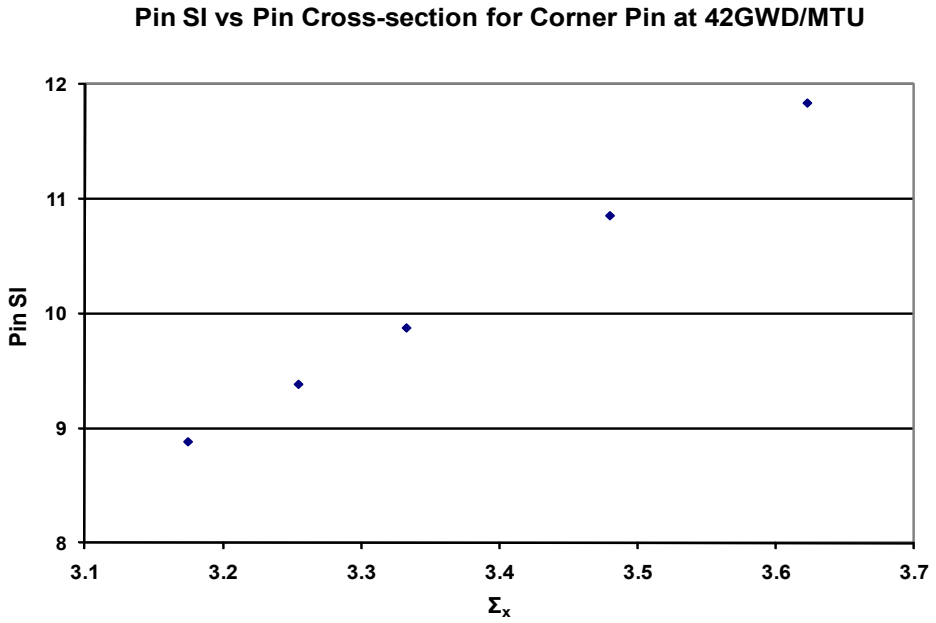

Figure 4.3 Spectrum index changes with pin cross-sections for corner pin at 42GWD/MTU

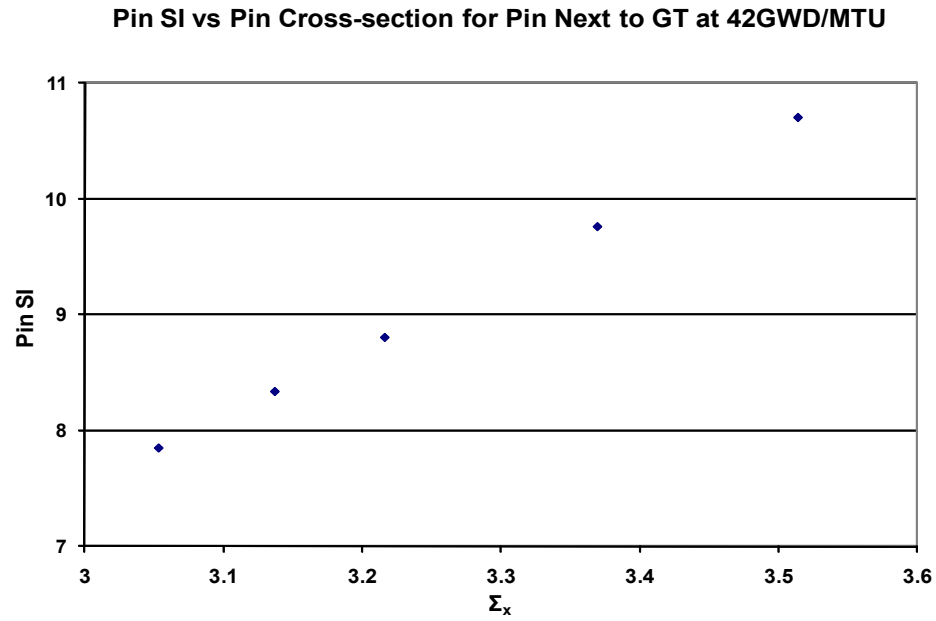

Figure 4.4 Spectrum index changes with pin cross-sections for pin next to guide thimble at 42GWD/MTU

From the figures, along with more extensive investigation, a reasonable approximation was developed. That is, for a fuel assembly at a given burnup state, the actual spectrum index of each pin can be adjusted from the reference value based on the spectrum history impact on the pin cross-sections.

$$\frac{\delta^k\left(\Sigma_x^{k,refh}\right)}{S^{k,refh}} = \frac{\delta^k\left(\Sigma_x^k\right)}{S^k} \tag{4.8}$$

Therefore:

$$S^k = \frac{\delta^k\left(\Sigma_x^k\right)}{\delta^k\left(\Sigma_x^{k,refh}\right)} \cdot S^{k,refh} = \frac{S^{k,refh}}{F^k\left(\Sigma_x^{k,refh}, \Sigma_x^k\right)}$$

Bringing the definition $S^k = \frac{\phi_1^k}{\phi_2^k} = \frac{f_1^k}{f_2^k} \cdot \frac{\phi_1^{k,Hom}}{\phi_2^{k,Hom}}$ and $S^{k,refh} = \frac{f_1^{k,refh}}{f_2^{k,refh}} \cdot \frac{\phi_1^{k,Hom}}{\phi_2^{k,Hom}}$ into the above correlation, the final pin thermal flux form factor becomes:

$$f_2^k = F^k\left(\Sigma_x^{k,refh}, \Sigma_x^k\right) \cdot f_2^{k,refh} \tag{4.9}$$

4.3 Qualification of Pin Thermal Flux Form Factor

The thermal flux form factor adjustment model was tested explicitly. To qualify the model, it is assumed that the pin cross-sections for both reference and actual depletion history can be well constructed. Therefore, the cross-sections used in this qualification are directly from the lattice calculations. Since the pin cross-section representation model has been discussed and verified in the previous chapter, the above assumption is considered true.

The four cases described in Chapter 2 were analyzed and the results with the control rod insertion history were taken as reference. The comparisons of the pin thermal flux form factors again the references of PARAGON are given in Figure 4.5 and Figure 4.6. The results of "After history correction" were obtained through the spectrum index correction of Eq.(4.9) to the base case, which doesn't have control rod insertion history.

The "Error" shown in the figures is defined as:

$$\varepsilon = \frac{f_2^{k,corr} - f_2^{k,ref}}{f_2^{k,ref}} \times 100\%$$

and $f_2^{k,corr}$ is the result of "After history correction", i.e. predicted using the spectrum index correction model.

The comparison of the results confirms that the correction model that uses the spectrum index approach captures the majority of the control rod history effects on the pin thermal flux form factors and the predicted pin flux form factors are in good agreement with the reference data.

With the pin flux form factors, the heterogeneous pin cross-sections and the homogeneous fluxes, the heterogeneous pin power can be directly computed by Eq.(3.3).

1.390 1.339 1.394 0.312								
1.330 1.288 1.336 0.456	1.262 1.229 1.270 0.593		Case 2 Case 3 After history correction Error (%)					
1.274 1.242 1.282 0.594	1.193 1.171 1.200 0.614	1.081 1.072 1.084 0.262						
1.216 1.194 1.225 0.675	1.117 1.106 1.123 0.529	0.936 0.938 0.929 -0.749						
1.170 1.156 1.179 0.728	1.047 1.045 1.051 0.384	0.867 0.876 0.860 -0.804	0.798 0.813 0.792 -0.705	0.835 0.853 0.836 0.199				
1.128 1.120 1.136 0.682	0.959 0.961 0.956 -0.401		0.806 0.820 0.801 -0.521	0.803 0.819 0.800 -0.391				
1.121 1.115 1.130 0.848	1.011 1.014 1.016 0.568	0.870 0.880 0.867 -0.377	0.892 0.907 0.897 0.606	0.884 0.900 0.890 0.623	0.833 0.847 0.831 -0.352	0.925 0.937 0.930 0.533		
1.114 1.109 1.124 0.864	1.007 1.012 1.013 0.593	0.871 0.881 0.868 -0.344	0.899 0.914 0.905 0.647	0.891 0.907 0.897 0.636	0.844 0.857 0.841 -0.356	0.959 0.968 0.964 0.504	1.057 1.059 1.064 0.629	
1.103 1.099 1.112 0.760	0.947 0.951 0.944 -0.267		0.835 0.848 0.832 -0.285	0.829 0.842 0.826 -0.311		0.921 0.928 0.917 -0.398	1.131 1.126 1.134 0.236	

Figure 4.5 Comparison of pin thermal flux form factors at 22GWD/MTU with CR insertion

0.997 0.949 0.986 -1.136								
0.972 0.930 0.963 -0.889	0.951 0.917 0.945 -0.588		Case 4 Case 1 After history correction Error (%)					
0.964 0.930 0.959 -0.541	0.950 0.925 0.947 -0.235	0.970 0.958 0.968 -0.194						
0.967 0.942 0.965 -0.198	0.962 0.948 0.962 0.036	1.027 1.025 1.016 -1.064						
0.972 0.955 0.972 0.064	0.980 0.974 0.980 0.003	1.045 1.051 1.033 -1.124	1.055 1.073 1.045 -0.917	1.016 1.041 1.021 0.445				
0.981 0.969 0.983 0.181	1.023 1.020 1.014 -0.880		1.043 1.063 1.038 -0.479	1.039 1.062 1.037 -0.185				
0.978 0.967 0.981 0.314	0.982 0.982 0.984 0.262	1.028 1.038 1.022 -0.573	0.988 1.007 0.997 0.847	0.988 1.010 0.999 1.022	1.033 1.052 1.032 -0.126	0.993 1.008 1.002 0.911		
0.977 0.968 0.981 0.354	0.980 0.981 0.983 0.301	1.026 1.035 1.020 -0.549	0.985 1.002 0.993 0.837	0.986 1.005 0.996 0.964	1.032 1.049 1.030 -0.212	0.996 1.007 1.004 0.805	1.004 1.008 1.013 0.904	
0.982 0.974 0.985 0.319	1.019 1.018 1.012 -0.722		1.026 1.042 1.023 -0.322	1.028 1.046 1.026 -0.223		1.041 1.049 1.037 -0.321	1.053 1.051 1.058 0.513	

Figure 4.6 Comparison of pin thermal flux form factors at 22GWD/MTU without CR insertion

4.4 Concluding Remarks

The P3C methodology for both pin cross-sections and flux calculation have been derived and discussed in Chapter 3 and Chapter 4. Based on the pin cross-section change caused by the different spectrum history, a pin thermal flux form factor adjustment model was developed. The philosophy of P3C methodology and the form factor correction is summarized in Figure 4.7.

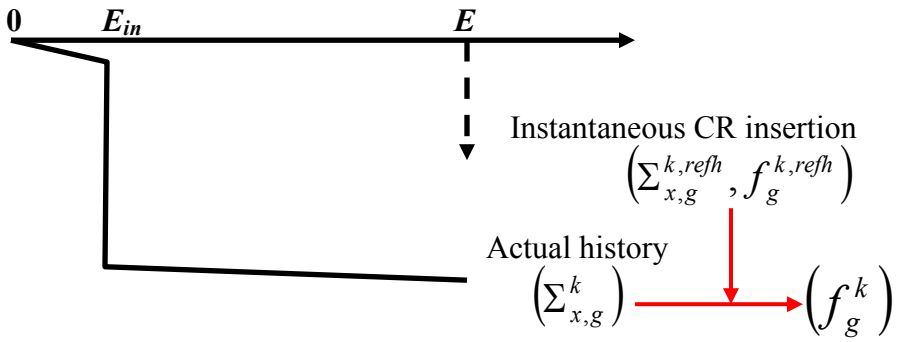

Figure 4.7 Illustration of P3C methodology

The preliminary verification calculations performed for PWR fuel have shown that the pin flux form factors can be accurately predicted by the P3C methodology based on the pin-by-pin cross-sections.

CHAPTER 5

QUALIFICATION OF P3C METHODOLOGY FOR PWR PIN POWER RECOVERY

5.1 Introduction

NEXUS/ANC9 [29], as shown in Figure 1.1, has been developed at Westinghouse to replace the current APA (ALPHA/PHOENIX-P/ANC8) system. ANC is the PWR core design code developed and maintain by Westinghouse, in which the semi-analytic nodal method is used as the nodal solver. The conventional pin power recovery method was implemented in 1989 [28] to compute the fuel rod power distribution.

A new pin power recovery package has been developed using P3C methodology. The new pin power recovery modules developed in this study were incorporated into ANC9 so that NEXUS/ANC9 can model the reactor operated with control rod insertion and meet the needs of AP1000 design calculations.

Other than the conventional pin power method, the P3C methodology requires pin-by-pin cross-sections and history data. To meet the needs of the new pin power recovery

methodology, NEXUS system was modified to generate and process the pin data and write them to Cell Data (CD) files. ANC9 was also changed to be able to read the pin data from the CD files and to call the new pin power recovery modules in order to generate the pin-by-pin fluxes and power distributions.

Using the updated NEXUS/ANC9 system, several PWR fuels were modeled so as to qualify the P3C methodology.

5.2 Implementation of P3C Methodology in ANC9

Based on the proposed P3C methodology in the previous chapters, a new pin power calculation software package has been developed, which includes the modules for generating nodal corner fluxes, calculating homogeneous flux distribution, calculating pin cross-sections and flux form factors, and computing the pin power distribution. The P3C modules have been implemented in ANC9 to perform the pin power calculation.

Similar to the conventional pin power methodology, the corner flux calculation module obtains the corner fluxes for each node through the nodal coupling as described in Appendix A.2. From the node-wise data, such as nodal average cross-sections, average, surface and corner fluxes, the homogeneous pin flux module computes the response matrix for each node and derives the pin-by-pin homogeneous fluxes. Although the same method is used to calculate the pin homogeneous flux distribution, the calculation module was newly developed in such way that it can be directly applied to multiple energy groups.

Since the P3C methodology constructs the pin cross-sections based on the local spectrum conditions and pin history data, such as pin burnups and fast (>1MeV) fluences, the pin history data is explicitly tracked and saved for each node with the application of predictor/corrector method [27].

After completing 3D nodal calculation, ANC9 calls the newly developed P3C modules to generate pin-by-pin fluxes, powers and fast (>1MeV) fluxes. The algorithm of the new pin power calculation in ANC9 is depicted in Figure 5.1.

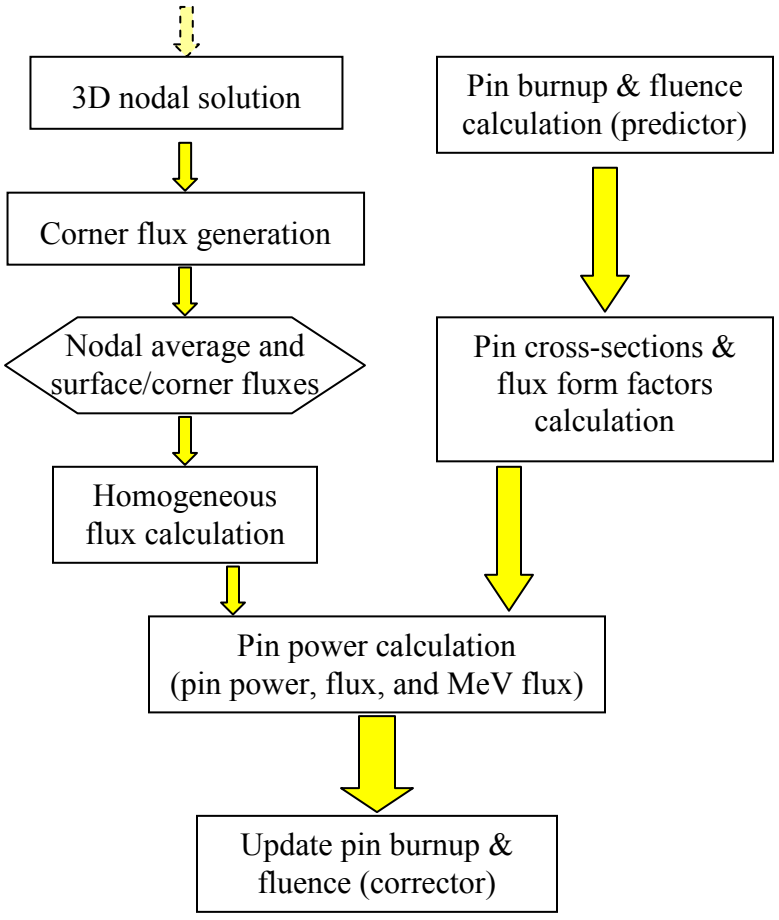

Figure 5.1 Algorithm of new pin power calculation in ANC9

5.3 Qualification of P3C methodology

The evaluation of the new pin power methodology is initially done using single fuel assembly models. The analysis cover different fuel assemblies with different control rod insertion scenarios so as to assess the performance of the P3C methodology in different fuel type with different control rod insertion strategies.

5.3.1 Fuel Assembly Descriptions

The fuel assemblies modeled in the qualification are standard Westinghouse 17x17 fuel assemblies with and without burnable absorbers.

Figure 5.2 shows the configurations, i.e. pin maps, of the non-BA fuel assembly and enrichment 4.95 w/o ^{235}U. The qualification also covers a fuel assembly with 168-IFBA rods, a fuel assembly with the combination of IFBA and WABA, and a fuel assembly with 8 Gd fuel rods.

5.3.2 Control Rod Modeling

Corresponding to 17x17 fuel assemblies, Westinghouse type 24-finger Ag-In-Cd control rod cluster is modeled.

For the non-BA assembly, four CR history scenarios, depicted in Figure 5.3 to Figure 5.6, are simulated. The UA cases are expected to have very non-homogeneous intra-assembly flux distributions and spectral history during the depletion, and are therefore adequately challenging for the new pin power methodology. The chosen CR history scenarios bound

the AP1000 heavy banks movement during both base load operation and load following maneuver. For instance, longer intervals of depletion with CR inserted as simulated in the sequences may happen in the top part of the fuel under the axial offset (AO) control rod bank; multiple insertion and extraction of CR with variable length may occur at intermediate part of the fuel stack; depletion with CR extracted simulates fuel shuffle into an unrodded location, etc. Due to their reduced worth, the gray bank impact on power distribution and fuel depletion history is also bound by the simulations performed in this study using heavy Ag-In-Cd bank. Therefore the sequences simulated for UAs are adequate to cover the range of CR history expected.

5.3.3 3x3 Mini-Core Modeling

One 3x3 mini-core is modeled using standard 17x17 assembly with 4.95 w/o ^{235}U fuel and no BA. A bank of 24 full-size Ag-In-Cd rodlets is present in the center assembly and inserted from 0 to 11GWD/MTU and 22 to 33GWD/MTU, while the CR is extracted during 11 to 22GWD/MTU. The same mini-core is modeled with PARAGON code.

5.4 Qualification Results

For each single assembly case, PARAGON model is created to provide the reference pin power distribution. Comparisons of the ANC results obtained with the new and the conventional pin power methods against the reference results are made for all single assembly cases.

As discussed earlier, the CR insertion induces power depression around the CR rods and

leads to relative power increase at the assembly corners. In other words, the largest impact of the CR insertion on the pin power is located at the assembly corners or near the guide thimbles. Therefore, special attention was paid to these pins, and an extensive comparison is made for the corner pins and pin at (5,4) next to the CR location (guide thimble).

5.4.1 Results of Non-BA Assembly

The pin power difference between ANC with new and current methodology vs. PARAGON is shown as a function of burnup in Figure 5.7 through Figure 5.10 for the 4.95 w/o ^{235}U fuel. Namely, Figure 5.7 shows the agreement for the corner pin and Figure 5.8 for the pin at location (5,4), which is close to the GT/CR. These locations are important, since the power migrates to the corners as a consequence of CR insertion, and redistributes and typically peaks at (5,4) when the CR are extracted. The agreement for these two pins is typically within +/- 1%, and practically always within +/-2% in the new methodology. The new methodology shows a significant improvement over the conventional pin power methodology, which yields pin power errors up to 8% as CR history builds up during the irradiation.

Figure 5.9 shows the results for the limiting pin of the assembly, which is in line with the results discussed above, and Figure 5.10 shows the average pin power difference, i.e. root mean square error (RMSE), for all the pin locations. The RMSE is calculated as the square root of the sum of the squared percent differences, divided by the number of fuel pins in an assembly. This figure, which is indicative of the overall accuracy of the

methodology, shows practically no difference with PARAGON results.

Figure 5.11 shows a summary comparison of the RMSE between new and conventional methodology for non-BA fuel cases. While RMSE up to 9% are observed with the conventional methodology, RMSE is within 1% with the new methodology, and typically below 0.5%. Furthermore, there is a consistent behavior and accuracy throughout the control rod histories simulated. This makes the agreement in the control rod simulations performed with the P3C methodology as accurate as that observed for a standard unrodded depletion calculation.

Results relative to 2.6 w/o ^{235}U fuel are in line with the above results, with some slightly higher discrepancy especially at very high burnup. This trend should not be of any concern however, given the persisting overall good agreement, plus the fact that low enrichment fuel will be placed in locations with low power and reduced importance, such as the axial blankets.

5.4.2 Results of BA Assemblies

The calculations of BA assemblies cover typical BA types, such as the Westinghouse ZrB_2 IFBA, the Wet Annular Burnable Absorber (WABA), and gadolinia (Gd_2O_3) rods. Several loading patterns, including enrichment zoning have been considered. The BA concentrations chosen exceed those used in standard PWR core designs. The high BA concentration is intended to further challenge the new pin power methodology and the associated spectral history corrections. The strong local power suppression and typical

collocation of BA bearing pins close to the water holes/control rods (or in place of control rods before WABA rods are removed) enhances the heterogeneity of the assembly and the severity of the depletion environment.

Since the discrete BA, e.g. WABA, rods take the same guide thimbles as the control rods, control rod cannot be inserted when the discrete BA rods are in. Different CR insertion sequences are adopted for BA assembly calculation, which are shown in Figure 5.12.

The results for an assembly with 156 IFBA rods are presented in Figure 5.16. A summary of the RMSE for all the IFBA and WABA cases analyzed is given in Figure 5.14. Results for a gadolinia fuel assembly (8 w/o Gd_2O_3 in 16 gadolinia rods) are given in some detail in Figure 5.15.

The pin power results obtained with the P3C methodology for IFBA and WABA assemblies are similar to those described earlier for non-BA assemblies (while the disagreement with the conventional methodology becomes even larger due to the increased heterogeneity effect of the BAs), as shown in Figure 5.16 for 156 IFBA rods and in summary results in Figure 5.14. This confirms a consistent improvement in the pin power prediction with the P3C methodology compared to the conventional methodology for these standard Westinghouse BA designs.

Results for the gadolinia fuel assembly in Figure 5.15 also show a substantial improvement with respect to the conventional methodology. However slightly larger RMSE are observed in the first part of the depletion, driven by the miss-prediction of the

gadolinia pin power during the gadolinium burnout depletion range (compare RMSE of the gadolinia assembly with and without taking Gd rods into account, second plot on the right in Figure 5.15. It is important to note that the P3C methodology yields substantial improvements with respect to the conventional methodology also for the gadolinia assembly and that the gadolinia rod power is still considerably lower than the limiting rod power when the larger differences occur and thereby do not represent a safety or an operational concern (plots in the bottom of Figure 5.15, showing the behavior of a typical gadolinia rod, on the left, and the RMSE for all gadolinia rods, on the right). While the P3C methodology predicts the gadolinia rods power with same accuracy as that of the non-BA rods after gadolinium burns out (i.e. max difference <1%, RMSE <0.5%), the error remains substantial throughout the rods depletion with the conventional methodology.

5.4.3 Mini-core results

The pin power comparisons between PARAGON and ANC are made for both new and conventional methodologies. With both pin power methodologies, the pin powers between ANC and PARAGON are in good agreement at 0 burnup. The new pin power methodology well reproduce the PARAGON pin power results throughout the modeled sequence and do not seem to be particularly challenged by the presence of CR, or the CR history built-up. This is not true for the current methodology, where differences up to 7% are observed in the corner pin of the central assembly as history accumulates see in Figure 5.16 and Figure 5.17.

5.5 Concluding Remarks

Pseudo Pin-by-Pin Calculation (P3C) methodology was developed and implemented in ANC9. This methodology is superior to conventional pin power methodologies since it directly follows the real history of each fuel rod and takes into account the history effect on the pin cross-sections and flux form factors. The qualification results demonstrated that the P3C methodology can adequately predict fuel rod powers for any control rod insertion scenario, thereby verifying that the P3C methodology well captures the control rod history effects.

This methodology has been incorporated into Westinghouse new system NEXUS/ANC and will be released for PWR core design calculations.

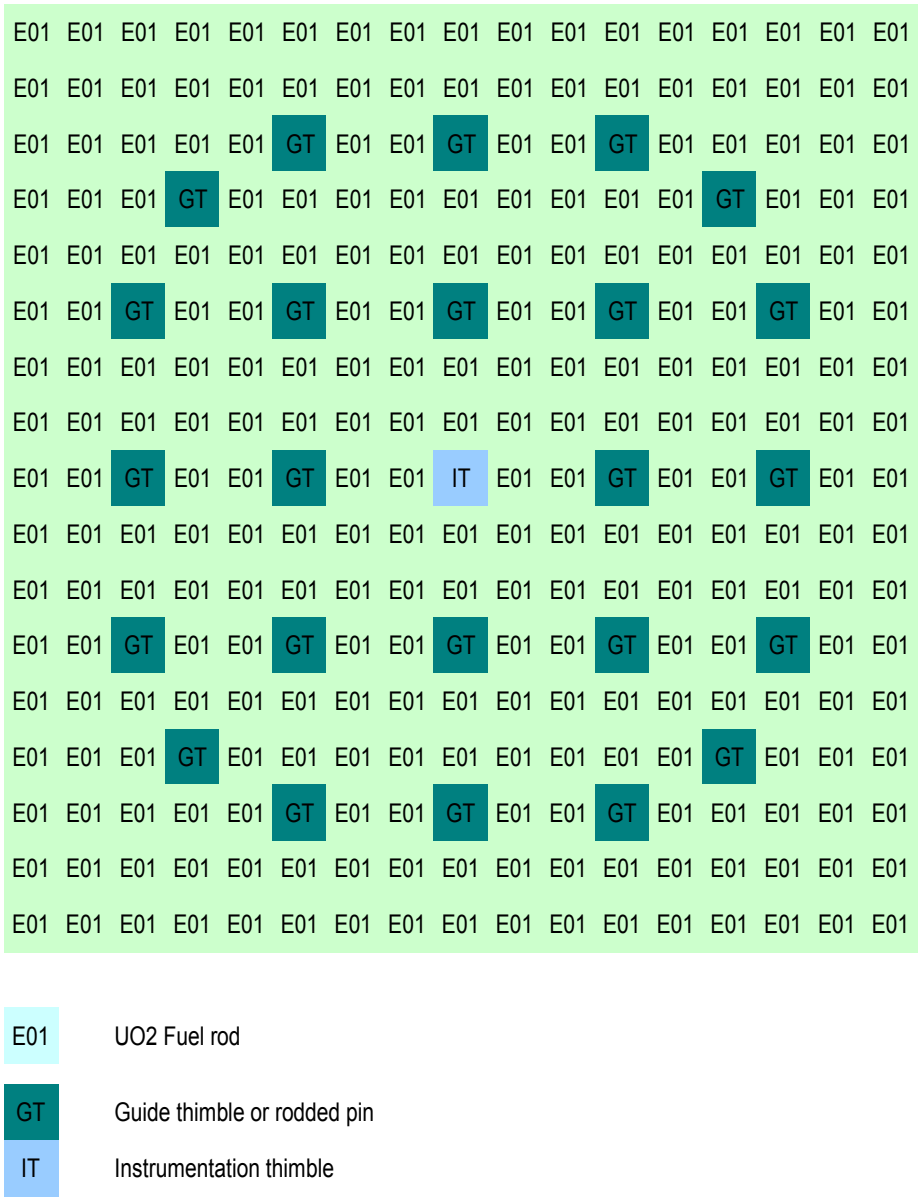

Figure 5.2 Pin map of non-BA assembly

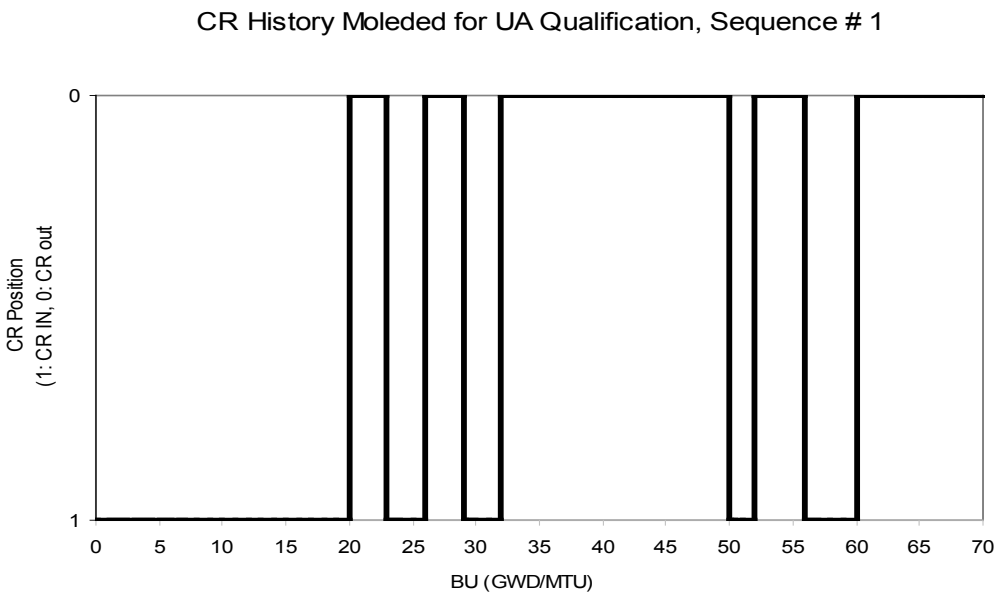

Figure 5.3 Control rod insertion sequence #1

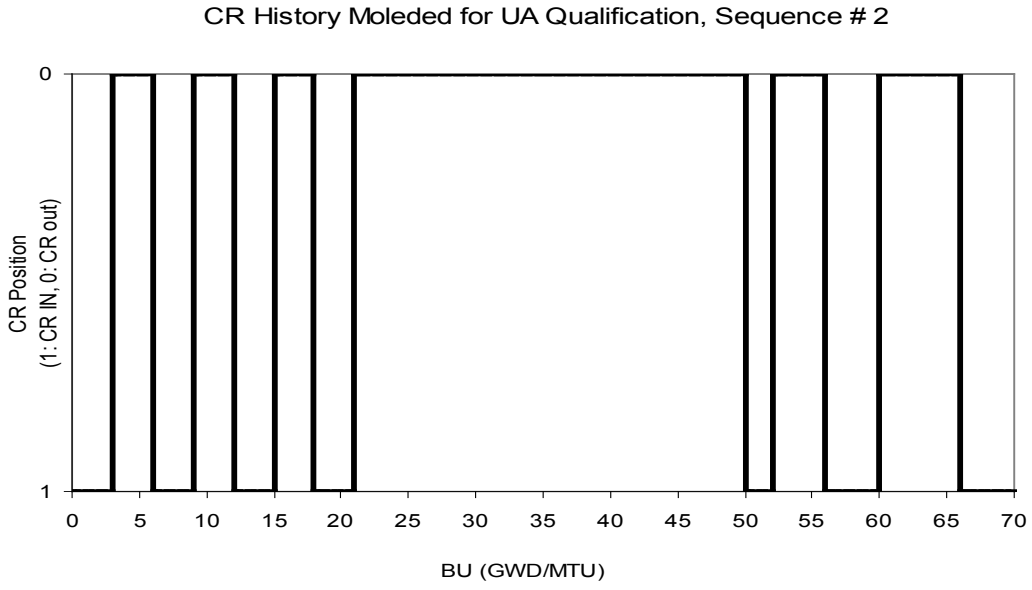

Figure 5.4 Control rod insertion sequence #2

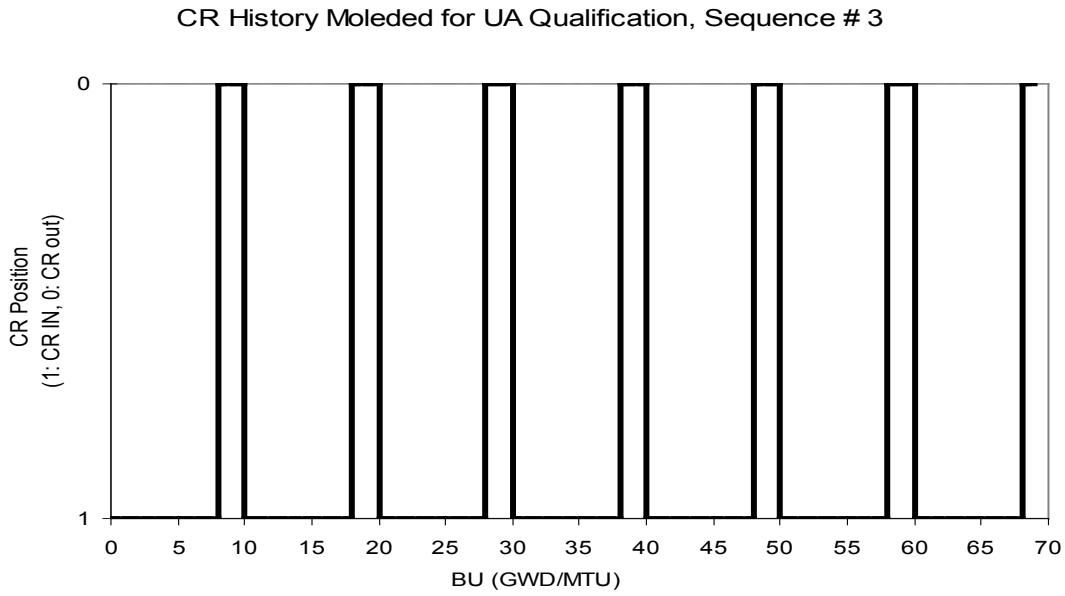

Figure 5.5 Control rod insertion sequence #3

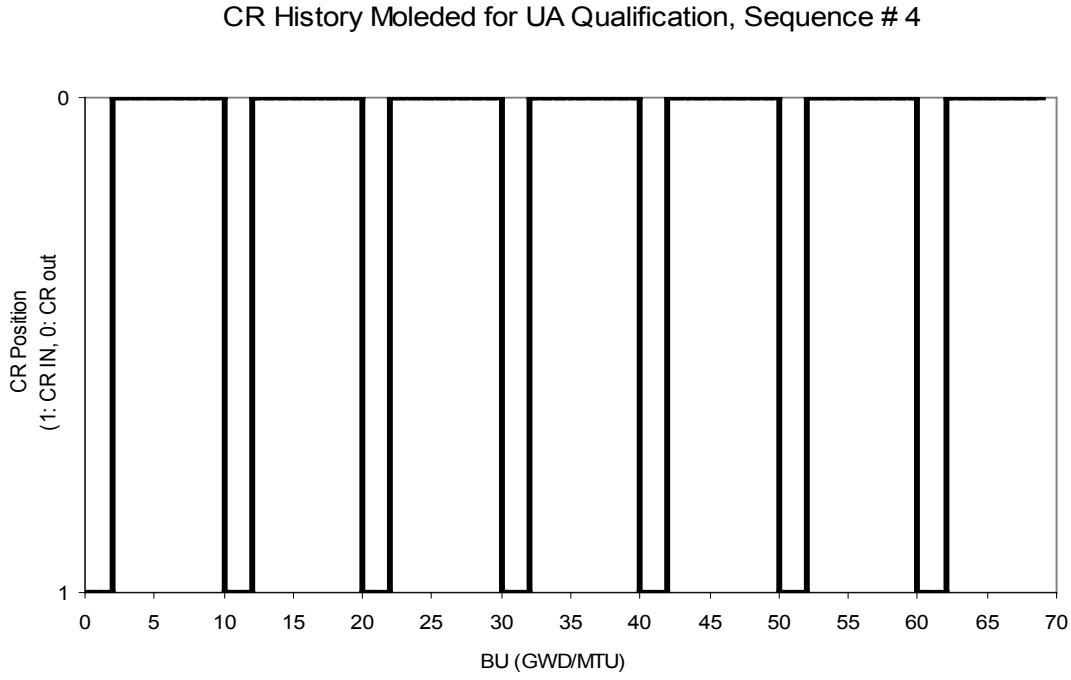

Figure 5.6 Control rod insertion sequence #4

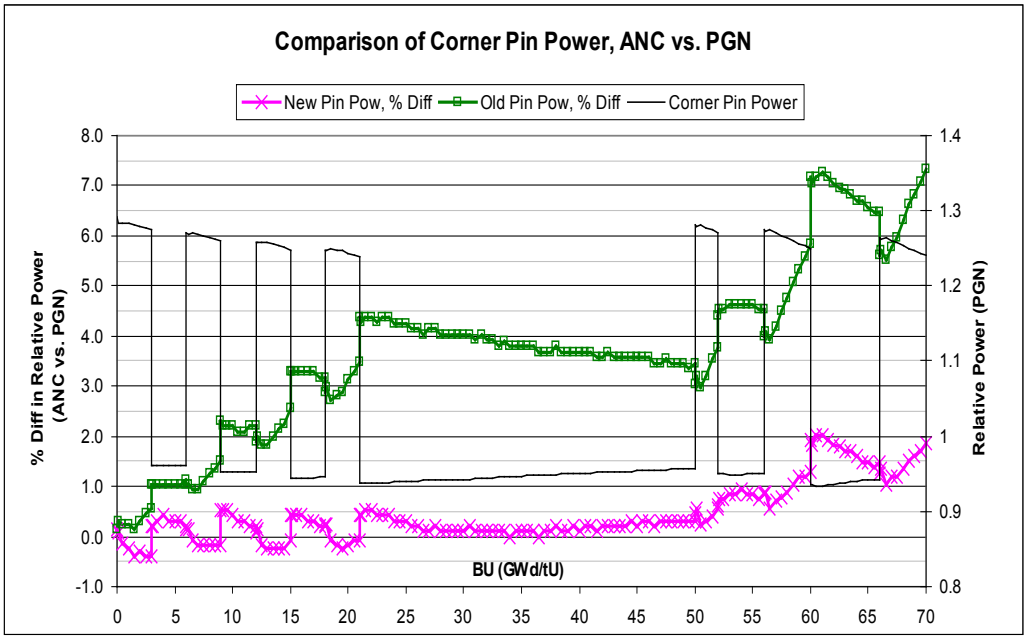

Figure 5.7 Comparison of corner pin power for 4.95wt% non-BA assembly with CR sequence #2

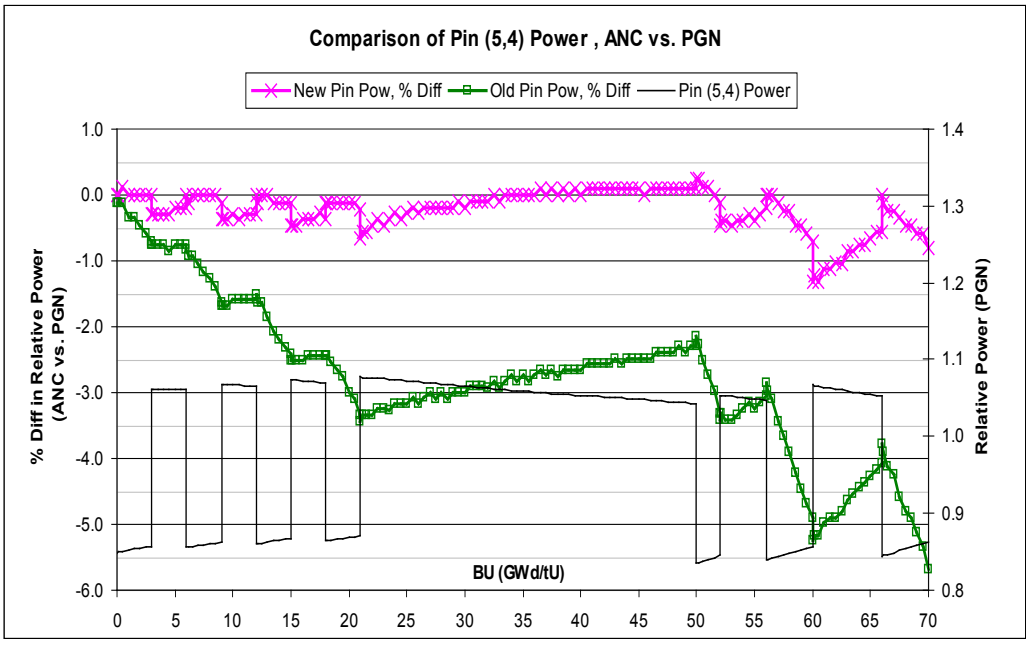

Figure 5.8 Comparison of pin power at (5,4) for 4.95wt% non-BA assembly with CR sequence #2

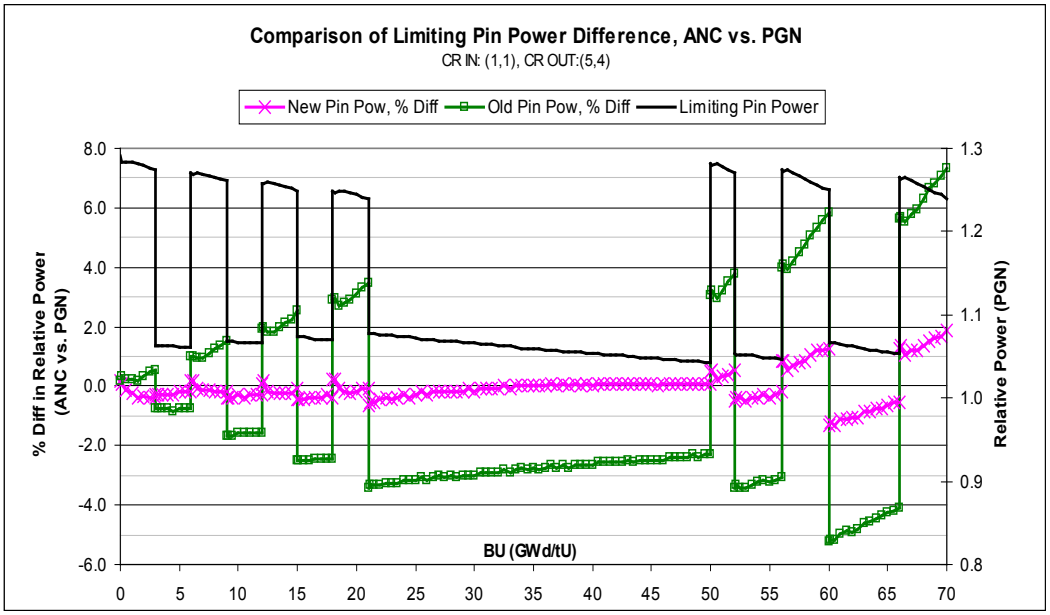

Figure 5.9 Limiting pin power comparison for 4.95wt% non-BA assembly with CR sequence #2

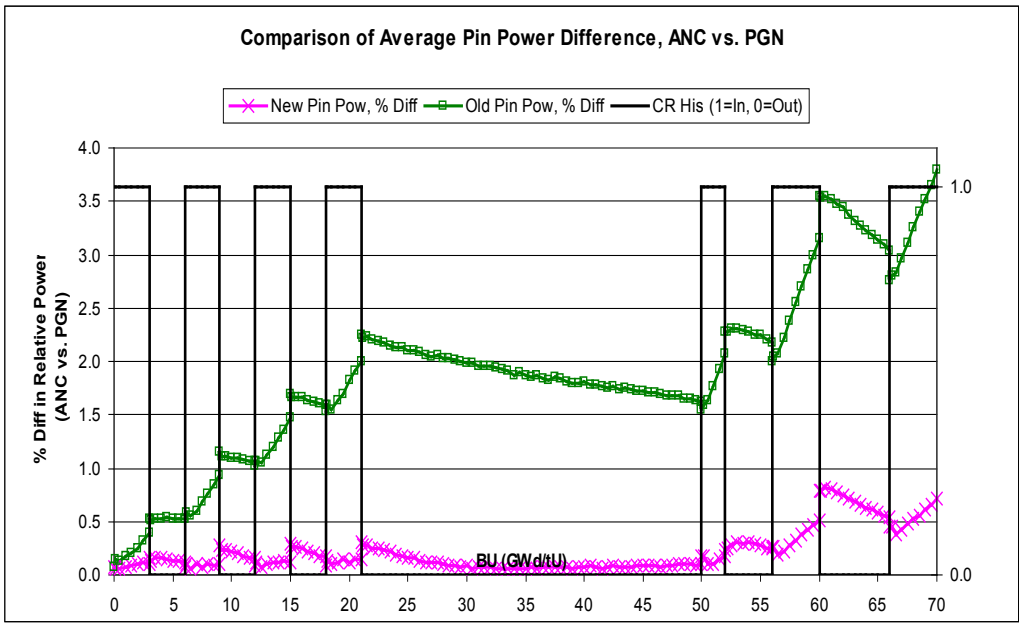

Figure 5.10 Comparison of average pin power difference for 4.95wt% non-BA assembly with CR sequence #2

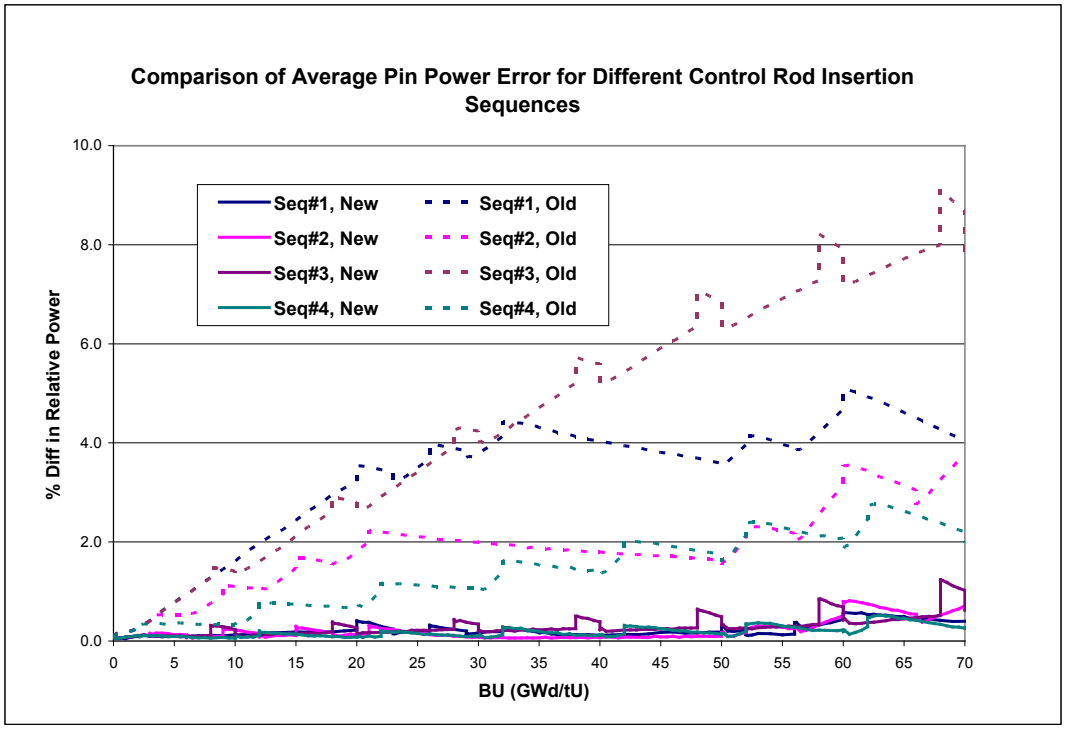

Figure 5.11 Comparison of average pin power error for different CR sequences

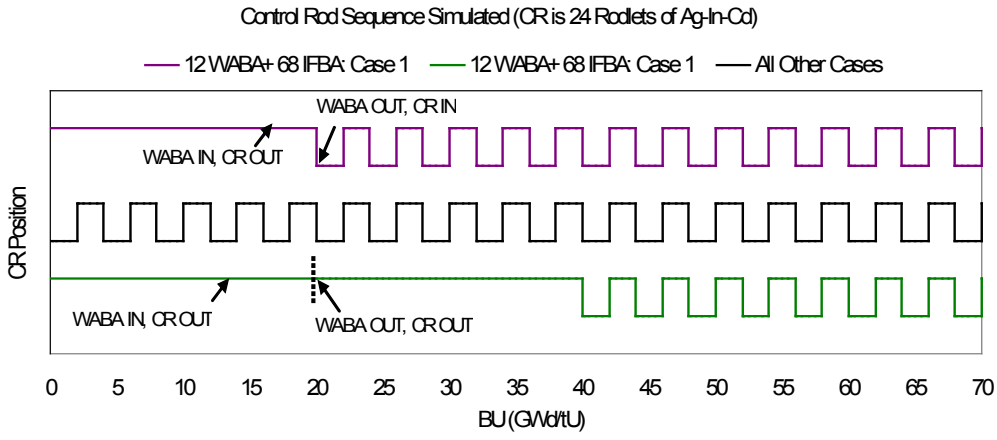

Figure 5.12 Control rod insertion sequence for BA assemblies

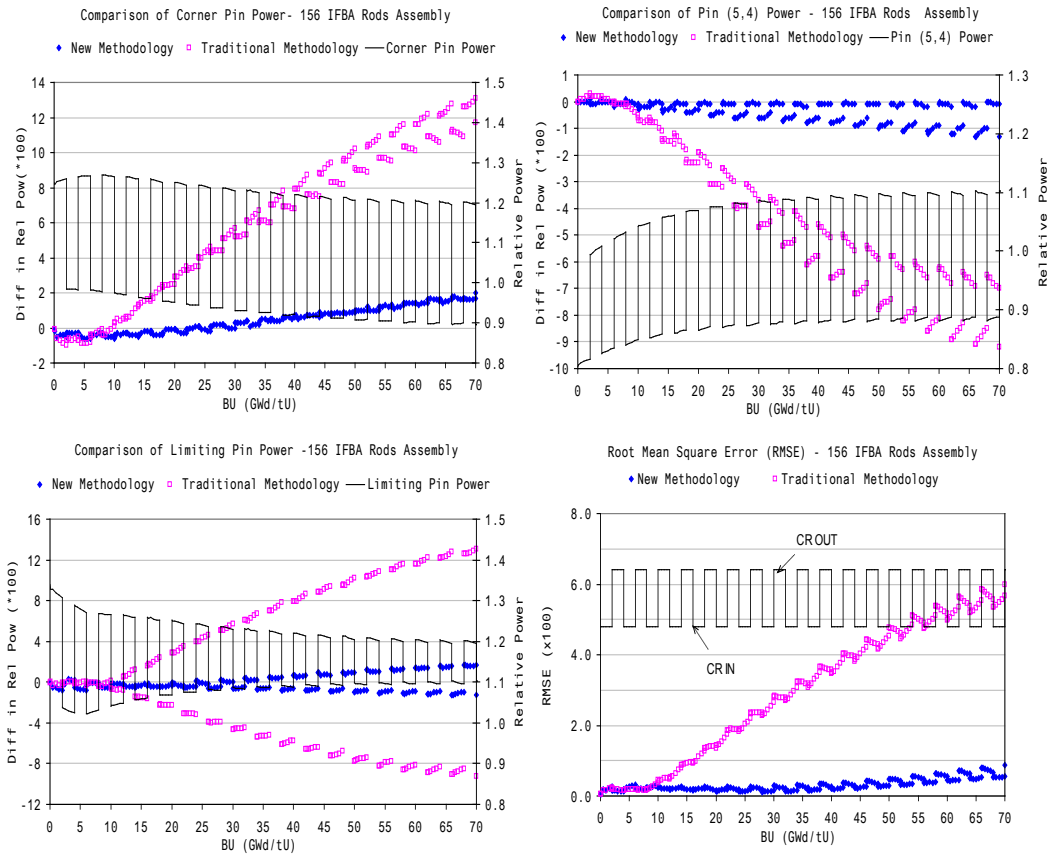

Figure 5.13 Comparisons of pin power for 156 IFBA assembly

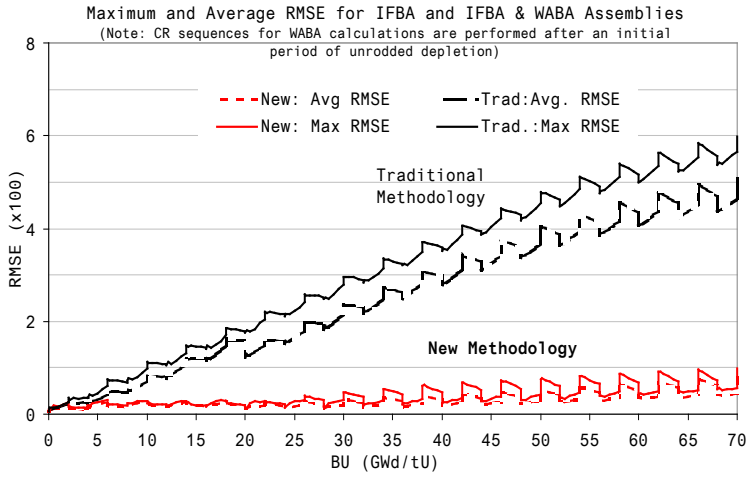

Figure 5.14 Root mean square error (average and maximum) for all IFBA and WABA assemblies

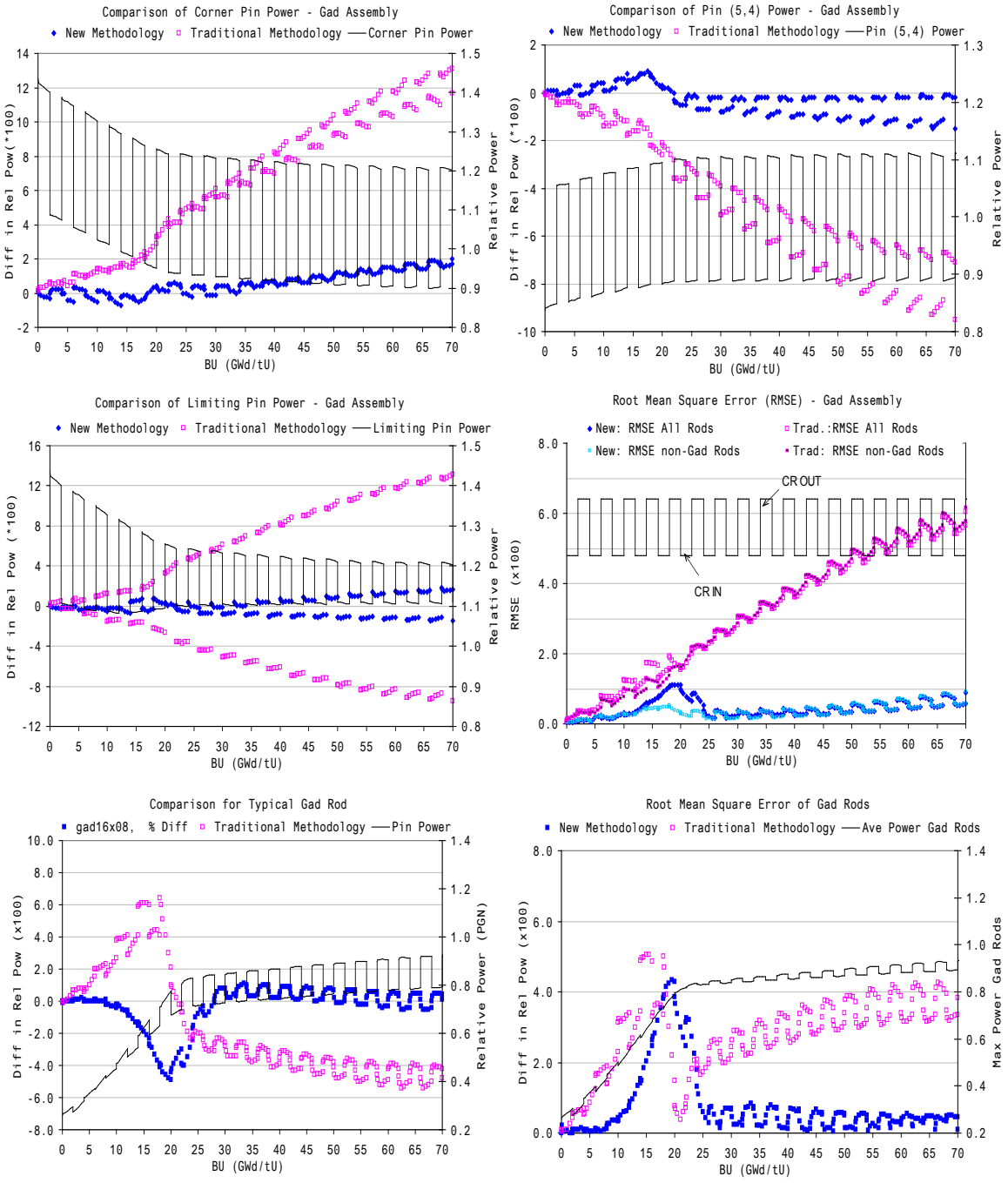

Figure 5.15 Comparison of pin power for gadolinia assembly

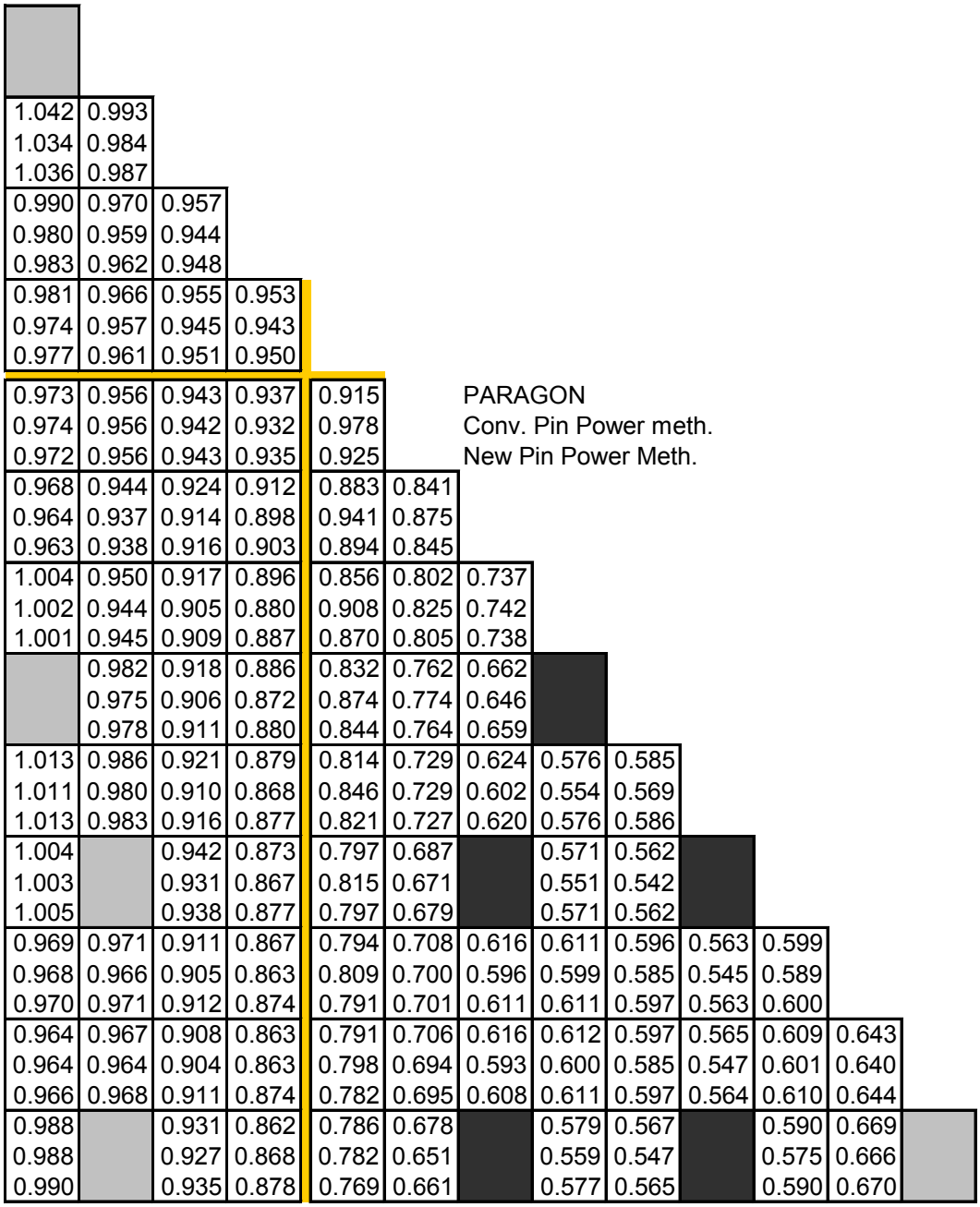

Figure 5.16 Pin power distribution of 3x3 mini-core model at 28GWD/MTU

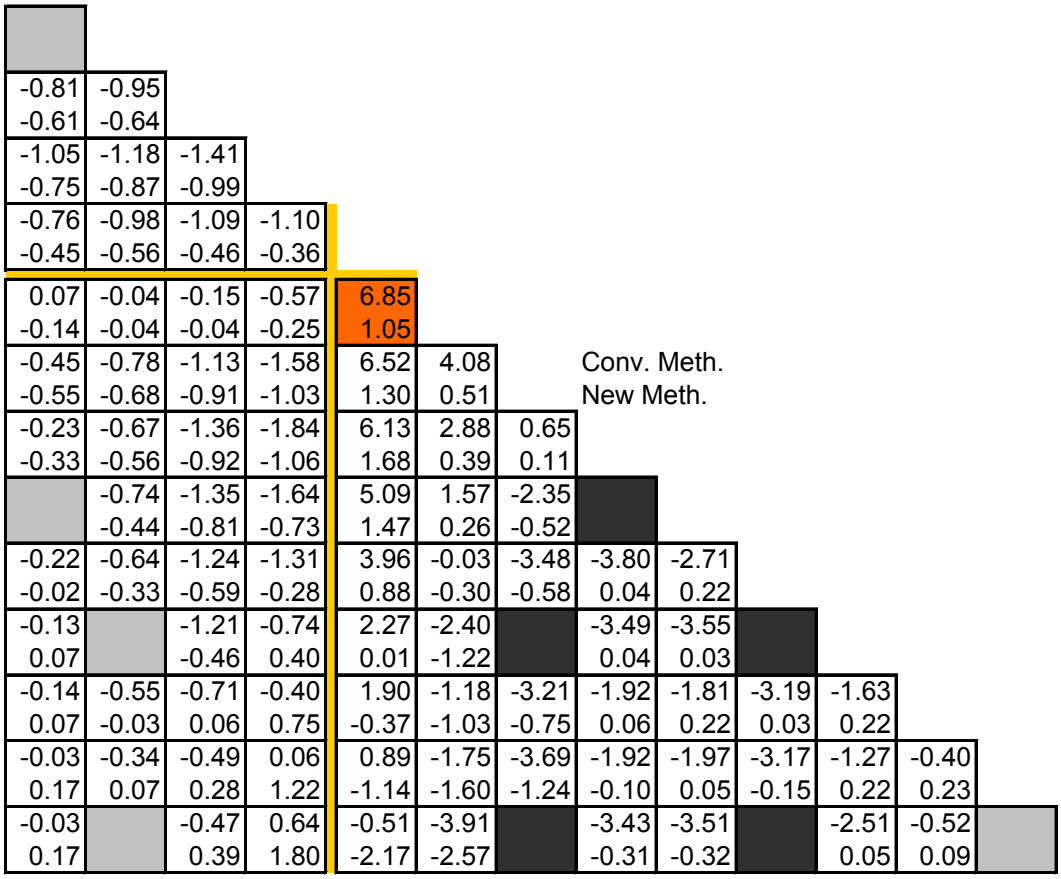

Figure 5.17 Error comparison of pin power predictions between conventional and new pin power methodologies at 28GWD/MTU

CHAPTER 6

FEASIBILITY STUDY OF P3C METHODOLOGY FOR BWR PIN POWER CALCULATION

6.1 Introduction

The application of P3C methodology for PWR fuel assemblies has been evaluated. The qualification results demonstrate that the new methodology could overcome the difficulties that the conventional methodology is facing in handling the strong heterogeneity changes and the accumulating effects on the pin power distribution. Therefore, the methodology meets the core design needs for Westinghouse AP1000, a plant that will be operated with control rod insertion during normal operation.

Since the spectrum history correction used in the P3C methodology is not limited to the fuel assembly type, it is expected that the new methodology would be robust enough to work for both PWR and BWR. However, compared to PWR core, the BWR fuel may bring an extra challenge to the pin power methodology since:

- Multiple water regions create additional heterogeneity in the BWR fuel assembly
- Unlike the PWR control rods, the BWR control blade creates significant flux or power tilt in the affected fuel assembly. The control blade impact on the neighboring fuel rods is much stronger than that of the PWR control rod. The applicability of the spectrum index approach to BWR fuel should be investigated.

To fully qualify the new pin power method for BWR application, the lattice code should be able to handle BWR assembly, and a system similar to NEXUS should be created to generate CD files for BWR fuel assemblies. Unfortunately, the PARAGON code and the NEXUS system are not ready to model BWR assembly. The expansion of the system for BWR application is out of the scope for this study.

Due to the above limitations, the preliminary test of the new pin power methodology for BWR application was focused on the assessment of spectrum index model for the pin flux form factor adjustment. So in the following discussion, it is assumed that the pin cross-sections representation model in P3C method works for BWR assembly as well.

6.2 BWR Assembly Description

A 4-sub-bundle 10x10 BWR fuel assembly is modeled for this study. The assembly pin map is shown in Figure 6.1. The different pin number in the figure stands for different fuel type, and the description of each pin type is also given in Figure 6.1. Each pin will be located by its coordinates, i.e. row and column shown in the figure. There is a slightly larger water gap in both west and north sides. At the north-west (upper-left in the figure)

corner, the control blade is modeled for the control rod inserted case. The absorber material of the control blade is B_4C.

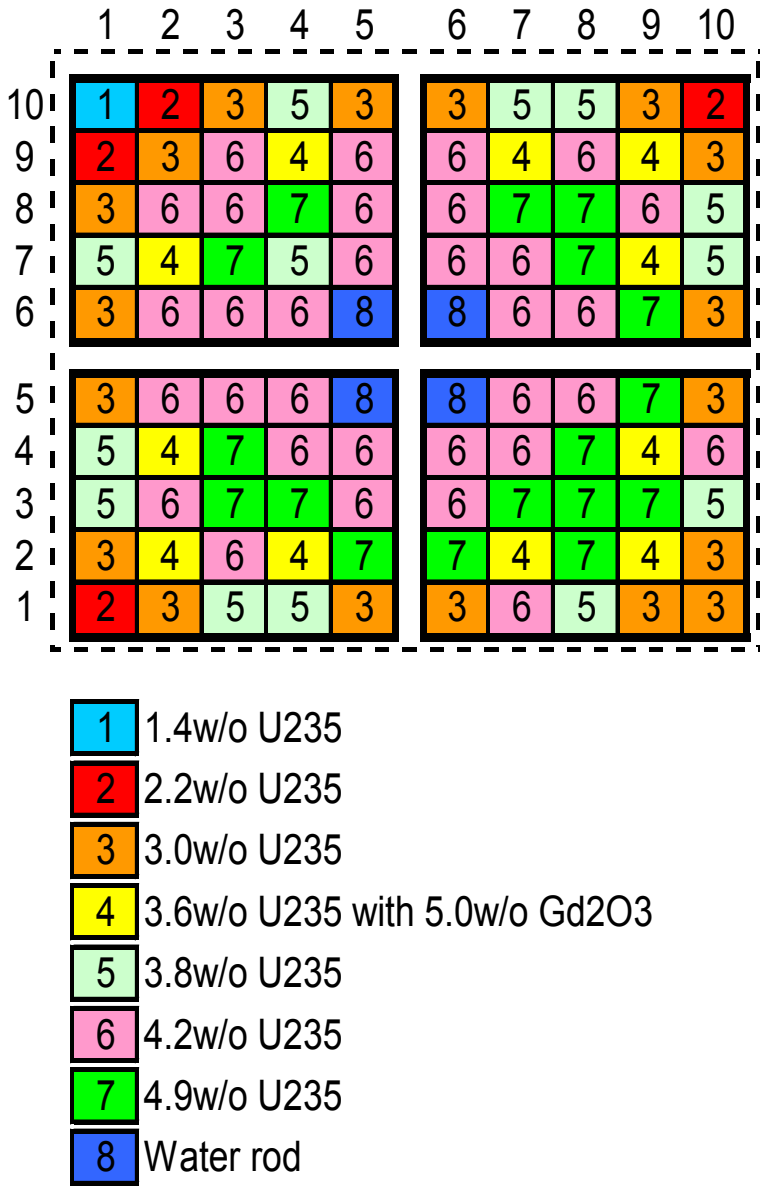

Figure 6.1 Pin map of BWR assembly

There are three water regions in the BWR assembly. They are

1) Coolant, which is included in each fuel pin

2) Water gap, bypass water region to separate fuel assemblies (bundles)

3) Water cross, the water region in the center of the fuel assembly to separate the sub-bundles.

In water regions 2 and 3, water is normally at the saturated state. A large void may happen in the coolant water region, where the void fraction can vary significantly along the axial direction from 0% up to about 90%. To focus on control rod effect, a 40% void condition is selected for the coolant region.

6.3 Calculated Results

6.3.1 Case Description

Since PARAGON code is not ready to model BWR fuel assembly, Westinghouse BWR lattice code PHOENIX-4 [32] is used in this study. Whole lattice code calculations include 9 cases. Case 1 is the standard no control rod depletion case, and case 2 is the control rod branch case. These two cases generate the basic data without control rod history effect. Various control rod insertion scenarios with different insertion periods are simulated. These control rod insertion cases elicit a wide range of spectrum history during the depletion, and therefore are challenging enough to the new pin power methodology. Among the control rod inserted cases, case 3 is the depletion case while the control rod stays inserted throughout depletion. Figure 6.2 to Figure 6.7 specify the

control rod insertion sequences of the simulated BWR case 4 to case 9.

For all cases, water temperature in all water regions was set to 559K, and fuel temperature to 784K.

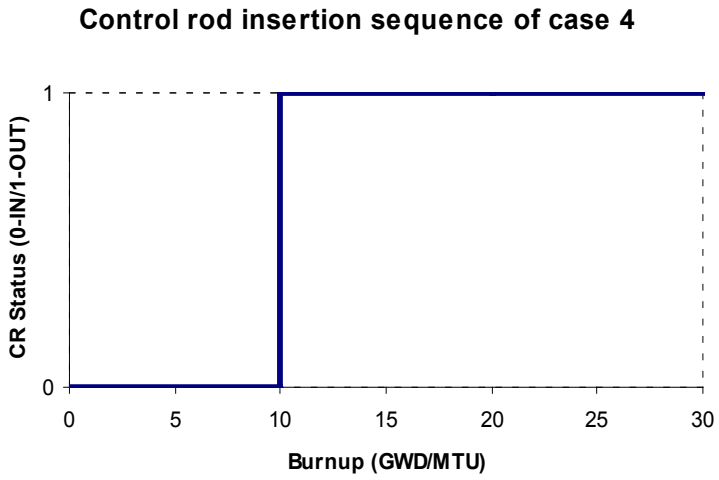

Figure 6.2 Case 4 control rod sequence

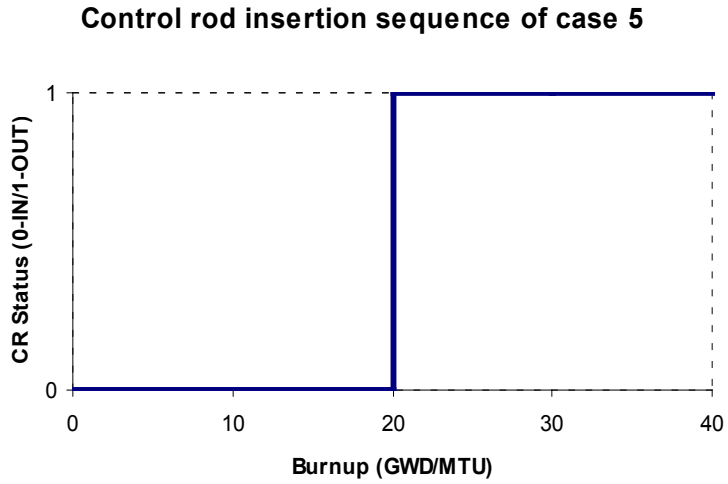

Figure 6.3 Case 5 control rod sequence

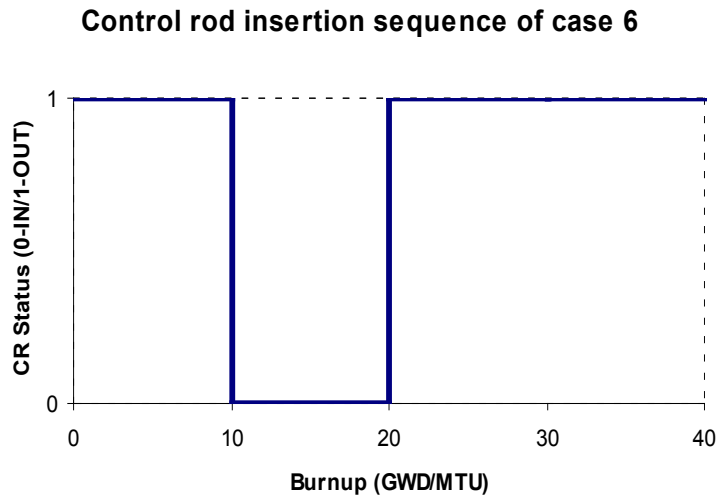

Figure 6.4 Case 6 control rod sequence

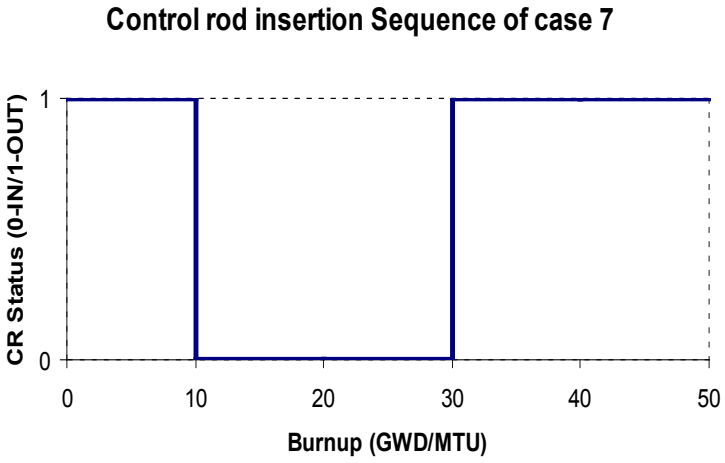

Figure 6.5 Case 7 control rod sequence

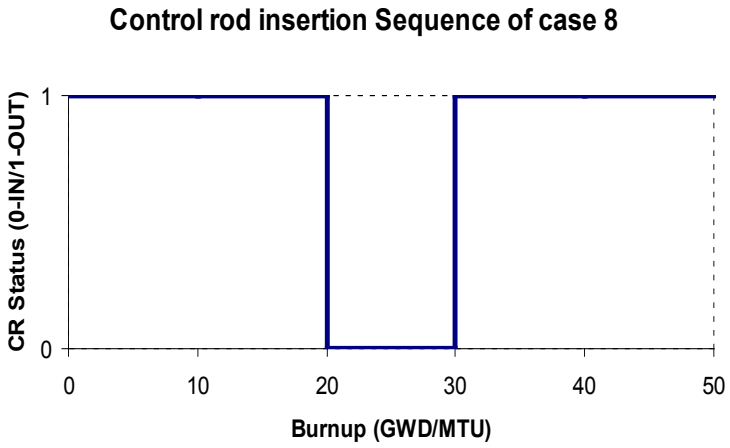

Figure 6.6 Case 8 control rod sequence

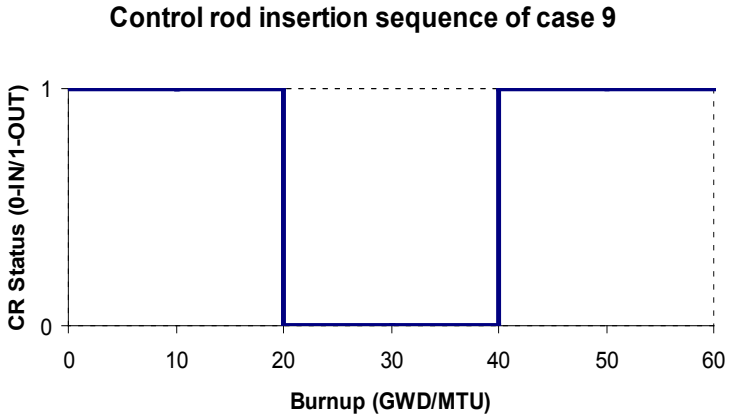

Figure 6.7 Case 9 control rod sequence

6.3.2 Calculation Results

Based on the assembly symmetry, PHOENIX-4 models the diagonal half assembly for the simulated cases. To look into the spectrum index approach model for BWR application, both thermal absorption and down-scattering cross-sections for each pin are evaluated against the pin spectrum index. In this evaluation, two burnup steps,

20GWD/MTU and 30GWD/MTU, are selected. Figure 6.8 to Figure 6.10 show the pin thermal absorption, down-scattering cross-sections, and spectrum index at 20GWD/MTU with CR insertion, At 30GWD/MTU, Figure 6.11 to Figure 6.16 list the results for cases with and without CR insertion respectively.

6.91E-02		Case 2							
9.91E-02		Case 3							
8.99E-02		Case 6							
7.86E-02	9.07E-02								
1.09E-01	1.18E-01								
9.85E-02	1.08E-01								
9.05E-02	1.10E-01	1.15E-01							
1.22E-01	1.36E-01	1.35E-01							
1.10E-01	1.26E-01	1.27E-01							
1.02E-01	1.07E-01	1.27E-01	1.13E-01						
1.34E-01	1.63E-01	1.43E-01	1.24E-01						
1.22E-01	1.24E-01	1.37E-01	1.20E-01						
9.46E-02	1.15E-01	1.18E-01	1.18E-01	9.56E-03					
1.23E-01	1.36E-01	1.32E-01	1.27E-01	9.53E-03					
1.12E-01	1.28E-01	1.27E-01	1.24E-01	9.54E-03					
9.52E-02	1.15E-01	1.19E-01	1.19E-01	9.57E-03	9.58E-03				
1.22E-01	1.35E-01	1.31E-01	1.25E-01	9.56E-03	9.58E-03				
1.12E-01	1.27E-01	1.26E-01	1.23E-01	9.56E-03	9.58E-03				
1.04E-01	1.09E-01	1.29E-01	1.20E-01	1.19E-01	1.20E-01	1.20E-01			
1.32E-01	1.32E-01	1.40E-01	1.25E-01	1.22E-01	1.20E-01	1.20E-01			
1.21E-01	1.22E-01	1.36E-01	1.23E-01	1.21E-01	1.20E-01	1.21E-01			
1.03E-01	1.15E-01	1.29E-01	1.31E-01	1.21E-01	1.21E-01	1.32E-01	1.31E-01		
1.29E-01	1.31E-01	1.38E-01	1.35E-01	1.23E-01	1.21E-01	1.30E-01	1.29E-01		
1.19E-01	1.25E-01	1.35E-01	1.34E-01	1.23E-01	1.22E-01	1.31E-01	1.30E-01		
9.10E-02	1.05E-01	1.17E-01	1.12E-01	1.28E-01	1.29E-01	1.13E-01	1.28E-01	1.08E-01	
1.11E-01	1.19E-01	1.24E-01	1.16E-01	1.28E-01	1.26E-01	1.12E-01	1.23E-01	1.04E-01	
1.04E-01	1.14E-01	1.21E-01	1.15E-01	1.29E-01	1.28E-01	1.13E-01	1.26E-01	1.06E-01	
7.94E-02	9.20E-02	1.06E-01	1.08E-01	9.87E-02	9.90E-02	1.14E-01	1.08E-01	9.44E-02	9.05E-02
9.23E-02	1.01E-01	1.11E-01	1.09E-01	9.93E-02	9.78E-02	1.09E-01	1.02E-01	9.00E-02	8.53E-02
8.82E-02	9.83E-02	1.09E-01	1.09E-01	9.95E-02	9.88E-02	1.12E-01	1.05E-01	9.24E-02	8.78E-02

Figure 6.8 Pin-wise $\Sigma_{a,2}$ at 20GWD/MTU with CR insertion

6.96E-03		Case 2							
6.79E-03		Case 3							
6.86E-03		Case 6							
6.56E-03	6.89E-03								
6.40E-03	6.71E-03								
6.47E-03	6.80E-03								
6.54E-03	7.02E-03	7.28E-03							
6.37E-03	6.84E-03	7.09E-03							
6.45E-03	6.93E-03	7.18E-03							
6.52E-03	7.19E-03	7.53E-03	8.05E-03						
6.35E-03	7.01E-03	7.34E-03	7.87E-03						
6.44E-03	7.10E-03	7.44E-03	7.96E-03						
6.62E-03	7.42E-03	7.83E-03	8.57E-03	3.00E-02					
6.46E-03	7.24E-03	7.66E-03	8.42E-03	2.97E-02					
6.54E-03	7.33E-03	7.75E-03	8.50E-03	2.98E-02					
6.66E-03	7.43E-03	7.84E-03	8.58E-03	2.99E-02	2.98E-02				
6.51E-03	7.27E-03	7.70E-03	8.47E-03	2.97E-02	2.99E-02				
6.59E-03	7.35E-03	7.77E-03	8.53E-03	2.98E-02	2.99E-02				
6.68E-03	7.30E-03	7.67E-03	8.15E-03	8.69E-03	8.70E-03	8.28E-03			
6.52E-03	7.15E-03	7.53E-03	8.05E-03	8.64E-03	8.69E-03	8.28E-03			
6.60E-03	7.23E-03	7.61E-03	8.10E-03	8.67E-03	8.70E-03	8.29E-03			
6.98E-03	7.43E-03	7.69E-03	7.96E-03	8.29E-03	8.30E-03	8.07E-03	8.03E-03		
6.81E-03	7.28E-03	7.56E-03	7.87E-03	8.23E-03	8.28E-03	8.07E-03	8.04E-03		
6.89E-03	7.36E-03	7.63E-03	7.92E-03	8.27E-03	8.30E-03	8.08E-03	8.04E-03		
7.77E-03	8.07E-03	8.23E-03	8.35E-03	8.47E-03	8.45E-03	8.37E-03	8.40E-03	8.76E-03	
7.59E-03	7.91E-03	8.10E-03	8.26E-03	8.43E-03	8.45E-03	8.38E-03	8.43E-03	8.80E-03	
7.68E-03	7.99E-03	8.17E-03	8.31E-03	8.46E-03	8.46E-03	8.38E-03	8.41E-03	8.78E-03	
9.40E-03	9.17E-03	9.19E-03	9.23E-03	9.37E-03	9.35E-03	9.19E-03	9.30E-03	9.60E-03	1.03E-02
9.24E-03	9.05E-03	9.10E-03	9.18E-03	9.36E-03	9.38E-03	9.24E-03	9.36E-03	9.67E-03	1.04E-02
9.31E-03	9.11E-03	9.14E-03	9.21E-03	9.37E-03	9.37E-03	9.22E-03	9.33E-03	9.64E-03	1.04E-02

Figure 6.9 Pin-wise $\Sigma_{1\to2}$ at 20GWD/MTU with CR insertion

13.740		Case 2							
16.440		Case 3							
15.389		Case 6							
15.158	14.684								
18.651	18.275								
17.213	16.740								
15.513	14.387	13.386							
19.260	17.861	16.155							
17.617	16.278	14.899							
15.264	13.424	12.075	9.853						
18.880	16.785	14.130	11.058						
17.231	15.037	13.209	10.549						
14.085	12.118	10.367	7.919	4.833					
16.903	14.304	11.741	8.607	5.063					
15.680	13.333	11.154	8.326	4.971					
13.300	11.526	9.986	7.692	4.727	4.629				
15.708	13.310	11.072	8.195	4.874	4.687				
14.704	12.566	10.631	8.001	4.821	4.674				
12.791	11.458	10.565	8.883	7.195	7.028	8.110			
15.089	13.230	11.656	9.423	7.402	7.059	8.054			
14.139	12.492	11.224	9.225	7.340	7.075	8.119			
10.751	10.296	9.997	9.213	8.108	7.916	8.462	8.240		
12.448	11.651	10.896	9.687	8.297	7.897	8.308	7.980		
11.766	11.116	10.557	9.527	8.254	7.943	8.422	8.142		
7.752	7.914	8.024	7.785	7.368	7.236	7.310	7.007	5.932	
8.688	8.738	8.589	8.093	7.460	7.141	7.116	6.726	5.667	
8.333	8.434	8.391	8.003	7.459	7.220	7.241	6.889	5.813	
5.008	5.537	5.792	5.779	5.470	5.387	5.537	5.201	4.561	3.749
5.407	5.929	6.069	5.924	5.512	5.313	5.367	4.997	4.373	3.600
5.265	5.793	5.981	5.890	5.519	5.369	5.468	5.110	4.474	3.678

Figure 6.10 Pin-wise spectrum index at 20GWD/MTU with CR insertion

6.88E-02		Case 2							
1.14E-01		Case 3							
1.06E-01		Case 7							
9.30E-02		Case 9							
7.58E-02	8.60E-02								
1.22E-01	1.28E-01								
1.13E-01	1.19E-01								
9.88E-02	1.06E-01								
8.54E-02	1.03E-01	1.10E-01							
1.33E-01	1.43E-01	1.40E-01							
1.23E-01	1.33E-01	1.33E-01							
1.08E-01	1.22E-01	1.24E-01							
9.46E-02	1.02E-01	1.20E-01	1.08E-01						
1.43E-01	1.39E-01	1.45E-01	1.25E-01						
1.32E-01	1.31E-01	1.39E-01	1.21E-01						
1.17E-01	1.21E-01	1.32E-01	1.17E-01						
8.99E-02	1.08E-01	1.13E-01	1.12E-01	9.60E-03					
1.33E-01	1.40E-01	1.33E-01	1.24E-01	9.56E-03					
1.24E-01	1.33E-01	1.29E-01	1.21E-01	9.57E-03					
1.11E-01	1.23E-01	1.23E-01	1.18E-01	9.58E-03					
9.05E-02	1.09E-01	1.13E-01	1.12E-01	9.61E-03	9.63E-03				
1.31E-01	1.38E-01	1.31E-01	1.21E-01	9.59E-03	9.62E-03				
1.22E-01	1.31E-01	1.27E-01	1.19E-01	9.59E-03	9.62E-03				
1.11E-01	1.23E-01	1.22E-01	1.17E-01	9.60E-03	9.62E-03				
9.67E-02	1.04E-01	1.23E-01	1.14E-01	1.13E-01	1.13E-01	1.16E-01			
1.38E-01	1.32E-01	1.38E-01	1.22E-01	1.15E-01	1.12E-01	1.13E-01			
1.28E-01	1.26E-01	1.35E-01	1.20E-01	1.15E-01	1.13E-01	1.14E-01			
1.16E-01	1.19E-01	1.30E-01	1.18E-01	1.15E-01	1.13E-01	1.15E-01			
9.48E-02	1.08E-01	1.22E-01	1.24E-01	1.16E-01	1.16E-01	1.26E-01	1.25E-01		
1.32E-01	1.31E-01	1.35E-01	1.29E-01	1.17E-01	1.14E-01	1.21E-01	1.18E-01		
1.24E-01	1.26E-01	1.32E-01	1.29E-01	1.17E-01	1.15E-01	1.22E-01	1.20E-01		
1.13E-01	1.19E-01	1.29E-01	1.27E-01	1.17E-01	1.16E-01	1.24E-01	1.23E-01		
8.45E-02	9.74E-02	1.09E-01	1.07E-01	1.20E-01	1.20E-01	1.08E-01	1.19E-01	1.01E-01	
1.11E-01	1.16E-01	1.19E-01	1.11E-01	1.18E-01	1.15E-01	1.04E-01	1.10E-01	9.39E-02	
1.06E-01	1.12E-01	1.17E-01	1.11E-01	1.19E-01	1.17E-01	1.06E-01	1.13E-01	9.60E-02	
9.83E-02	1.08E-01	1.14E-01	1.10E-01	1.20E-01	1.19E-01	1.07E-01	1.16E-01	9.83E-02	
7.55E-02	8.54E-02	9.69E-02	9.98E-02	9.36E-02	9.41E-02	1.05E-01	9.92E-02	8.81E-02	8.36E-02
9.11E-02	9.70E-02	1.03E-01	1.01E-01	9.39E-02	9.19E-02	9.78E-02	9.22E-02	8.31E-02	7.89E-02
8.86E-02	9.51E-02	1.02E-01	1.02E-01	9.43E-02	9.28E-02	9.99E-02	9.42E-02	8.45E-02	8.01E-02
8.49E-02	9.23E-02	1.01E-01	1.02E-01	9.45E-02	9.36E-02	1.02E-01	9.65E-02	8.61E-02	8.16E-02

Figure 6.11 Pin-wise $\Sigma_{a,2}$ at 30GWD/MTU with CR insertion

6.98E-03		Case 2							
6.66E-03		Case 3							
6.73E-03		Case 7							
6.83E-03		Case 9							
6.56E-03	6.87E-03								
6.26E-03	6.54E-03								
6.33E-03	6.63E-03								
6.43E-03	6.73E-03								
6.54E-03	7.01E-03	7.26E-03							
6.23E-03	6.66E-03	6.91E-03							
6.31E-03	6.76E-03	7.01E-03							
6.41E-03	6.87E-03	7.12E-03							
6.53E-03	7.17E-03	7.50E-03	8.04E-03						
6.22E-03	6.84E-03	7.19E-03	7.75E-03						
6.30E-03	6.93E-03	7.28E-03	7.83E-03						
6.40E-03	7.04E-03	7.38E-03	7.93E-03						
6.63E-03	7.41E-03	7.82E-03	8.59E-03	3.03E-02					
6.34E-03	7.10E-03	7.54E-03	8.35E-03	2.97E-02					
6.42E-03	7.19E-03	7.62E-03	8.42E-03	2.99E-02					
6.51E-03	7.29E-03	7.71E-03	8.50E-03	3.00E-02					
6.67E-03	7.42E-03	7.82E-03	8.60E-03	3.01E-02	3.01E-02				
6.40E-03	7.14E-03	7.59E-03	8.42E-03	2.99E-02	3.01E-02				
6.48E-03	7.22E-03	7.66E-03	8.47E-03	3.00E-02	3.01E-02				
6.56E-03	7.31E-03	7.74E-03	8.53E-03	3.00E-02	3.01E-02				
6.68E-03	7.28E-03	7.64E-03	8.12E-03	8.70E-03	8.69E-03	8.24E-03			
6.41E-03	7.03E-03	7.43E-03	7.98E-03	8.63E-03	8.72E-03	8.27E-03			
6.49E-03	7.10E-03	7.49E-03	8.02E-03	8.65E-03	8.71E-03	8.26E-03			
6.57E-03	7.18E-03	7.56E-03	8.07E-03	8.67E-03	8.71E-03	8.26E-03			
6.98E-03	7.41E-03	7.65E-03	7.92E-03	8.26E-03	8.26E-03	8.01E-03	7.97E-03		
6.71E-03	7.16E-03	7.46E-03	7.80E-03	8.21E-03	8.28E-03	8.07E-03	8.05E-03		
6.78E-03	7.23E-03	7.51E-03	7.83E-03	8.22E-03	8.27E-03	8.05E-03	8.03E-03		
6.87E-03	7.31E-03	7.58E-03	7.88E-03	8.24E-03	8.27E-03	8.04E-03	8.01E-03		
7.79E-03	8.06E-03	8.20E-03	8.31E-03	8.45E-03	8.43E-03	8.32E-03	8.36E-03	8.74E-03	
7.50E-03	7.82E-03	8.03E-03	8.21E-03	8.43E-03	8.47E-03	8.40E-03	8.46E-03	8.85E-03	
7.57E-03	7.88E-03	8.08E-03	8.24E-03	8.43E-03	8.46E-03	8.38E-03	8.43E-03	8.82E-03	
7.66E-03	7.96E-03	8.14E-03	8.28E-03	8.45E-03	8.45E-03	8.36E-03	8.40E-03	8.79E-03	
9.46E-03	9.21E-03	9.22E-03	9.26E-03	9.40E-03	9.37E-03	9.21E-03	9.32E-03	9.63E-03	1.04E-02
9.23E-03	9.03E-03	9.10E-03	9.19E-03	9.40E-03	9.44E-03	9.32E-03	9.45E-03	9.76E-03	1.05E-02
9.28E-03	9.07E-03	9.13E-03	9.21E-03	9.39E-03	9.42E-03	9.29E-03	9.41E-03	9.73E-03	1.05E-02
9.35E-03	9.13E-03	9.17E-03	9.23E-03	9.40E-03	9.40E-03	9.26E-03	9.37E-03	9.69E-03	1.05E-02

Figure 6.12 Pin-wise $\Sigma_{1\to 2}$ at 30GWD/MTU with CR insertion

13.323		Case 2							
17.430		Case 3							
16.549		Case 7							
15.308		Case 9							
14.544	13.962								
19.803	19.317								
18.598	18.032								
16.998	16.414								
14.747	13.577	12.617							
20.208	18.505	16.540							
18.890	17.296	15.587							
17.237	15.820	14.423							
14.419	12.658	11.373	9.327						
19.508	16.746	14.235	11.032						
18.264	15.758	13.556	10.644						
16.735	14.553	12.712	10.147						
13.343	11.430	9.794	7.516	4.653					
17.399	14.486	11.721	8.481	4.976					
16.434	13.760	11.279	8.271	4.910					
15.222	12.858	10.717	7.994	4.817					
12.549	10.835	9.409	7.284	4.543	4.442				
16.030	13.363	10.918	7.968	4.736	4.500				
15.211	12.776	10.585	7.830	4.703	4.501				
14.182	12.037	10.151	7.638	4.650	4.488				
11.963	10.713	9.882	8.352	6.795	6.630	7.604			
15.215	13.114	11.359	9.050	7.036	6.608	7.430			
14.445	12.569	11.043	8.919	7.008	6.645	7.514			
13.491	11.880	10.622	8.727	6.948	6.662	7.577			
10.031	9.572	9.299	8.603	7.604	7.418	7.878	7.629		
12.369	11.408	10.483	9.187	7.792	7.300	7.564	7.193		
11.832	11.005	10.244	9.092	7.786	7.369	7.685	7.342		
11.158	10.483	9.914	8.937	7.746	7.418	7.794	7.487		
7.280	7.373	7.462	7.262	6.878	6.745	6.795	6.476	5.494	
8.529	8.454	8.187	7.629	6.951	6.558	6.474	6.058	5.138	
8.267	8.237	8.056	7.582	6.971	6.639	6.588	6.192	5.246	
7.922	7.943	7.863	7.493	6.964	6.708	6.696	6.328	5.361	
4.762	5.211	5.422	5.416	5.158	5.072	5.165	4.844	4.262	3.522
5.281	5.718	5.776	5.591	5.189	4.946	4.921	4.569	4.023	3.344
5.185	5.628	5.722	5.578	5.207	5.000	5.004	4.656	4.096	3.398
5.049	5.496	5.632	5.539	5.207	5.045	5.084	4.744	4.172	3.454

Figure 6.13 Pin-wise spectrum index at 30GWD/MTU with CR insertion

6.96E-02		Case 1							
7.38E-02		Case 4							
8.31E-02		Case 5							
7.67E-02		Case 6							
1.07E-01		Case 7							
9.36E-02		Case 8							
7.72E-02	8.83E-02								
8.40E-02	9.68E-02								
9.59E-02	1.09E-01								
8.68E-02	9.93E-02								
1.15E-01	1.22E-01								
1.01E-01	1.09E-01								
8.76E-02	1.06E-01	1.12E-01							
9.64E-02	1.16E-01	1.20E-01							
1.10E-01	1.28E-01	1.30E-01							
9.91E-02	1.18E-01	1.22E-01							
1.26E-01	1.37E-01	1.36E-01							
1.11E-01	1.25E-01	1.27E-01							
9.74E-02	1.05E-01	1.22E-01	1.09E-01						
1.08E-01	1.12E-01	1.29E-01	1.14E-01						
1.22E-01	1.23E-01	1.37E-01	1.19E-01						
1.10E-01	1.14E-01	1.30E-01	1.15E-01						
1.36E-01	1.35E-01	1.41E-01	1.22E-01						
1.21E-01	1.25E-01	1.34E-01	1.17E-01						
9.20E-02	1.10E-01	1.14E-01	1.12E-01	9.70E-03					
9.99E-02	1.18E-01	1.19E-01	1.15E-01	9.68E-03					
1.12E-01	1.28E-01	1.25E-01	1.19E-01	9.65E-03					
1.02E-01	1.20E-01	1.20E-01	1.16E-01	9.67E-03					
1.26E-01	1.35E-01	1.30E-01	1.21E-01	9.64E-03					
1.13E-01	1.26E-01	1.24E-01	1.18E-01	9.66E-03					
9.25E-02	1.11E-01	1.15E-01	1.13E-01	9.69E-03	9.69E-03				
9.99E-02	1.18E-01	1.19E-01	1.15E-01	9.68E-03	9.69E-03				
1.11E-01	1.26E-01	1.24E-01	1.17E-01	9.67E-03	9.68E-03				
1.02E-01	1.19E-01	1.20E-01	1.15E-01	9.68E-03	9.68E-03				
1.25E-01	1.33E-01	1.28E-01	1.19E-01	9.65E-03	9.67E-03				
1.13E-01	1.25E-01	1.23E-01	1.17E-01	9.67E-03	9.68E-03				
9.91E-02	1.06E-01	1.24E-01	1.15E-01	1.13E-01	1.13E-01	1.16E-01			
1.08E-01	1.12E-01	1.28E-01	1.17E-01	1.13E-01	1.13E-01	1.15E-01			
1.19E-01	1.19E-01	1.32E-01	1.19E-01	1.14E-01	1.12E-01	1.14E-01			
1.10E-01	1.14E-01	1.29E-01	1.17E-01	1.14E-01	1.13E-01	1.15E-01			
1.32E-01	1.28E-01	1.36E-01	1.21E-01	1.15E-01	1.13E-01	1.14E-01			
1.19E-01	1.21E-01	1.31E-01	1.19E-01	1.15E-01	1.13E-01	1.15E-01			
9.67E-02	1.09E-01	1.23E-01	1.25E-01	1.16E-01	1.16E-01	1.26E-01	1.25E-01		
1.04E-01	1.15E-01	1.26E-01	1.26E-01	1.16E-01	1.15E-01	1.24E-01	1.23E-01		
1.15E-01	1.22E-01	1.30E-01	1.27E-01	1.16E-01	1.15E-01	1.22E-01	1.20E-01		
1.06E-01	1.16E-01	1.27E-01	1.26E-01	1.16E-01	1.15E-01	1.24E-01	1.23E-01		
1.26E-01	1.27E-01	1.33E-01	1.29E-01	1.17E-01	1.15E-01	1.22E-01	1.20E-01		
1.15E-01	1.21E-01	1.29E-01	1.27E-01	1.17E-01	1.16E-01	1.24E-01	1.23E-01		
8.54E-02	9.83E-02	1.10E-01	1.07E-01	1.20E-01	1.20E-01	1.08E-01	1.19E-01	1.01E-01	
9.02E-02	1.02E-01	1.12E-01	1.08E-01	1.19E-01	1.18E-01	1.07E-01	1.16E-01	9.85E-02	
9.73E-02	1.07E-01	1.14E-01	1.09E-01	1.18E-01	1.17E-01	1.05E-01	1.13E-01	9.61E-02	
9.18E-02	1.03E-01	1.13E-01	1.08E-01	1.19E-01	1.19E-01	1.07E-01	1.16E-01	9.85E-02	
1.07E-01	1.13E-01	1.17E-01	1.11E-01	1.19E-01	1.17E-01	1.05E-01	1.13E-01	9.60E-02	
9.91E-02	1.08E-01	1.15E-01	1.10E-01	1.20E-01	1.19E-01	1.07E-01	1.16E-01	9.83E-02	
7.56E-02	8.55E-02	9.71E-02	9.99E-02	9.37E-02	9.42E-02	1.05E-01	9.93E-02	8.82E-02	8.37E-02
7.79E-02	8.76E-02	9.82E-02	9.99E-02	9.34E-02	9.32E-02	1.02E-01	9.67E-02	8.62E-02	8.17E-02
8.16E-02	9.06E-02	9.97E-02	1.00E-01	9.33E-02	9.24E-02	9.99E-02	9.43E-02	8.46E-02	8.02E-02
7.90E-02	8.85E-02	9.88E-02	1.00E-01	9.36E-02	9.33E-02	1.02E-01	9.67E-02	8.63E-02	8.18E-02
8.84E-02	9.50E-02	1.02E-01	1.02E-01	9.43E-02	9.28E-02	9.99E-02	9.42E-02	8.45E-02	8.02E-02
8.48E-02	9.22E-02	1.01E-01	1.02E-01	9.45E-02	9.36E-02	1.02E-01	9.65E-02	8.61E-02	8.16E-02

Figure 6.14 Pin-wise $\Sigma_{a,2}$ at 30GWD/MTU without CR

1.08E-02		Case 1							
1.06E-02		Case 4							
1.04E-02		Case 5							
1.06E-02		Case 6							
1.03E-02		Case 7							
1.05E-02		Case 8							
9.94E-03	9.07E-03								
9.79E-03	8.92E-03								
9.60E-03	8.76E-03								
9.76E-03	8.90E-03								
9.55E-03	8.75E-03								
9.70E-03	8.89E-03								
9.60E-03	8.67E-03	8.29E-03							
9.44E-03	8.53E-03	8.16E-03							
9.27E-03	8.38E-03	8.04E-03							
9.42E-03	8.52E-03	8.16E-03							
9.26E-03	8.41E-03	8.07E-03							
9.40E-03	8.53E-03	8.17E-03							
9.43E-03	8.58E-03	8.27E-03	8.48E-03						
9.27E-03	8.45E-03	8.16E-03	8.38E-03						
9.12E-03	8.32E-03	8.06E-03	8.30E-03						
9.26E-03	8.44E-03	8.16E-03	8.38E-03						
9.12E-03	8.35E-03	8.09E-03	8.32E-03						
9.25E-03	8.46E-03	8.18E-03	8.40E-03						
9.50E-03	8.66E-03	8.46E-03	8.88E-03	3.03E-02					
9.37E-03	8.54E-03	8.37E-03	8.81E-03	3.01E-02					
9.24E-03	8.43E-03	8.28E-03	8.73E-03	2.99E-02					
9.36E-03	8.54E-03	8.37E-03	8.81E-03	3.01E-02					
9.23E-03	8.45E-03	8.30E-03	8.75E-03	2.99E-02					
9.35E-03	8.55E-03	8.39E-03	8.82E-03	3.01E-02					
9.48E-03	8.63E-03	8.44E-03	8.86E-03	3.02E-02	3.01E-02				
9.36E-03	8.53E-03	8.36E-03	8.80E-03	3.01E-02	3.01E-02				
9.24E-03	8.44E-03	8.29E-03	8.75E-03	3.00E-02	3.02E-02				
9.35E-03	8.53E-03	8.36E-03	8.80E-03	3.01E-02	3.01E-02				
9.23E-03	8.45E-03	8.31E-03	8.77E-03	3.01E-02	3.02E-02				
9.34E-03	8.54E-03	8.38E-03	8.82E-03	3.01E-02	3.02E-02				
9.36E-03	8.52E-03	8.21E-03	8.42E-03	8.84E-03	8.82E-03	8.39E-03			
9.25E-03	8.43E-03	8.15E-03	8.37E-03	8.81E-03	8.82E-03	8.39E-03			
9.13E-03	8.34E-03	8.08E-03	8.33E-03	8.80E-03	8.83E-03	8.40E-03			
9.24E-03	8.42E-03	8.15E-03	8.37E-03	8.82E-03	8.83E-03	8.39E-03			
9.12E-03	8.35E-03	8.11E-03	8.34E-03	8.81E-03	8.85E-03	8.42E-03			
9.23E-03	8.44E-03	8.17E-03	8.39E-03	8.83E-03	8.84E-03	8.41E-03			
9.48E-03	8.57E-03	8.19E-03	8.20E-03	8.40E-03	8.39E-03	8.17E-03	8.14E-03		
9.37E-03	8.49E-03	8.13E-03	8.15E-03	8.38E-03	8.39E-03	8.17E-03	8.15E-03		
9.26E-03	8.41E-03	8.07E-03	8.12E-03	8.37E-03	8.40E-03	8.18E-03	8.17E-03		
9.36E-03	8.49E-03	8.13E-03	8.16E-03	8.39E-03	8.39E-03	8.18E-03	8.16E-03		
9.24E-03	8.42E-03	8.09E-03	8.14E-03	8.39E-03	8.42E-03	8.21E-03	8.20E-03		
9.35E-03	8.49E-03	8.14E-03	8.17E-03	8.40E-03	8.41E-03	8.20E-03	8.18E-03		
9.80E-03	8.94E-03	8.58E-03	8.50E-03	8.57E-03	8.55E-03	8.46E-03	8.51E-03	8.87E-03	
9.70E-03	8.87E-03	8.53E-03	8.46E-03	8.56E-03	8.56E-03	8.47E-03	8.53E-03	8.89E-03	
9.60E-03	8.80E-03	8.47E-03	8.43E-03	8.55E-03	8.57E-03	8.49E-03	8.56E-03	8.92E-03	
9.69E-03	8.87E-03	8.52E-03	8.46E-03	8.56E-03	8.56E-03	8.48E-03	8.53E-03	8.90E-03	
9.57E-03	8.79E-03	8.48E-03	8.45E-03	8.57E-03	8.59E-03	8.52E-03	8.59E-03	8.95E-03	
9.66E-03	8.86E-03	8.53E-03	8.48E-03	8.57E-03	8.58E-03	8.50E-03	8.55E-03	8.91E-03	
1.06E-02	9.80E-03	9.49E-03	9.36E-03	9.46E-03	9.45E-03	9.31E-03	9.43E-03	9.72E-03	1.04E-02
1.05E-02	9.75E-03	9.45E-03	9.34E-03	9.45E-03	9.46E-03	9.33E-03	9.46E-03	9.75E-03	1.05E-02
1.05E-02	9.69E-03	9.42E-03	9.32E-03	9.45E-03	9.48E-03	9.36E-03	9.49E-03	9.79E-03	1.05E-02
1.05E-02	9.74E-03	9.45E-03	9.34E-03	9.45E-03	9.46E-03	9.34E-03	9.46E-03	9.75E-03	1.05E-02
1.04E-02	9.68E-03	9.42E-03	9.33E-03	9.47E-03	9.50E-03	9.39E-03	9.52E-03	9.81E-03	1.05E-02
1.05E-02	9.73E-03	9.45E-03	9.35E-03	9.46E-03	9.47E-03	9.35E-03	9.48E-03	9.77E-03	1.05E-02

Figure 6.15 Pin-wise $\Sigma_{1\to2}$ at 30GWD/MTU without CR

2.9650		Case 1							
3.1598		Case 4							
3.4667		Case 5							
3.2268		Case 6							
3.9158		Case 7							
3.5515		Case 8							
3.6395	4.6601								
3.9265	5.0948								
4.3681	5.7470								
4.0159	5.2193								
4.9393	6.5143								
4.4267	5.7681								
4.2072	5.5478	6.5679							
4.5703	6.0932	7.1882							
5.1014	6.8737	8.0438							
4.6689	6.2319	7.3383							
5.6862	7.6684	8.8329							
5.0965	6.8128	7.9288							
4.5949	5.9853	6.9525	6.7545						
4.9890	6.5331	7.5272	7.1981						
5.5432	7.2928	8.2824	7.7558						
5.0869	6.6677	7.6576	7.2989						
6.0925	8.0375	8.9290	8.2032						
5.4960	7.2275	8.1566	7.6533						
4.6028	5.9750	6.6210	5.9796	4.0887					
4.9487	6.4515	7.0665	6.2708	4.2105					
5.4288	7.0952	7.6391	6.6276	4.3533					
5.0375	6.5678	7.1710	6.3372	4.2375					
5.8996	7.6817	8.1136	6.9053	4.4598					
5.3920	7.0141	7.5458	6.5652	4.3276					
4.6582	6.0546	6.7074	6.0494	4.1207	4.1512				
4.9673	6.4667	7.0688	6.2631	4.1986	4.1841				
5.3936	7.0186	7.5309	6.5249	4.2896	4.2235				
5.0490	6.5707	7.1586	6.3170	4.2184	4.1972				
5.8118	7.5218	7.9218	6.7394	4.3642	4.2682				
5.3660	6.9575	7.4704	6.4951	4.2824	4.2360				
4.7449	6.1998	7.1998	6.9922	6.1269	6.1813	7.1620			
5.0478	6.5869	7.5446	7.2020	6.2157	6.1879	7.1180			
5.4626	7.1085	7.9919	7.4639	6.3272	6.2060	7.0845			
5.1261	6.6885	7.6360	7.2620	6.2486	6.2082	7.1372			
5.8642	7.6108	8.3868	7.6979	6.4435	6.2680	7.1365			
5.4331	7.0793	7.9519	7.4561	6.3477	6.2613	7.1812			
4.4556	5.8805	6.9862	7.2917	6.8915	6.9659	7.5022	7.3421		
4.7028	6.1923	7.2636	7.4614	6.9581	6.9386	7.4094	7.2041		
5.0403	6.6111	7.6248	7.6804	7.0511	6.9241	7.3310	7.0774		
4.7686	6.2777	7.3436	7.5196	6.9944	6.9601	7.4263	7.2160		
5.3776	7.0208	7.9683	7.9041	7.1771	6.9860	7.3695	7.0993		
5.0312	6.6004	7.6215	7.7050	7.1011	7.0126	7.4564	7.2280		
3.8895	5.0188	5.9195	6.3251	6.3203	6.4040	6.5441	6.2922	5.3857	
4.0536	5.2185	6.0921	6.4267	6.3453	6.3483	6.4414	6.1536	5.2621	
4.2789	5.4888	6.3222	6.5660	6.3928	6.3058	6.3503	6.0279	5.1515	
4.1021	5.2795	6.1497	6.4708	6.3748	6.3654	6.4533	6.1616	5.2672	
4.5291	5.7883	6.5721	6.7400	6.4947	6.3529	6.3755	6.0360	5.1551	
4.3024	5.5219	6.3554	6.6165	6.4605	6.4035	6.4715	6.1632	5.2646	
3.1561	3.9073	4.5040	4.8422	4.8176	4.8763	5.0201	4.7483	4.2066	3.4995
3.2476	4.0128	4.5914	4.8906	4.8264	4.8360	4.9399	4.6543	4.1221	3.4356
3.3731	4.1572	4.7116	4.9623	4.8505	4.8063	4.8698	4.5708	4.0478	3.3800
3.2775	4.0491	4.6257	4.9177	4.8449	4.8470	4.9473	4.6592	4.1253	3.4379
3.5291	4.3353	4.8624	5.0696	4.9175	4.8382	4.8846	4.5765	4.0510	3.3827
3.4069	4.1968	4.7518	5.0081	4.9015	4.8729	4.9569	4.6599	4.1237	3.4363

Figure 6.16 Pin-wise spectrum index at 30GWD/MTU without CR

The above figures clearly show that the control rod insertion history has a strong impact on the pin cross-sections. The closer to the control rod is the pin; the larger is the change of the pin spectrum; the stronger is the impact of the control rod insertion history. For the above state points, five fuel pins, located at (10,1), (6,1), (7,2), (8,3), and (3,3) colored in the figures, are selected for further analysis. These pins cover the enrichment range from 1.4 to 4.9 w/o ^{235}U, with and without burnable absorber (Gd).

Similar to the PWR cases, the changes of the pin spectrum index against the pin cross-sections $\left(\Sigma_x^k\right)$ for the selected pins are plotted in Figure 6.17 to Figure 6.31.

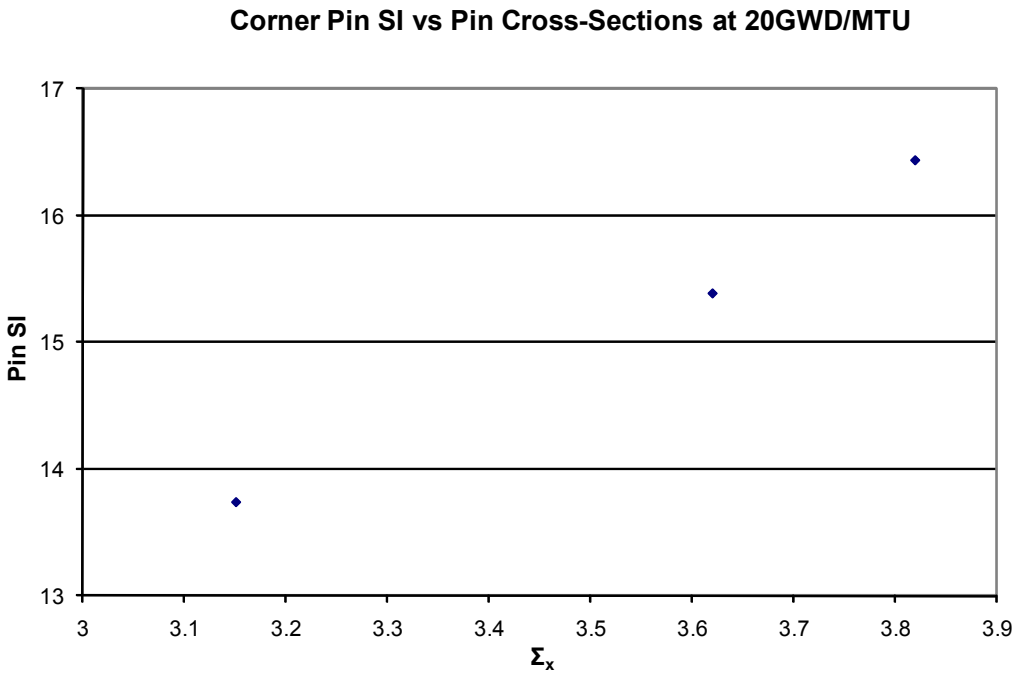

Figure 6.17 Spectrum index change with cross-sections for pin (10,1) at 20GWD/MTU

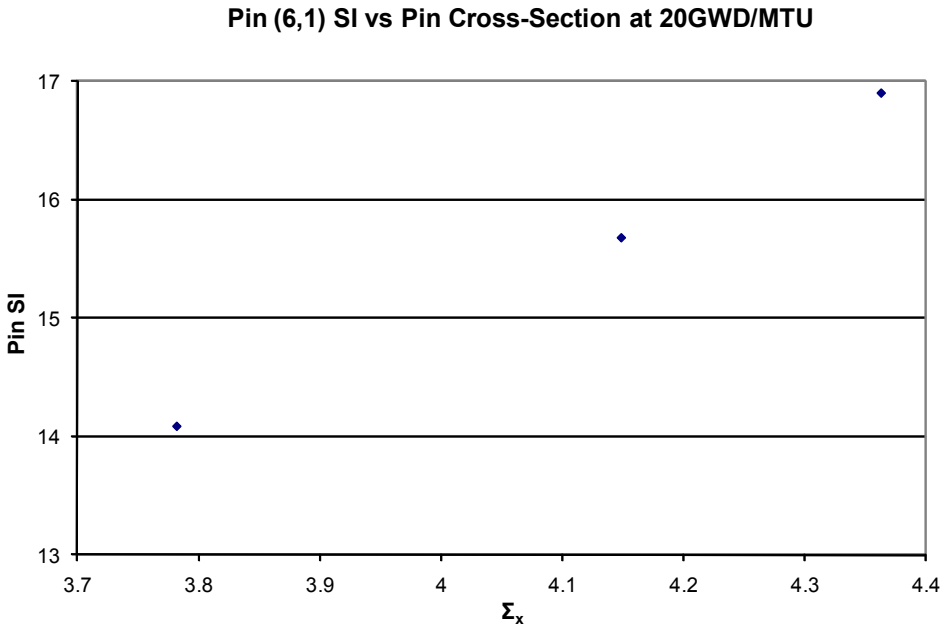

Figure 6.18 Spectrum index change with cross-sections for pin (6,1) at 20GWD/MTU

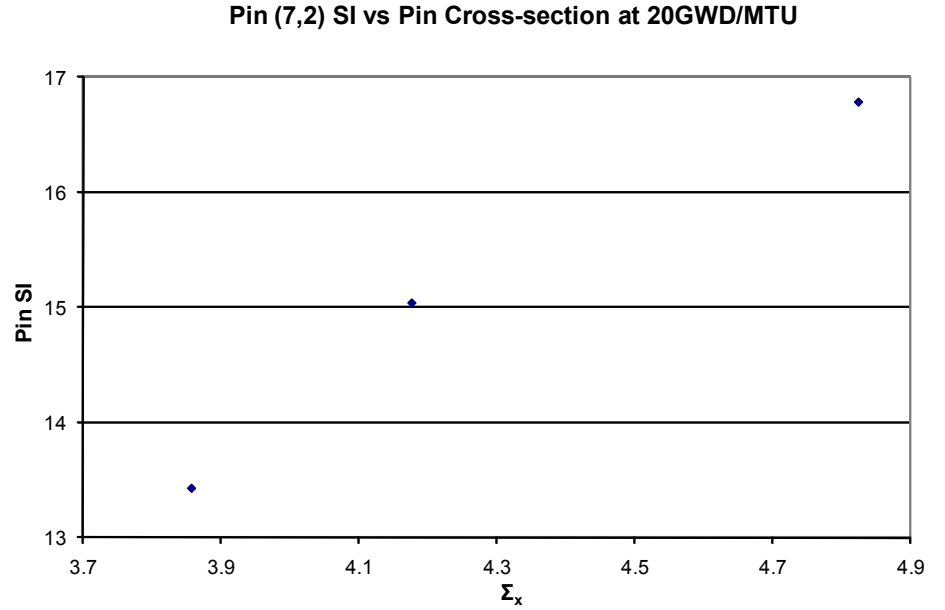

Figure 6.19 Spectrum index change with cross-sections for pin (7,2) at 20GWD/MTU

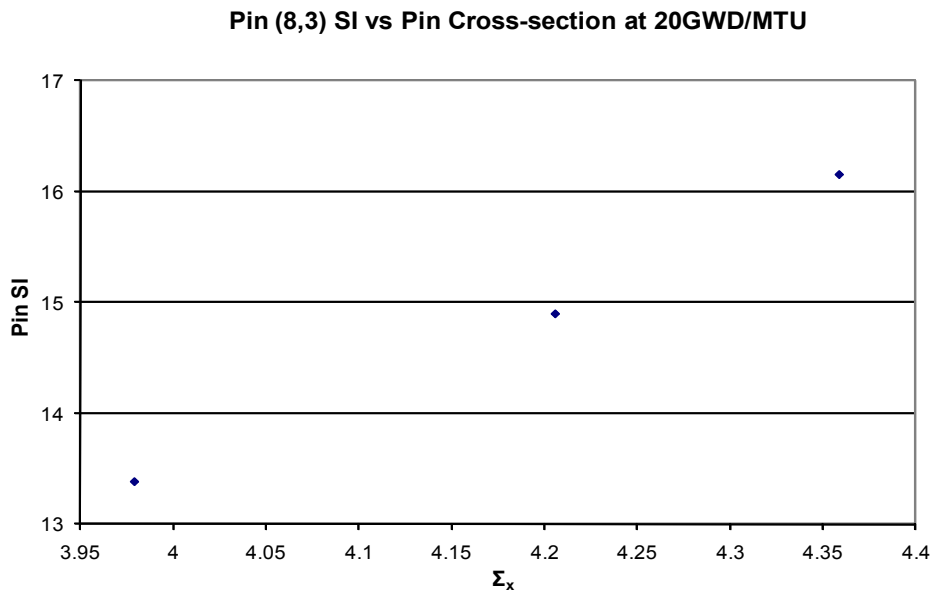

Figure 6.20 Spectrum index change with cross-sections for pin (8,3) at 20GWD/MTU

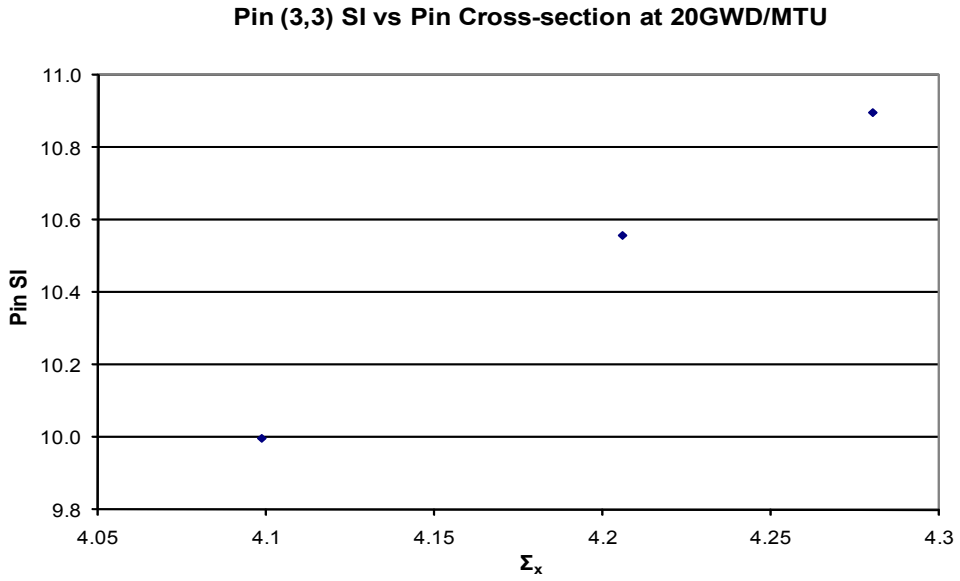

Figure 6.21 Spectrum index change with cross-sections for pin (3,3) at 20GWD/MTU

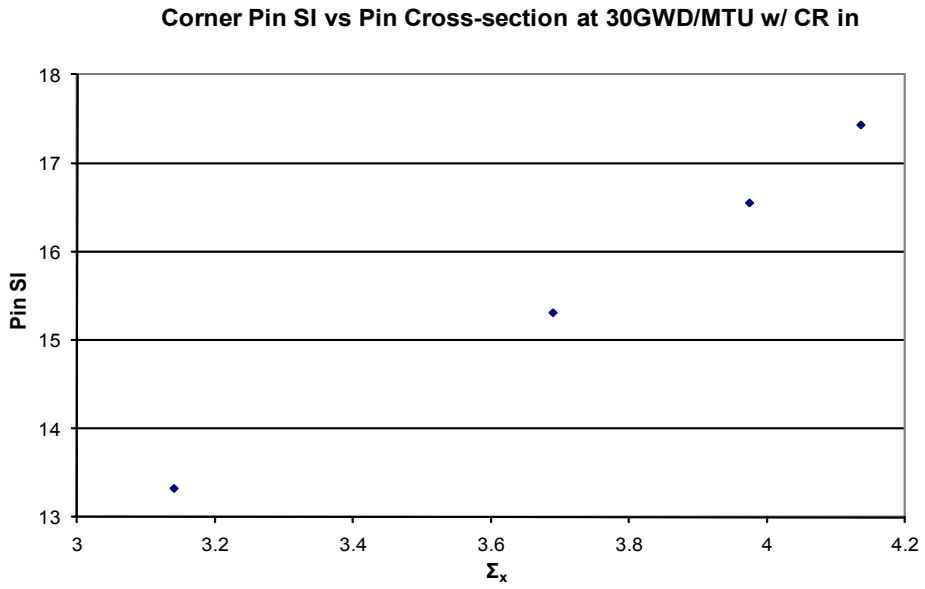

Figure 6.22 Spectrum index change with cross-sections for pin (10,1) at 30GWD/MTU with CR insertion

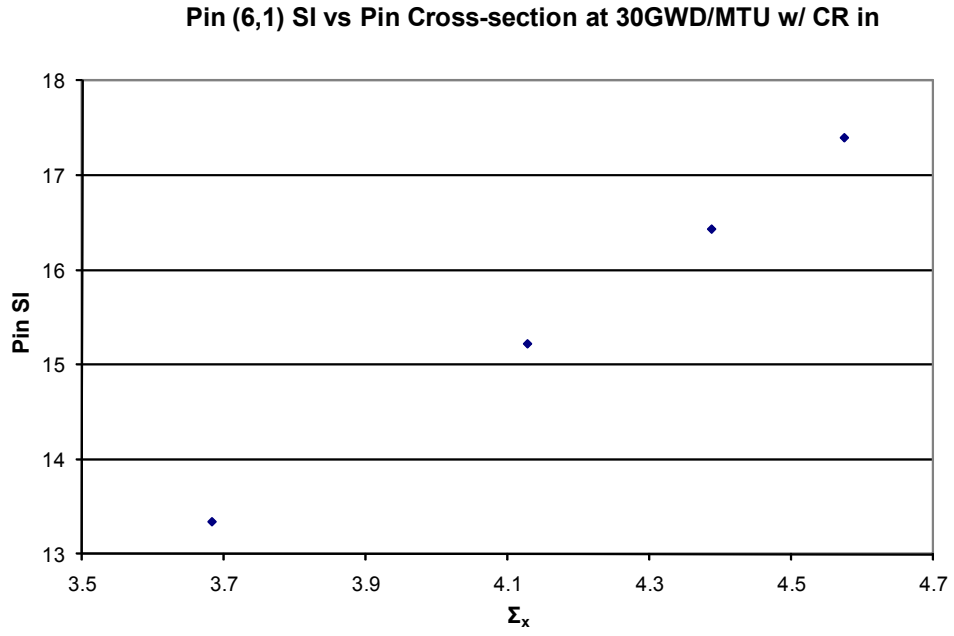

Figure 6.23 Spectrum index change with cross-sections for pin (6,1) at 30GWD/MTU with CR insertion

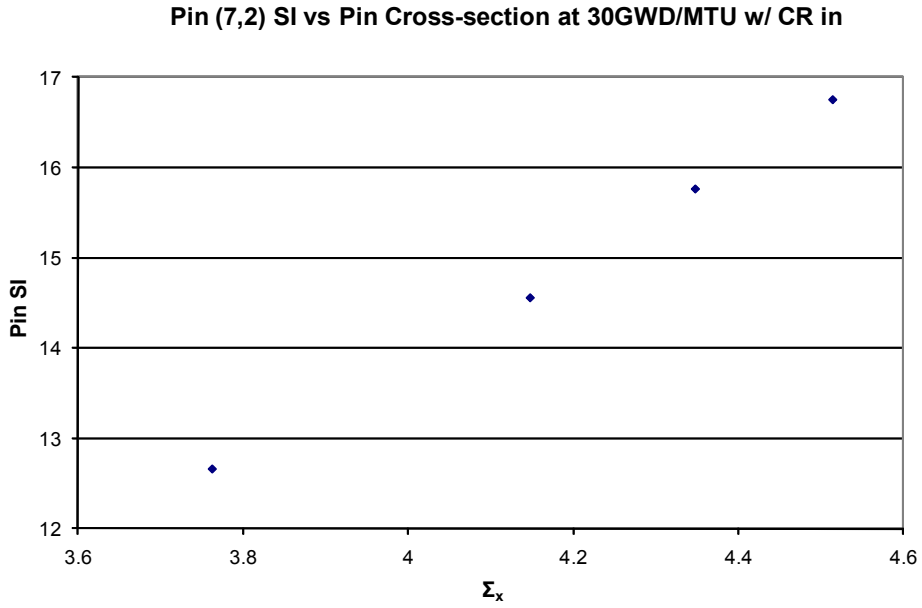

Figure 6.24 Spectrum index change with cross-sections for pin (7,2) at 30GWD/MTU with CR insertion

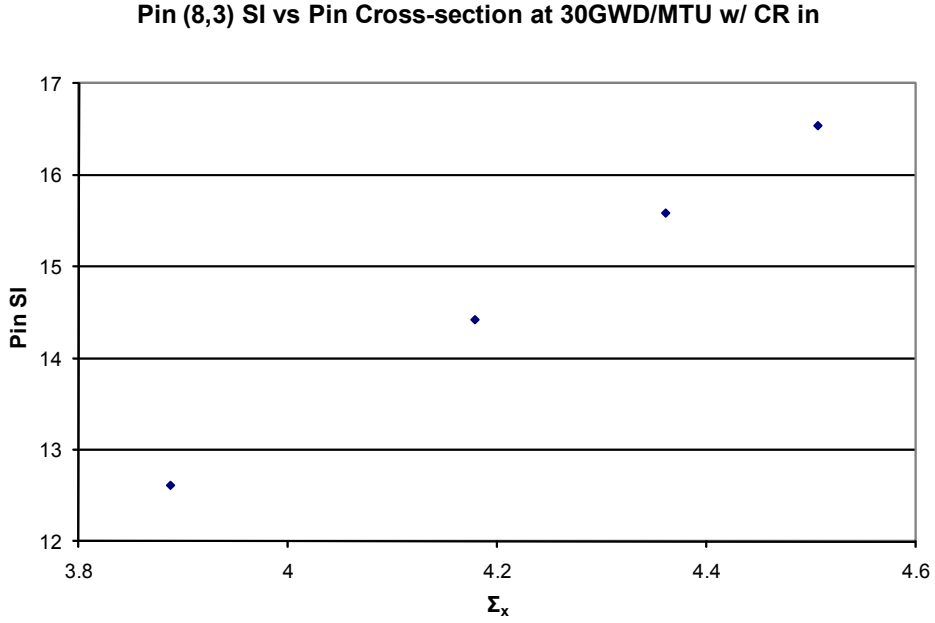

Figure 6.25 Spectrum index change with cross-sections for pin (8,3) at 30GWD/MTU with CR insertion

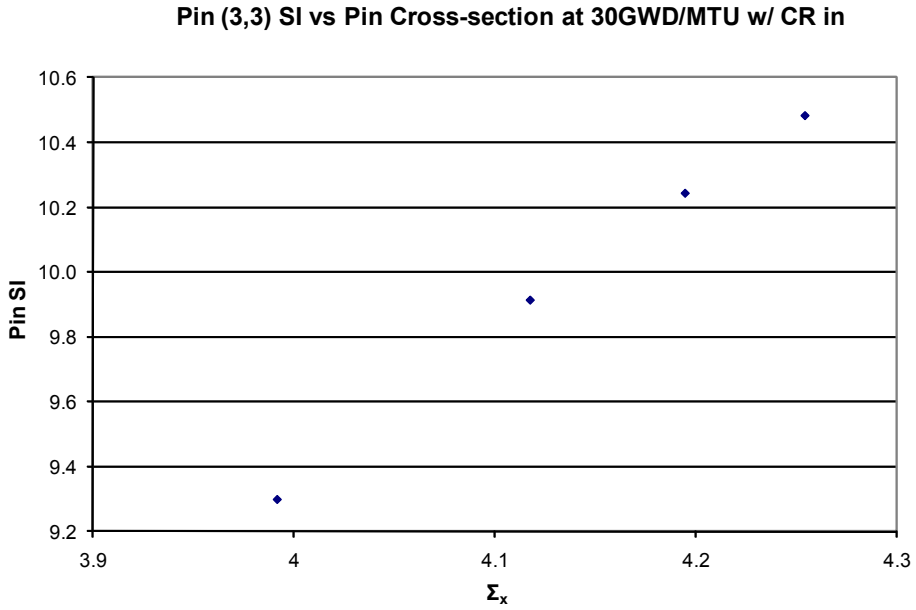

Figure 6.26 Spectrum index change with cross-sections for pin (3,3) at 30GWD/MTU with CR insertion

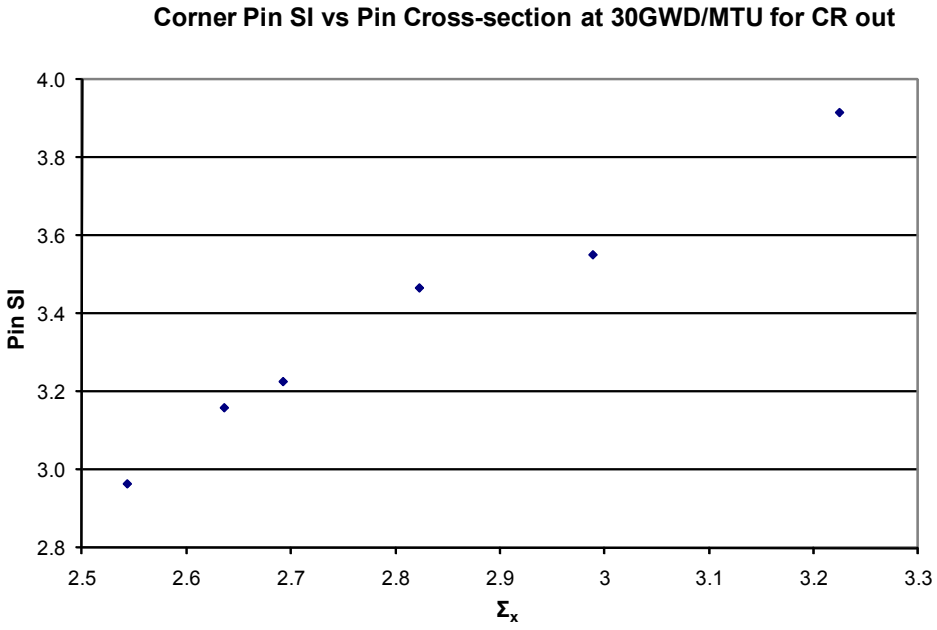

Figure 6.27 Spectrum index change with cross-sections for pin (10,1) at 30GWD/MTU without CR

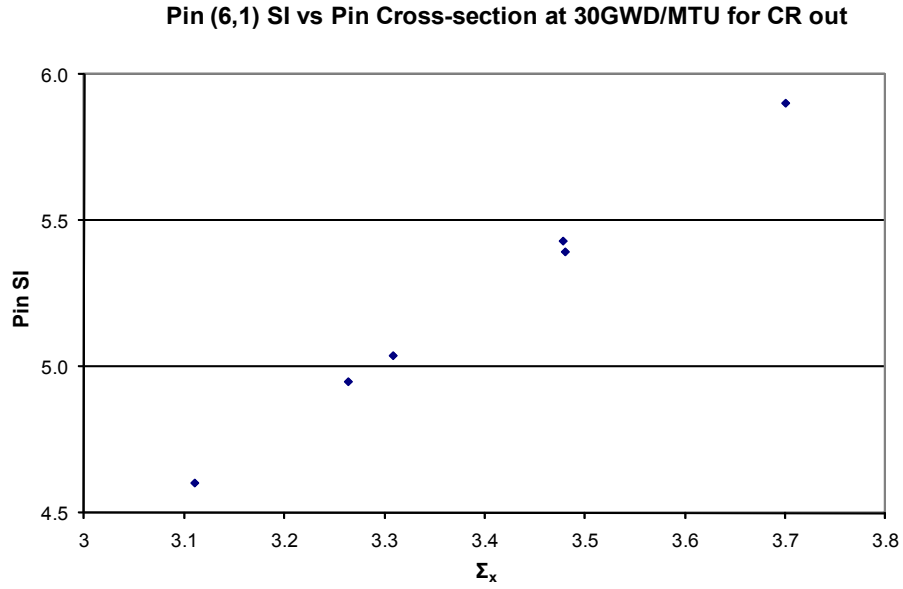

Figure 6.28 Spectrum index change with cross-sections for pin (6,1) at 30GWD/MTU without CR

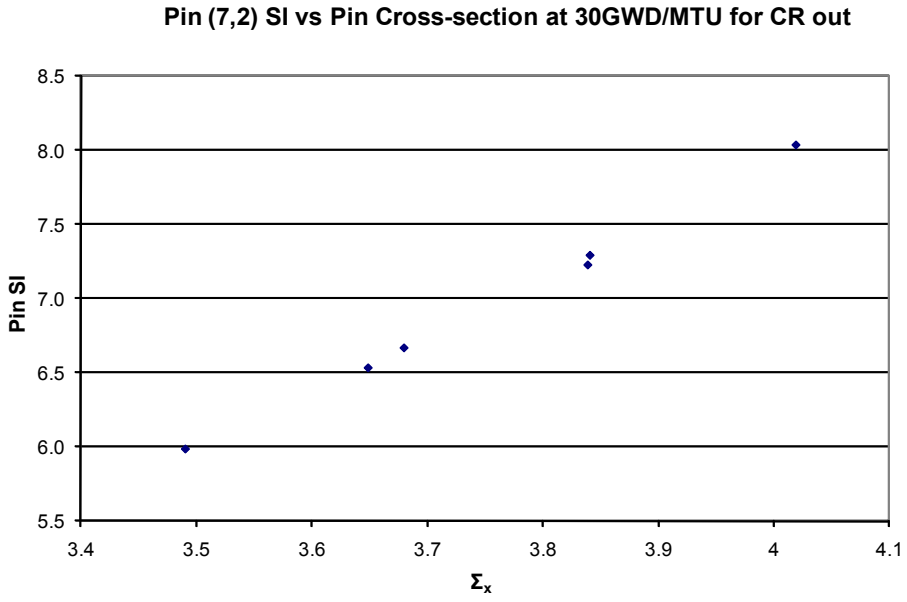

Figure 6.29 Spectrum index change with cross-sections for pin (7,2) at 30GWD/MTU without CR

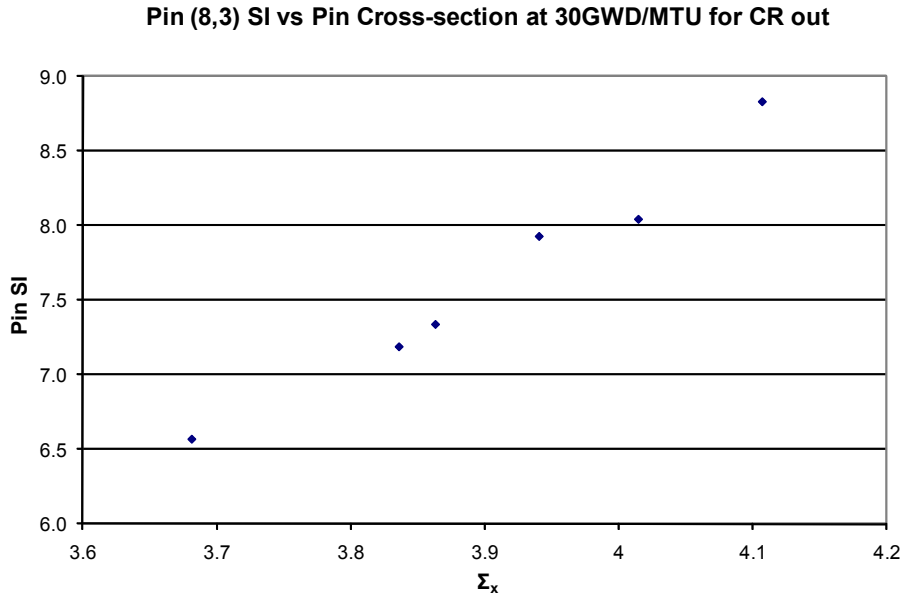

Figure 6.30 Spectrum index change with cross-sections for pin (8,3) at 30GWD/MTU without CR

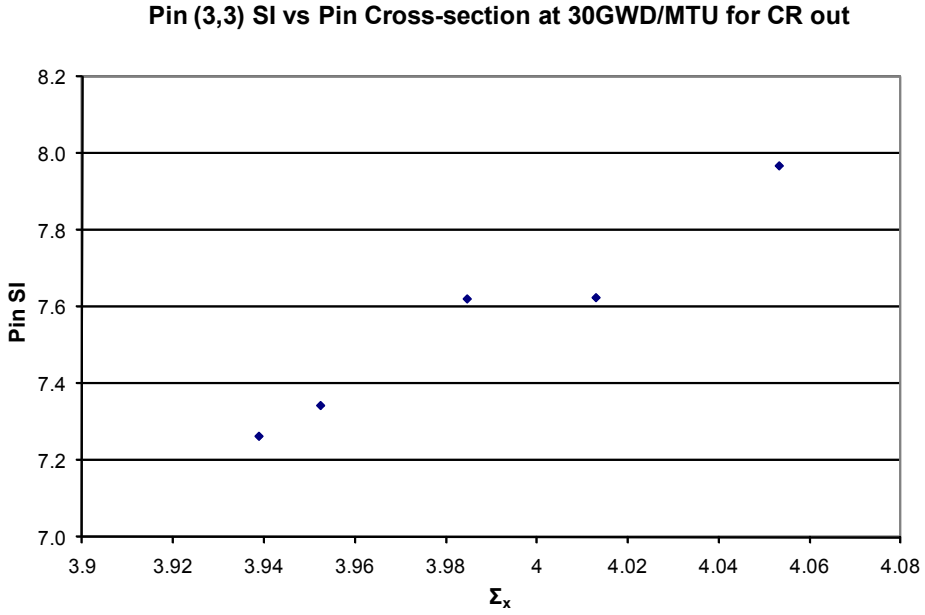

Figure 6.31 Spectrum index change with cross-sections for pin (3,3) at 30GWD/MTU without CR

Although the BWR control rod shows much stronger impact on local spectrum than PWR, for all selected pins of the BWR assembly, the figures demonstrate that the spectrum index behaviors against the pin cross-sections exactly in the same way as shown in PWR assemblies. From the limited evaluation, it is reasonable to believe that the pin spectrum index approach will work for BWR fuel to get the right pin thermal flux form factors.

6.4 Concluding Remarks

Since NEXUS/ANC9 is not ready to calculate BWR fuel, a BWR fuel assembly with and without control blade insertion was modeled offline with Westinghouse BWR lattice code PHOENIX-4. A preliminary test for the new pin power methodology in BWR application was carried out. As a key assumption of the new pin power method, the variation of the pin-wise spectrum index against the pin cross-sections was investigated. The results at different burnup steps and different states are consistent, encouraging, and promising, which suggests that the pin flux form factor correction model of the P3C methodology is applicable to BWR fuel.

Compared with PWR fuel assembly in the core, BWR coolant density varies significantly along the axial direction with different void fraction. The change of the void fraction introduces large change in both moderator composition (water) and the neutron spectrum. In radial direction, water density may be different from sub-bundle to sub-bundle and even pin to pin. From the water density information generated by the thermal-hydraulic calculation and through explicitly taking into account the water density contribution

coupled with the spectrum correction model, the updated pin cross-section representation model should be able to capture the void impact on the pin cross-sections for BWR fuel. As long as the pin cross-sections are precisely constructed, the P3C methodology should be able to capture the spectrum history effects for all control rod insertion scenarios and accurately predict the pin power distribution.

CHAPTER 7

CONCLUSIONS AND FUTURE WORK

7.1 Conclusions

The PWR operation strategy change, brought by the Westinghouse AP1000 reactor, introduced challenges to the conventional pin power methodology, which couldn't capture the CR history effect on the pin power during the irradiation of fuel assembly with the control rod insertion. A new pin power recovery (P3C, Pseudo Pin-by-Pin Calculation) methodology has been developed. The qualification results for PWR assemblies show that the P3C methodology overcomes the difficulties that the conventional methodology is facing in handling the strong heterogeneity changes and the accumulating effects on the pin power distribution.

In addition, the P3C methodology does not involve pin-by-pin isotopic tracking and fine-mesh diffusion or transport calculations. It is very efficient and therefore applicable for the regular core design calculation. For a PWR full core model, on Linux computer and without parallelization, ANC9 takes less than 5 second CPU time to complete the pin power calculations.

Since the spectrum history correction used in the P3C methodology is not limited to the

fuel assembly type, the new methodology is expected to be robust enough to work for both PWR and BWR. The P3C methodology for PWR pin power recovery has been fully qualified. For BWR fuel, the limited test results demonstrated that P3C flux form factor correction model is applicable to BWR fuel. As long as the application of the P3C spectrum history correction to pin cross-section is confirmed, the P3C methodology can be used for BWR pin power calculation.

7.2 Vision of Future Work

7.2.1 Full Qualification of P3C Methodology for BWR Pin Power Recovery

In order to qualify the P3C methodology for BWR pin power recovery, the NEXUS system will need to be modified to generate CD files for BWR fuel segments.

At the same time, the P3C modules should be incorporated into BWR simulator code. Once P3C methodology is implemented in BWR core design suite, the qualification calculations similar to those described in Chapter 5 will be performed for different BWR fuel assemblies with different control rod insertion scenarios.

7.2.2 Extension Application of P3C Methodology

The P3C method explicitly calculates pin-by-pin cross-sections and fluxes during the pin power recovery process. In fact, this is an important step and the key feature of the embedded models that has been studied around the world as a candidate for next generation methods (NGM). The next generation method follows each individual fuel rod

based on the local and boundary conditions and calculates fine mesh cross-sections and fluxes. From the fine mesh data, NGM can generate average effective cross-sections for each coarse mesh (node) on-the-fly if required, and those average cross-sections reflect the actual environment.

When NGM derives the nodal cross-sections on-the-fly, these cross-sections can capture the environmental effect precisely, including the interaction between fuel assemblies. A typical example for interaction between fuel assemblies important to be modeled is the UO_2 and MOX interface. There is very strong interaction on this interface due to the significant difference in the neutron spectrum between UO_2 and MOX assemblies.

Since the pin-wise cross-sections and fluxes are available in the P3C pin power calculation, this suggests that P3C methodology can play similar role as that of the embedded model. In other words, with P3C methodology, ANC9 could possibly capture the strong interaction between MOX and UO_2 assemblies through re-homogenization and the NEXUS/ANC9 system can be qualified for MOX core design applications. However, to meet the needs of MOX core calculation, both node-wise and pin-wise cross-sections must satisfy the accuracy requirements. As mentioned earlier, the interaction between MOX and UO_2 assemblies significantly changes the neutron spectrum for the pins along the interfaces. The spectrum change is much larger than the one covered in the current P3C spectrum correction model, described in Chapter 3. An extreme extrapolation could lead to unacceptable errors in the pin cross-sections and make the representation model invalid. Due to this fact, the P3C cross-section representation model requires further

qualification for MOX core application, especially for the pins around MOX/UO_2 interfaces. It might also require further improvement of the pin cross-section representation model to take the interaction effects into account. Theoretically, with the re-homogenization correction along with the above enhancement, NEXUS/ANC9 would be able to improve the accuracy for MOX/UO_2 core prediction.

In view of the fact that the cross-section representation method is based on the collapsed few-group data and cannot exactly capture the complex effect of the local spectrum and history in fine groups, it has to be pointed out that the P3C methodology won't be able to play the full role of NGM to eliminate the approximation although it could potentially function as the embedded model.

7.2.3 Expand P3C Methodology to Multiple Energy Groups

ANC9 is a two group nodal diffusion code. So the current P3C model is used for two-group calculations. In fact, the philosophy of the methodology is not limited to two energy groups. As a whole system, in order to expand to multi-group, the cross-section representation methods must be updated to generate multi-group cross-sections for each node and each pin. Once the multi-group pin cross-sections are available, the pin flux form factors can be developed in the same way as two-group model by ignoring the depletion history effect on the first group, i.e.

$$f_1^k = f_1^{k,refh}$$

Practically, in the multi-group nodal code, the energy group is normally wide enough and the probability of a neutron crossing 2 groups while slowing-down is negligible. By following the process of Section 4.2.2 and defining the multi-group pin spectrum index,

$$S_g^k = \begin{cases} \dfrac{\phi_g^k}{\phi_{g+1}^k} & g = 1 \\ \dfrac{\phi_{g-1}^k}{\phi_g^k} & g > 1 \end{cases}$$

the multi-group flux form factor adjustment model can be derived as:

$$f_g^k = \left(\prod_{g'=1}^{g} C_{g'}^k \right) \cdot f_g^{k,refh}$$

Here $C_{g'}^k = F_{g'}^k \left(\Sigma_{x,g'}^k, \Sigma_{x,g'}^{k,refh} \right)$ and $C_1^k = 1$.

Once the system is ready for multi-group calculation, the evaluation of the multi-group P3C model should be included in the system qualification.

7.3 Concluding Remarks

P3C methodology has been successfully developed and applied for pin power recovery. The new methodology allows the nodal code to predict the fuel rod power distribution for a core operated at any condition, including control rod insertion. By tracking and utilizing the real history of each individual fuel rod, the new pin power methodology accurately captures both the instantaneous and history effects of the heterogeneity change due to

control rod insertion during the operation.

The novel methodology has been implemented in the Westinghouse nodal code ANC, and qualified for PWR application. A BWR assembly was also tested and the limited results show that the P3C concept is valid and could be used in BWR pin power calculation.

By following each individual pin, the P3C methodology enables the conventional nodal code with a potential to solve the challenging theoretical issues in a new fashion with high efficiency and accuracy.

In addition, the pin power recovery calculation is executed independently for each fuel node. Therefore the P3C methodology is naturally ready for parallel computation.

APPENDIX

HOMOGENEOUS PIN FLUX CALCULATION

A.1 Derivation of Equation for Pin Homogeneous Flux Calculation

In order to make the derivation easier, we normalize the independent geometry variable to the range of -1 to 1 by simply dividing the actual coordinates by half of the nodal mesh size.

To get rod wise homogeneous fluxes for each node, the average fluxes of each node side and the nodal corner fluxes are taken as given information. For square node, to utilize this information in the rod fluxes calculation, 4 directions (and 4 opposite directions) are chosen in the right side of Eq.(3.4) to cover 4 sides and 4 corners. These directions are shown in the Figure A.1.

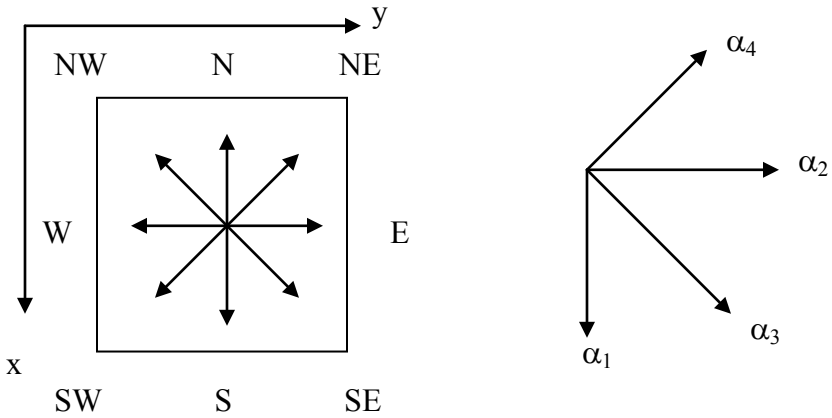

Figure A.1 4+4 directions used for expansion expression

For square geometry, m= 1, 4 represents directions respectively with angles (α) of ($0, \pi/2, \pi/4, 3\pi/4$) (see Fig.A.1). For each direction *m*, if we define $\phi_m^{\pm} = 0.5 \cdot \left(\phi_m^R \pm \phi_m^L\right)$, and ψ_m^R is the surface (or corner) flux in direction *m* while ψ_m^L is the flux on the opposite direction, i.e.:

$$\begin{cases} \psi_g^{\pm}(1) = \psi_{g,1}^{\pm} = 0.5 \cdot \left(\psi_g^S \pm \psi_g^N\right) \\ \psi_g^{\pm}(2) = \psi_{g,2}^{\pm} = 0.5 \cdot \left(\psi_g^E \pm \psi_g^W\right) \\ \psi_g^{\pm}(3) = \psi_{g,3}^{\pm} = 0.5 \cdot \left(\psi_g^{SE} \pm \psi_g^{NW}\right) \\ \psi_g^{\pm}(4) = \psi_{g,4}^{\pm} = 0.5 \cdot \left(\psi_g^{NE} \pm \psi_g^{SW}\right) \end{cases} \tag{A.1}$$

Clearly, before going further, we need to obtain the buckling flux boundary conditions by converting the available sides/corners fluxes using Eq. (3.2). The expansion coefficients can be determined from the available sides and corners fluxes as:

$$\vec{A}_g^{\pm} = \left[\hat{T}_g^{\pm}\right]^{-1} \cdot \vec{\psi}_g^{\pm} \tag{A.2}$$

Bringing the corner coordinates into the homogeneous flux expression, i.e. Eq.(3.2.b), at the North-East corner ($x = -1, y = 1$), the fluxes is:

$$\psi_g^{NE} = \sum_m \left\{ A_{g,m}^{+} \cos\left(-B_g \cos(\alpha_m) + B_g \sin(\alpha_m)\right) + A_{g,m}^{-} \sin\left(-B_g \cos(\alpha_m) + B_g \sin(\alpha_m)\right) \right\} \tag{A.3a}$$

Similarly, all the other corners can be expressed as:

$$\psi_g^{NW} = \sum_m \left\{ A_{g,m}^{+} \cos\left(B_g \cos(\alpha_m) + B_g \sin(\alpha_m)\right) - A_{g,m}^{-} \sin\left(B_g \cos(\alpha_m) + B_g \sin(\alpha_m)\right) \right\} \tag{A.3b}$$

$$\psi_g^{SW} = \sum_m \left\{ A_{g,m}^{+} \cos\left(-B_g \cos(\alpha_m) + B_g \sin(\alpha_m)\right) - A_{g,m}^{-} \sin\left(-B_g \cos(\alpha_m) + B_g \sin(\alpha_m)\right) \right\} \quad \text{(A.3c)}$$

$$\psi_g^{SE} = \sum_m \left\{ A_{g,m}^{+} \cos\left(B_g \cos(\alpha_m) + B_g \sin(\alpha_m)\right) + A_{g,m}^{-} \sin\left(B_g \cos(\alpha_m) + B_g \sin(\alpha_m)\right) \right\} \quad \text{(A.3d)}$$

Averaging over each nodal side for Eq.(2.7b), the homogeneous flux for the side can be generated and for side "North" ($x = -1$) the average flux is derived by integration of y over the range ($-1, 1$), there is:

$$\psi_g^{N} = 0.5 \cdot \sum_m \left\{ \frac{A_{g,m}^{+}}{B_g \sin(\alpha_m)} \cos\left(B_g \cos(\alpha_m)\right) \cdot \sin\left(B_g y \sin(\alpha_m)\right)\Big|_{-1}^{1} - \frac{A_{g,m}^{-}}{B_g \sin(\alpha_m)} \sin\left(B_g \cos(\alpha_m)\right) \cdot \sin\left(B_g y \sin(\alpha_m)\right)\Big|_{-1}^{1} \right\}$$

Or

$$\psi_g^{N} = \sum_m \left\{ \frac{A_{g,m}^{+}}{B_g \sin(\alpha_m)} \cos\left(B_g \cos(\alpha_m)\right) \cdot \sin\left(B_g \sin(\alpha_m)\right) - \frac{A_{g,m}^{-}}{B_g \sin(\alpha_m)} \sin\left(B_g \cos(\alpha_m)\right) \cdot \sin\left(B_g \sin(\alpha_m)\right) \right\}$$

For all the other sides, the average fluxes can be obtained similarly as shown below:

$$\psi_g^{S} = \sum_m \left\{ \frac{A_{g,m}^{+}}{B_g \sin(\alpha_m)} \cos\left(B_g \cos(\alpha_m)\right) \cdot \sin\left(B_g \sin(\alpha_m)\right) + \frac{A_{g,m}^{-}}{B_g \sin(\alpha_m)} \sin\left(B_g \cos(\alpha_m)\right) \cdot \sin\left(B_g \sin(\alpha_m)\right) \right\}$$

$$\psi_g^{W} = \sum_m \left\{ \frac{A_{g,m}^{+}}{B_g \cos(\alpha_m)} \cos\left(B_g \sin(\alpha_m)\right) \cdot \sin\left(B_g \cos(\alpha_m)\right) - \frac{A_{g,m}^{-}}{B_g \cos(\alpha_m)} \sin\left(B_g \cos(\alpha_m)\right) \cdot \sin\left(B_g \sin(\alpha_m)\right) \right\}$$

$$\psi_g^E = \sum_m \left\{ \frac{A_{g,m}^+}{B_g \cos(\alpha_m)} \cos\left(B_g \sin(\alpha_m)\right) \cdot \sin\left(B_g \cos(\alpha_m)\right) + \frac{A_{g,m}^-}{B_g \cos(\alpha_m)} \sin\left(B_g \cos(\alpha_m)\right) \cdot \sin\left(B_g \sin(\alpha_m)\right) \right\}$$

Combining the above equations and letting $\alpha_m = 0, \frac{\pi}{2}, \frac{\pi}{4}, \frac{3\pi}{4}$, and m = 1, 2, 3, and 4, according to the definition given by Eq. (A.1), there is:

$$\vec{\psi}_g^+ = \begin{pmatrix} \cos(B_g) & \frac{\sin(B_g)}{B_g} & \frac{\sin(\sqrt{2}B_g)}{\sqrt{2}B_g} & \frac{\sin(\sqrt{2}B_g)}{\sqrt{2}B_g} \\ \frac{\sin(B_g)}{B_g} & \cos(B_g) & \frac{\sin(\sqrt{2}B_g)}{\sqrt{2}B_g} & \frac{\sin(\sqrt{2}B_g)}{\sqrt{2}B_g} \\ \cos(B_g) & \cos(B_g) & \cos(\sqrt{2}B_g) & 1 \\ \cos(B_g) & \cos(B_g) & 1 & \cos(\sqrt{2}B_g) \end{pmatrix} \cdot \vec{A}_g^+$$

So the matrix of T_g^+ shown in Eq. (A.2) can be expressed as:

$$\hat{T}_g^+ = \begin{pmatrix} \cos(B_g) & \frac{\sin(B_g)}{B_g} & \frac{\sin(\sqrt{2}B_g)}{\sqrt{2}B_g} & \frac{\sin(\sqrt{2}B_g)}{\sqrt{2}B_g} \\ \frac{\sin(B_g)}{B_g} & \cos(B_g) & \frac{\sin(\sqrt{2}B_g)}{\sqrt{2}B_g} & \frac{\sin(\sqrt{2}B_g)}{\sqrt{2}B_g} \\ \cos(B_g) & \cos(B_g) & \cos(\sqrt{2}B_g) & 1 \\ \cos(B_g) & \cos(B_g) & 1 & \cos(\sqrt{2}B_g) \end{pmatrix} \tag{A.4a}$$

In the same way, there is

$$\hat{T}_g^- = \begin{pmatrix} \sin(B_g) & 0 & \frac{\left(1-\cos\left(\sqrt{2}B_g\right)\right)}{\sqrt{2}B_g} & \frac{-\left(1-\cos\left(\sqrt{2}B_g\right)\right)}{\sqrt{2}B_g} \\ 0 & \sin(B_g) & \frac{\left(1-\cos\left(\sqrt{2}B_g\right)\right)}{\sqrt{2}B_g} & \frac{\left(1-\cos\left(\sqrt{2}B_g\right)\right)}{\sqrt{2}B_g} \\ \sin(B_g) & \sin(B_g) & \sin\left(\sqrt{2}B_g\right) & 0 \\ -\sin(B_g) & \sin(B_g) & 0 & \sin\left(\sqrt{2}B_g\right) \end{pmatrix} \tag{A.4b}$$

Bringing Eq. (A.2) into Eq. (2.7b), the buckling flux for a rod at (x, y) becomes:

$$\begin{aligned} \psi_g(x,y) = \sum_n \Bigg\{ & \left(\sum_m \left[T_g^+\right]_{mn}^{-1} \cdot \cos\left(B_g x\cos(\alpha_m) + B_g y \sin(\alpha_m)\right) \right) \cdot \psi_{g,n}^+ + \\ & \left(\sum_m \left[T_g^-\right]_{mn}^{-1} \cdot \sin\left(B_g x\cos(\alpha_m) + B_g y \sin(\alpha_m)\right) \right) \cdot \psi_{g,n}^- \Bigg\} \end{aligned} \tag{A.5}$$

After obtaining the buckling fluxes for all eigenvalues, the homogeneous fluxes at (x, y) can be calculated by multiplying the eigenmode to the buckling fluxes (Eq. 3.2), i.e.:

$$\vec{\phi}^{\,\mathrm{hom}}(x,y) = \hat{R} \cdot \vec{\psi}(x,y) \tag{A.6}$$

A.2 Determination of Corner Fluxes

In the above discussion, it is assumed that the corner fluxes are given. In fact, only the nodal and surface average fluxes are generated from the nodal solution. Therefore, in order to apply the above method to calculate the pin-wise homogeneous fluxes, the corner fluxes have to be determined first.

The corner fluxes are initialized as the average values of all adjacent surface fluxes. From

the diffusion equations of each node, the corner neutron current can be derived as a function of nodal surface and corner fluxes. Based on the corner neutron balance, for a given corner, the sum of all corner neutron currents from the nodes around the corner should be zero [30][37][38]. The corner fluxes of each node is determined through an iterative update scheme, which adjusts the corner fluxes based on the summation of the corner neutron currents until the corner neutron balance is met.

REFERENCES

[1] B. Zhang et al, NEXUS – A New Nuclear Data System for Light-Water Core Analysis, Proceedings of ICAPP '05, Seoul, Korea, May 15-19, 2005.

[2] B. Zhang, T. Ida, and Y.A. Chao, A Study on Generic Two-Group Cross-Section Representation Methodology, Proceedings of the PHYSOR 2002, Seoul, Korea, October 7-10, 2002.

[3] K.S. Smith, An Analytic Nodal Method for Solving the Two-group Multidimensional, Static and Transient Neutron Diffusion Equations, MS Thesis, MIT, USA, 1979.

[4] R.A. Shober, A Nodal Method for Fast Reactor Analysis, Proceedings of Computational Methods in Nuclear Engineering, Williamsburg, VA, 1979.

[5] M.R. Wagner, Three-dimensional Nodal Diffusion and Transport Theory Methods for Hexagonal-z Geometry, Nucl. Sci. & Eng., 103, p.377, 1989.

[6] H.L. Rajic, A.M. Ougouag, ILLICO: A Nodal Neutron Diffusion Method for Modern Computer Architectures, Nucl. Sci. & Eng., 103, P.392, 1989.

[7] H. Finnemann, F. Bennewitz, M.R. Wagner, Interface Current Techniques for Multidimensional Reactor Calculations, Atomkernenergie, 30, No.2, p.123, 1977.

[8] K. Koebke and M. R. Wagner, The Determination of the Pin Power Distribution in a Reactor Core on the Basic of Nodal Coarse Mesh Calculations, Atomkernenergie, 30, No. 2, 136, 1977.

[9] B. Ivanov, Methodology for Embedded Transport Core Calculation, PhD Thesis, PSU, USA December 2007.

[10] P. Mondot and R. Sanchez, An iterative homogenization technique that preserves assembly core exchanges, Proc. Int. Conf. On Supecomputing in Nuclear Applications, SNA-2003, September 22-24, 2003.

[11] N.Z. Cho, G.S. Lee, S.G. Hong, C.K. Jo, K.T. Lee, "Whole–Core Heterogeneous Transport Calculations and Their Comparison with Diffusion Results," Trans. Am. Nucl. Soc., Winter Mtg., Washington D.C., pp. 292-294, (2000).

[12] H.G. Joo, J.Y. Cho, Y.H. Kim, "Dynamic Implementation of the Equivalence Theory in the Heterogeneous Whole Core Transport Calculation," PHYSOR 2002, Seoul, Korea, Oct. 7-10 (2002).

[13] Y.S. Liu, et al, ANC: A Westinghouse Advanced Nodal Computer Code, WCAP-10965, Westinghouse Electric Company, Dec., 1989.

[14] F. Schliephacke, Computer Code Description, BWR application, Westinghouse Atom AB Report BTU 01-149, Rev 0.

[15] K. Kobke and L. Hetzelt, On the Construction of Local Homogeneous Neutron Flux and Current Distribution of LWR from Nodal Schemes, Nucl. Sci. Eng., 91, 123, 1991.

[16] Y.S. Liu et al, Pin Power Prediction in the Westinghouse Advanced Nodal Code, Trans. Am. Nuclear Soc., 53, 246, 1986.

[17] K.R. Rampe et al, SIMULATE-3 Pin Power Reconstruction: Methodology and Benchmarking, Proc. Int. Reactor Phys. Conf., III-19, Jackson Hole, WY, USA, 1988. (Nucl. Sci. Eng. 103:4, Dec 01 1989).

[18] P. Forslund, E. Muller, and S-Ö Lindahl, Investigation of Intranodal Depletion Effects, Annals of Nuclear Energy, Vol. 28 (3), p.225-250, Feb. 2001.

[19] F. Nissen, "Determination of Local Pin Powers in the Framework of Nodal Coarse-Mesh Solutions, Riso-R-474, August 1982.

[20] C.J., Park; Y.H. Kim, N.Z. Cho, On the Reconstruction of Pinwise Flux Distribution Using Several Types of Boundary Conditions, Nuclear Engineering and Technology, Vol 28, No.3, pp.311-319.

[21] S-Ö Lindahl, POLCA7 – Data and Calculation Flow, Westinghouse Atom AB Report BR 94-1061, Rev 3.

[22] E. Müller, NEXUS – Cross-Section Representation Model, BTU 03-021, Rev 3.

[23] PARAGON User Manual, Westinghouse Electric Company, 2005.

[24] L. Mayhue, Status of APA Performance for US PWR, Internal annual report for Westinghouse customers.

[25] R.E. MacFarlane, D.W. Muir, and R.M. Boicourt, The NJOY Nuclear Data Processing System, Los Alamos National Laboratory, Dec. 1978.

[26] B. Ivanov. "Methodology for Nuclear Cross-Sections Generation and Implementation". RDFMG-BI-D-001(04) rev.0, January 2004.

[27] R.J. Stammler and M.J. Abbate, Methods of Steady State Reactor Physics in Nuclear Design, (Academic Press, 1983)

[28] Y.S. Liu, et. al., ANC: A Westinghouse Advanced Nodal Computer Code, WCAP-10965-A-AD1, April, 1989

[29] L. Mayhue, et al, Qualification of NEXUS/ANC Nuclear Design System for PWR Analysis, Proceedings of PHSOR 2008, Interlaken, Switzerland, Sept. 14-19, 2008.

[30] V. Mecir, Y.A. Chao, Consistent Corner Flux Calculation for Pin Power Reconstruction, Trans. of the American Nuclear Society, Vol. 27, December 1995.

[31] D. Ziabletsev, K. Ivanov, Investigation of Alternative Boundary Conditions in the Analytical Pin Power Reconstruction Method, Proceedings of ANS Winter Meeting, Reno, Nevada, November 11-15, 2001.

[32] R. J. J. Stamm'ler, S. Olsson, Ö. Bernander, The PHOENIX Computer Program for Fuel Assembly and Pin Cell Calculations, ASEA-ATOM Report RCA-77-12 (1977).

[33] T. Bahadir, S-Ö Lindahl, Studsvik's Next Generation Nodal Code SIMULATE-5, Proceedings of Advances in Nuclear Fuel Management IV (ANFM IV), April 12-15, 2009, Hilton Head Island, South Carolina, USA

[34] T. Bahadir, S-Ö Lindahl, STIMULATE-4 Pin Power Calculations, Proceedings of PHSOR 2008, Interlaken, Switzerland, Sept. 14-19, 2008.

[35] S-Ö Lindahl, T. Bahadir, Evaluation of Gamma Scanning in Oskarshamn2 with SIMULATE-5, Proceedings of PHSOR 2010, Pittsburgh, Pennsylvannia, USA, May. 08-13, 2010.

[36] P. Forslund, The Effect of Control Rod History on Reactor Physcis Parameters, ABB Atom Report BCA 98-029.

[37] H.G. Joo, J.I. Yoon, S.G. Baek, Multigroup Pin Power Reconstruction with Two-dimensional Source Expansion and Corner Flux Discontinuity, Annals of Nuclear Energy, Vol.36 (1), p85-97, January 2009.

[38] M.H. Chang, K.S. Moon, J.M. Noh, and S.H. Kim, A Nodal Expansion Method with Spatially Coupled Effects Incorporated Into The Transverse Leakage Approximation, Nucl. Sci. Eng. 103, p.343, 1989.

Vita

Baocheng Zhang was born in Jiangsu, China on November 7, 1965. Baocheng received his M.S. degree in Nuclear Reactor Physics and Engineering from China Institute of Atomic Energy (CIAE), Beijing, China in July of 1991. From July 1991, he worked at China Nuclear Data Center of CIAE as an Engineer, on the nuclear data evaluation and benchmarking, method development of resonance integration and interference. During 1994 to 1995, Baocheng worked at the Netherlands Energy Research Foundation (ECN) as the guest researcher on the lattice model development for LEU-HTR. After returning to CIAE, he was appointed as an associate professor and continued his research work.

In 1998, he left China for Japan working in Mitsubishi Heavy Industries, Ltd. He was working on the methods development of Westinghouse core design code system (APA) till 2001.

Baocheng Zhang came to US in March of 2001. Since then, he has been working in Westinghouse as a senior and principal engineer on the development and implementation of new methodologies for the Westinghouse core design system. In 2008, he started his study at the Pennsylvania State University and earned the Ph.D. degree in Nuclear Engineering in December, 2010.